NEW DESIGN OF HIGH VOLTAGE SURGE ARRESTERS

(REKABENTUK BARU PENANGKAP PUSUAN VOLTAN TINGGI)

AHMAD B. DARUS

ZULKURNAIN ABDUL MALEK

MOHAMED AFENDI MOHAMED PIAH

Institut Voltan & Arus Tinggi
Fakulti Kejuruteraan Elektrik
Universiti Teknologi Malaysia

2004

Acknowledgement

Abstract

Zinc-oxide material is an important and widely used element in the high voltage gapless surge arresters. Equally important is the usually polymeric insulating material used for the surge arrester housing. This work aims to develop a new design of gapless high voltage surge arrester using an improved zinc-oxide material and a new natural rubber based insulating material. The first part of this work deals with the development of a newly formulated thermoplastic elastomes (TPE) compound based on the linear low-density polyethylene (LLDPE) and natural rubber (NR) blends. The effects of alumina trihydrate (ATH) fillers on the TPE compound were also studied. The electrical tracking performance of the compound was investigated using a newly constructed surface tracking system based on incline-planned test method. The LLDPE and natural rubber blend was found to be reliable as an alternative high voltage insulating material. The second part of the work involves the development of a new test module suitable for transient response studies of zinc-oxide surge arresters. It companies of a high voltage transducer based on the D-dot probe principle and a coaxial high current transducer as well as the high current impulse generator. The module is suitable for testing arresters with voltage and current ratings at up to 100kV and 10kA respectively. Initial tests on distribution level zinc-oxide surge arresters provide some data for the development of a new equivalent circuit representation of the zinc-oxide surge arrester under fast transient condition and hence better characterization of its electrical behavior.

Abstrak

Bahan zink-oksida merupakan elemen penting dan digunakan secara meluas dalam penangkap pusuan voltan tinggi tanpa sela. Sama pentingnya ialah bahan penebatan polimer yang biasa digunakan sebagai perumah kepada penangkap pusuan tersebut. Kajian ini bertujuan untuk membina satu rekabentuk baru penangkap pusuan tanpa sela dengan menggunakan bahan zink-oksida yang diperbaiki dan bahan penebatan baru berasaskan getah asli.Bahagian pertama kajian ini melibatkan penghasilan sebatian baru thermoplastik elastomer (TPE) berasaskan campuran *linear low-density polyethylene* (LLDPE) dan getah asli (NR). Kesan penambahan alumina trihydrate (ATH) juga dikaji. Prestasi treking elektrik sebatian diselidik dengan menggunakan sistem treking permukaan yang diterima berasaskan kaedah pengujian *incline-planned*. Campuran LLDPE dan NR didapati boleh digunakan sebagai alternatif kepada bahan penebatan voltan tinggi. Bahagian kedua kajian ini melibatkan pembinaan satu modul pengajian yang sesuai untuk kajian sambutan fana pantas penangkap pusuan zink-oksida. Modul tersebut mengandungi transduser voltan tinggi berasaskan prinsip *D-dot probe* dan satu transduser arus sepaksi di samping penjana arus tinggi. Modul tersebut sesuai digunakan untuk menguji penangkap pusuan dengan kadaran voltan dan arus masing-masing 100kV dsan 10kA. Pengujian awal pada penangkap pusuan zink-oksida tahap agihan menyediakan sebahagian data bagi pembinaan satu perwakilan litar setara yang baru bagi penangkap pusuan zink-oksida di bawah tegasan fana pantas dan seterusnya pencirian sifat elektrik bahan yang lebih baik.

CONTENTS

TOPICS   **PAGE**

CHAPTER 1   INTRODUCTION

PART ONE

CHAPTER 2   Surface Tracking

CHAPTER 6   Tubular Current Shunt Design and Construction

CHAPTER 7   **High Current Switch Design and Construction**

LIST OF TABLES

LIST OF FIGURES

CHAPTER 1

INTRODUCTION

1.0   Objectives

Since the introduction of zinc-oxide material in 1968 much research has been directed towards the characterization of the electrical behavior of the material under various stress conditions.The main aim of these characteristics is to develop a new design of high voltage zinc oxide surge arresters for fast transient applications. Both the zinc oxide material as well as the insulating material can play important roles in the overall performance of the complete surge arrester.

Based on the above, two main objectives of the work are identified. Firstly, to identify a new equivalent circuit representation of the zinc oxide surge arresters under fast transient conditions. Secondly, to develop a new design of insulating material for high voltage surge arresters incorporating locally available material namely the natural rubber.

In part II of this project, the research work is focused on development of a new test set-up for testing zinc oxide surge arresters under fast transient condition. This includes the development of a new voltage transducer based on the D-dot probe principle, and a new current transducer based on a coaxial configuration. SF_6-insulated triggerable high-current spark-gaps were also developed to provide the fast

switching requirement of the low inductance charging capacitors. This set-up is capable of providing more data and analysis on 11kV-rated distribution surge arresters in terms of their characteristics, performance, and effectiveness. The results can be used to further improve the performance of surge arresters by refining the design criteria especially with respect to the housing insulation characteristics that is carried out in Part I of this research.

1.1   Significant Output

The work had produced the following significant output :

- A new test module comprising the high voltage transducer based on the D-dot probe principle and a new high current transducer based on the coaxial configuration. This module is suitable for testing arresters with voltage and current ratings of up to 100kV and 10kA respectively.

- A new surface tracking system based on incline-planed test method.

- The LLDPE and natural rubber blend (for example 80% LLDPE and 20% NR) is reliable as an alternative high voltage insulating material.

1.2   Organization of Report

The project consists of two parts:

Part I:

In Part I, the work on the development of a new insulating material is discussed in detail. The work is reported in three chapters. The theory on surface tracking is described in Chapter 2, followed by a detailed description on the inclined plane technique in Chapter 3. Finally, in Chapter 4, the study on the new material composition is described in detail.

Part II:

In Part II, the work on fast transient study is reported. The D-dot voltage and the coaxial current shunt transducers are described in Chapters 5 and 6 respectively. Chapter 7 discusses the design of the triggerable high current switch followed by the description on high voltage and high current test facility in Chapter 8. A general discussion and conclusion is gives in Chapter 9.

PART ONE

CHAPTER 2

SURFACE TRACKING

2.1   Introduction

Electric power supply should ensure reliability and continuity to the utility concerns. Hence the power lines and sub-stations are to be operated and protected against over voltages such that the numbers of failures are as few as possible. At the same time, the cost involved in the design, installation and operation of the protective devices should not be too high. Hence, a gradation of insulation system and protective device operation is to be followed.

The objective of this project is to develop a new design of high voltage surge zinc oxide surge arrester for fast transient applications. The project involves experimental and simulation work to determine suitable zinc oxide material for surge arrester applications as well as to determine suitable insulating material based on local materials of new formulated thermoplastic elastomer (TPE) compounds.

Generally, the project consists of two major parts conducted in parallel and the report is presented into two parts. This part reports on the development of a newly formulated TPE that to be used as a housing insulating material of a proposed design

of surge arrester. In this work, the linear low-density polyethylene (LLDPE) blends with natural rubber (NR) are used as polymer based material due to their good electrical properties. In order for the material to be used for high voltage insulating purpose as well as capable of withstanding the electrical discharge stress, heat retardance fillers are mixed into the polymer compounds. With proper formulation of selected polymer materials, this newly developed material can offer as an alternative material in the future for high voltage insulating applications.

For investigating the electrical tracking performance of the developed materials under the stress of leakage current (LC) and surface discharges, a surface tracking and erosion test is conducted under severe ambient conditions. This test is based on the IEC 587 test method and popularly known as inclined-plane tracking (IPT) test. The test procedure of IEC 587 is used because it is designed to be a short-time test compared to others tracking test. Besides that, this IPT test offers fast results as well as requires close attention.

Investigation on the electrical tracking performance of a newly formulated TPE material for outdoor high voltage insulating application is conducted by measuring the LC and the rate of carbon track propagation on the material surface. A computer-based leakage current monitoring system is developed to monitor the electrical tracking activity as well as to provide on-line information on the performance of the material. Morphological analysis is also carried out to study the surface microstructure before and after the tracking test. The experimental results show that different material compositions affect the leakage current and electrical tracking properties. It is observed that the use of natural rubber blended with thermoplastic material is reliable as an alternative high voltage insulating material in the future.

2.2   Polymeric Insulating Materials and Compounding Technology

Insulation plays an important role in order to determine the performance of the electrical power apparatus. A good insulation system will give the better design and performance of the apparatus. Today, the polymeric insulators are widely being used

in both the distribution and transmission voltage ranges and are steadily capturing a wider share of the market. In fact, during the past five decades, polymer insulators (PIs) are commonly used in place of traditional porcelain and glass for high voltage applications in electrical power systems.

Survey on the use of PIs all over the world, shows that almost 80% of electrical utilities would actively increase the use of PIs in the future (Kikuchi, *et.al* 1999). The tremendous growth in the applications of PIs are due to their advantages such as lightweight, higher mechanical strength to weight ratio, low surface energy, resistance to vandalism and better performance in the present of wet contaminated conditions (Mackevich, 1997a ; Hackam, 1999). The most widely used materials in the manufacture of polymer high voltage insulators are silicone rubber, ethylene propylene rubber and epoxy. These polymers that differ in terms of their properties and characteristics must be understood and carefully controlled to yield a material, which will serve as long-life high voltage outdoor insulators (Sundhar, *et.al* 1992).

Polymer insulating materials are formulated to provide a better performance characteristic for high voltage applications, which can offer advantages such as more compact products, reduced maintenance and lower operating cost (Gubanski, 1999). The insulator performance is the result of the interaction between material formulation, product design, and the manufacturing process. There are many physical properties of a polymer material that must be properly controlled to provide the characteristics necessary to serve a long life as a high-voltage insulating polymer (Mackevich, 1997b). These physical properties are evaluated by a variety design tests to ensure that the compound exhibits those characteristics required for use in high voltage insulators.

Thermosetting compound materials are the first polymer materials that used in high voltage applications. However, because of thermal expansion problem as well as possibility in electromechanical failure, the used of thermosetting compounds are limited. Compounding materials to correct this compatibility problem resulted in the development of thermoplastic and elastomer based compound. The use of thermoplastic elastomer (TPE) has been steadily increasing and has enjoyed outstanding growth during the last three decades. The decision to use a TPE in place

of conventional rubber (thermoset-rubber) is due to the flexible material that provides a better performance characteristic as well as easy processing, lower cost and fully recyclable.

Compounding is the technology of converting the raw rubber resin into useful materials through the addition of additives. Extensive work in the development of improved TPE compounds has contributed significantly to the penetration of TPEs in many electrical markets previously dominated by product based on thermoset rubbers and high performance thermoplastics. All commercially available TPEs can be formulated for electrical applications, either in blends with other polymers or through the use of suitable additives to meet specific industry standards.

A practical compound formulation typically consists of several of ingredients. Proper selection of the ingredient(s) in each category requires that consideration to be given to the desired physical, electrical and environmental properties, as well as cost, ease of mixing, chemical stability and ease of processing (Callister, 2000). Knowledge of the function and effectiveness of compounding ingredients is essential in the development of a compound.

Table 2.1 shows the typical additives and their function in a compound formulation. The fillers are incorporated into the base polymer compound in order to improve the electrical and mechanical properties as well as reduced the material cost. In this study, the alumina trihydrate (ATH) is incorporated into the newly formulated thermoplastic elastomer compounds. ATH filler is added to enhance the resistance to tracking and erosion as well as to provide better mechanical performance of some polymers (Hackam, 1998). The use of such filler in the polymer formulation was a giant step towards the application of certain plastics and elastomers for outdoor electrical insulation. Typically, the industry uses ATH in the compound to improve the electrical tracking performance. The presence of 30% - 55% weight of ATH could improve the tracking properties into optimum condition for the most compounds (Costa, 1991; Xuguang, 2000).

This project is carried out to discover the possibility of using local and low cost materials in the high voltage insulating application. The LLDPE and NR

materials are selected as a polymer-based component due to their good compatibility as well as easy to process. The properties of selected materials used in this work are shown in Table 2.2. Since the main scope of the work is to investigate the surface tracking phenomena under the activity of electrical discharges, ATH filler is incorporated into the based polymer component in order to increase the tracking and erosion resistance.The behaviour of leakage and discharge current that flows on the material surface will be discussed in the following section.

Table 2.1 : Additives and their functions

Additives	Functions
Fillers	- reinforced physical properties. - modify electrical and mechanical properties. - improve hardness. - electrical tracking. - fire retardance. - reduce cost.
Vulcanizing agent	- chemical reaction – crosslinking.
Coagent	- chemical reaction – rapid crosslinking, inhibit bond degradation.
Antidegradant (Stabilizer)	- retarding the deterioration of compound under prolonged heat and light. - provide effective oxidative stability. - maximum protection against UV degradation.
Processing aid	- improving the processability of compounds in terms of flow and mould release.
Coupling agent	- bridge the interface between polymer and filler. - improve chemical bonding.
Plasticizer	- improving the processability of compounds. - Aid mixing, modify viscosity or provide flexibility

Table 2.2 : Properties data of the selected materials used

Properties	POLYMERS	
	Linear Low Density Polyethylene (LLDPE)	**Natural Rubber (polyisoprene) (NR)**
Category	Thermoplastic	Elastomer
Density (g/cm^3)	0.926	0.95
Electrical Resistivity (Ω-cm)	10^{15}	10^{16}
Dielectric constant (permittivity)	2.4	2.9
Dielectric strength (kV/cm)	150	50
Dissipation factor (tangent loss)	0.0002	0.03
Melting point (°C)	130	90
Thermal conductivity (W/m-K)	0.40	0.15
Specific heat (J/kg-K)	2000	440

Note : Data given are average values.

2.3   Leakage Current and Surface Tracking Phenomena

Polymer insulators may suffer from environmental and electrical aging stresses in service that may cause their performance to deteriorate. It is well known that tracking has been the most common cause of insulation failure. Tracking is developed from the electrical surface discharge activity due to the flowing of leakage current (LC) on the insulator surface under wet contaminated conditions (Chang, 2000). This LC results in non-uniform heating of electrolyte that eventually causes dry-band to be formed at the narrow section where the LC density is highest. The whole voltage across the insulator appears across the dry-band and the surface discharge occurs when it reaches the air-gap critical flashover voltage (Fernando, 1999).

Arcs created from this surface discharge phenomenon burn the insulator material and create the carbonized tracks. This dry-band discharge phenomenon is a cumulative process, and insulation failure occurs when carbonized tracks bridge the distance between the electrodes. The mode of degradation from the formation of carbon track as well as progressive material weight loss is called a surface tracking. Environmental stresses influence the different tracking patterns that affect the performance of insulator material (Ugur, 1999). Figure 2.1 shows the sequential process of carbon track development due to the surface tracking phenomena. The surface tracking activity is developed from the generation of electrical discharges, which is caused by the variation of LC density under the condition of wet contaminated. The mechanism of contamination and degradation due to the surface tracking phenomena is illustrated in Figure 2.2.

The electrical stresses, including LC and dry-band discharges, are directly responsible for the occurrence of tracking and erosion. Generation of scintillation discharge is closely related to the variation trends of the LC (Young, *et.al* 1992) and produces high temperature spots that lead to bond scissions and other chemical changes (Kim, 1994).
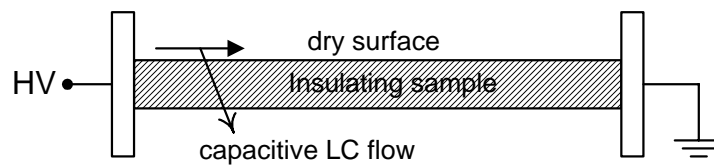
(a) dry condition
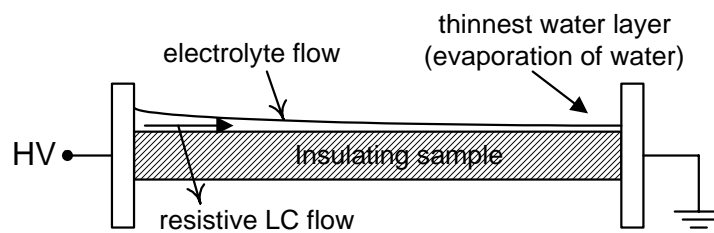
(b) completely dry
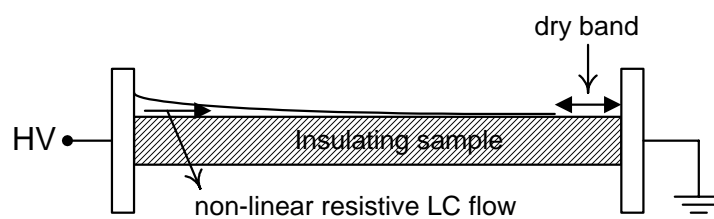
(c) formation of dry band
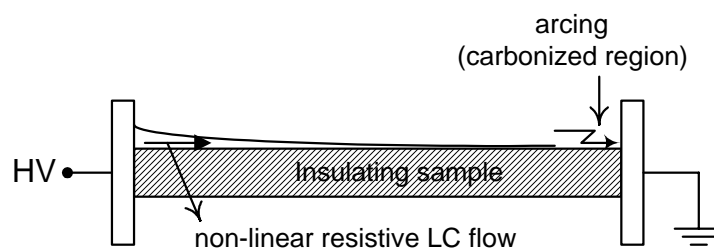
(d) arcing development

Figure 2.1 : Surface tracking development process
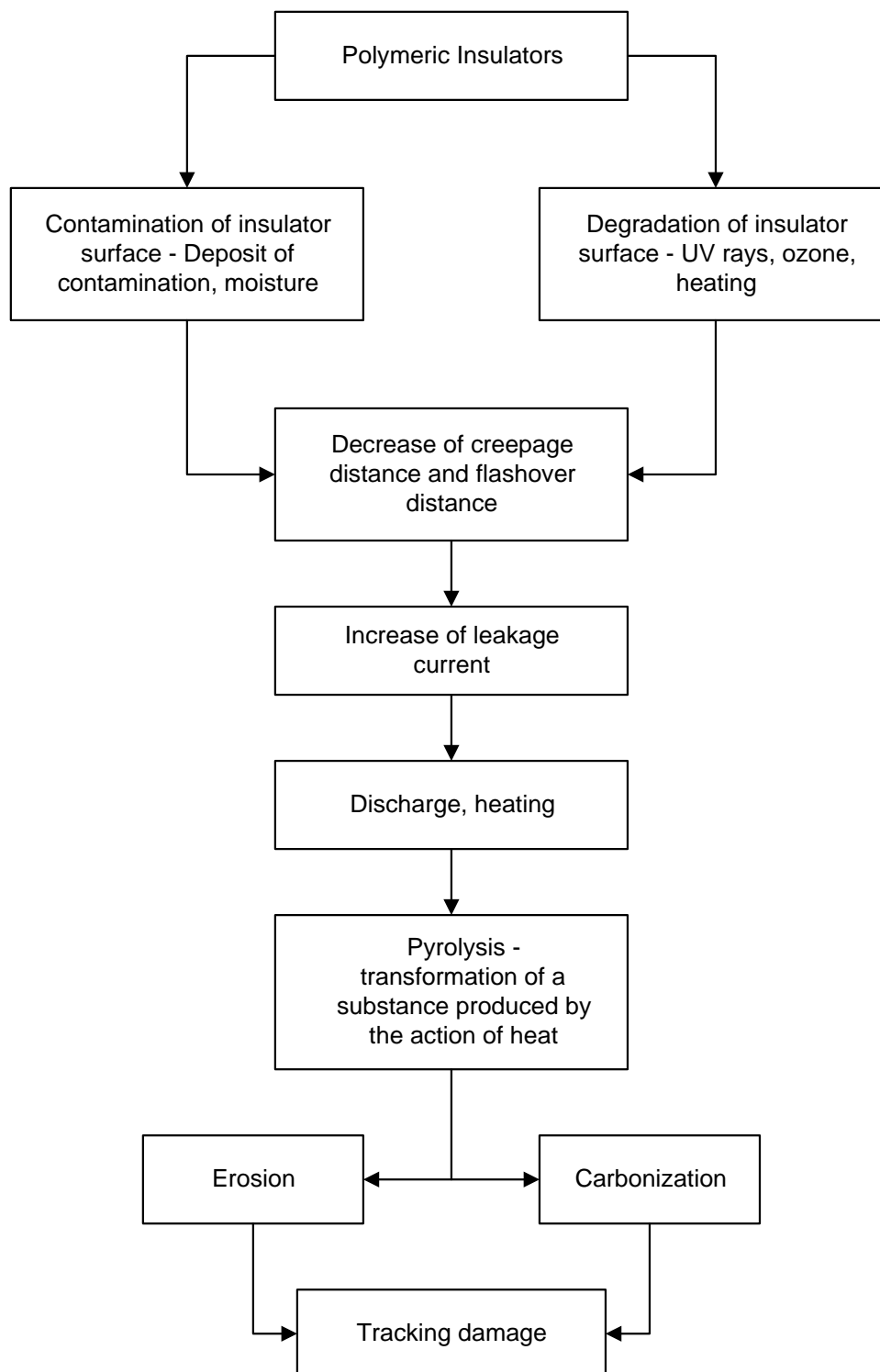
Figure 2.2 : Degradation process from tracking phenomena

The formation of dry band and scintillation discharges varied the level of LC as well as deformed the waveform pattern and thus increased the harmonic contents of the waveform (Fernando, 1999). The LC pulses observed at around the peaks of applied ac voltage due to the discharges generated from the tips of deformed water droplets (Katada, *et.al* 2000). When the dry band is formed, the crest of the LC waveform pattern showed many small spikes. These fast spikes indicate the discharge activity due to the corona effect.

The information gathered from the LC waveforms can be used to evaluate the tracking and erosion resistance of polymeric outdoor insulating materials. The condition where the materials have an experience surface degradation can be determined from the LC properties and the discharge duration, and could be used for early failure detection. Gorur, *et.al* (1997a) has found that the magnitude and harmonic content of the LC, and discharge duration are significantly different during the portion of the test when there is no visible degradation as compared to their values at the onset of visible degradation.

The description of the LC waveform patterns and their characteristics on describing the insulating performance of the polymeric materials will be discussed further in Chapter 3.

CHAPTER 3

DESIGN OF INCLINED-PLANE TRACKING SYSTEM

3.1 Introduction

The experimental set-up for evaluating the surface tracking and erosion resistance consists of two major parts, ie;

a) Inclined-plane tracking test system.
b) Computer-based leakage current monitoring system

An inclined-plane tracking test set-up is developed based on the standard procedures specified by IEC 587 test method. The complete schematic diagram of the test system is illustrated in Figure 3.1. The system is placed inside a Faraday cage to avoid any outside noise or disturbance that could affect the test measurement. All the high voltage equipments used and the Faraday cage is properly grounded for safety purposes. Furthermore, the material processing and the study on surface morphological are carried out accordingly.

(a) Inclined-plane tracking test set-up

(b) Leakage current monitoring system

Figure 3.1: Schematic diagram of the experimental set-up

3.2   Inclined-plane Tracking Test System

A 1.0 kVA, 0 to 10 kV high voltage transformer is used to supply a high voltage stress across a contaminated sample via a high power 200W (1k-50kΩ) resistor. The sample is wet-contaminated by flowing down continuously the contaminant solution on top of the sample through a PVC tube. A peristaltic pump is used to flow the contaminant solution at very low flow-rate according to the standard procedure. The contaminant electrolyte contains 0.1% by mass of ammonium chloride solution with Triton X-100 non-ionic wetting agent. The resistivity of the contaminant solution is maintained between 370 and 400 Ω-cm.

The slab-shaped sample with a dimension of 120x50x6 mm is mounted with the flat test surface on the underside, at an angle of 45° from the horizontal with the stainless steel electrodes 50 mm apart. All electrodes, fixtures and assembly elements associated with the electrodes must be made of stainless steel. In order to get the proper flowing of contaminant solution, eight layers of filter paper are clamped between the top electrode and the sample. For safety purposes, over current devices such as a relay or a fuse is installed in series with the sample. This over current device will operate when 60 mA or more current has persisted in the high voltage circuit for 2 seconds.

Figure 3.2 shows the photo pictures of the hardware set-up of complete test system. Basically the test is successfully conducted when the effective scintillation is observed, which means the existence of small yellow to white arc just above the teeth of the lower electrode. This arc appears within a few minutes of applying the voltage. The preferred test voltage depends on the contaminant flow-rate as well as the series resistor on the high voltage side as specified in the IEC 587 test procedures.
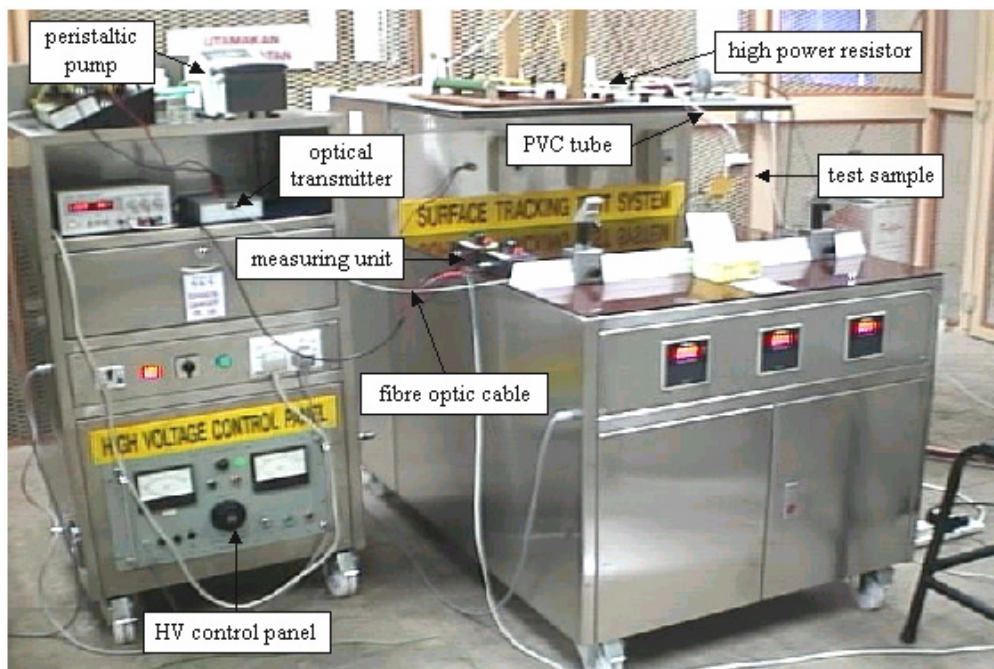
(a) Hardware set-up
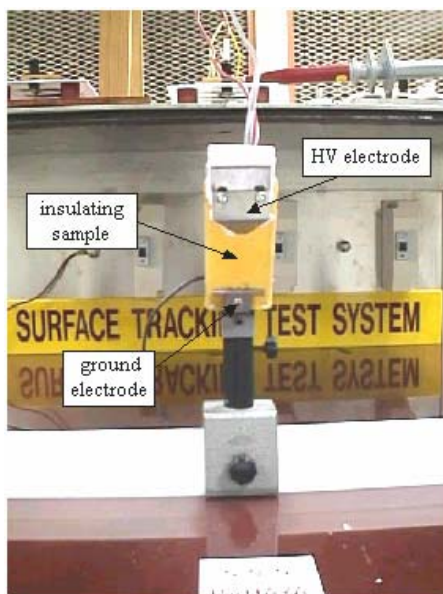
(b) Sample mounted and electrodes

(c) High voltage transformer

Figure 3.2 : Hardware set-up of tracking test system

3.3 Computer-based Leakage Current Monitoring System

An LC data acquisition system is developed to analyze the LC flowing on the sample surface under laboratory conditions. It consists of three parts;

1) Measuring Unit
2) Signal Conditioning
3) Analog to Digital Converter (ADC) with personal computer

The measuring unit is a component that is used to capture the LC that flows along the sample surface. It is done by measuring the voltage drop across a resistor, which is connected in series with the ground electrode. The resistor value can be changed from 50 Ω to 1 kΩ, depending on the LC level. This unit is also equipped with a protective circuit to protect the measurement system against occasional flashover during the test. The protective circuit consists of a 63mA fuse, which is connected in series with ground electrode and parallel connection of a gas discharge tube (with a few nanoseconds operation) and a back-to-back 12 V Zenner diode.

For a very small LC, the amplifier is developed to amplify the signal. The amplified signal is sent to a remote measuring system via a fibre optic cable. The use of an optical transceiver is to reduce the signal attenuation during transmission of the LC signal from the test system to the measurement system. A high power infrared photo emitter and a photo detector are used in the optical transceiver system. The high-speed photo emitter provides users with a universal LED emitter designed primarily for maximising the applications of polymer optical fibre. It also launches good levels of power into other multimode fibre types, and the fast response time makes it suitable for data rates up to 10 MB/s.

The LC signal is analysed by a computer with the help of an external analog-to- digital converter (ADC). 12 bits, 2 channels ADC with 3 MS/s sampling rate manufactured by Pico Technology is used. This ADC has large 32k waveform buffers, so it is possible to capture complex signals and then expand areas of interest to show fine detail. The program based on the LabVIEW package, is written to

communicate with the ADC to sort out the LC based on the magnitude and calculate the cumulative charge. In addition, the discrete Fourier Transform analysis of the LC waveform is performed on-line and its normalised harmonic components are sorted out.

For experimentation purposes, the LabVIEW program provides a variable sampling rate that can be chosen from. A faster sampling rate provides a more accurate reconstruction of the LC waveform for integration and lessens the degree of inaccuracy of the integration method. Besides the capability for on-line monitoring, a data storage feature is also added to the system to allow for future analysis.

Figure 3.3 shows a computer-based LC monitoring system. On-line information regarding on the characteristics of the LC is displayed on the computer screen. All the input data that has to be set into the measurement program in the computer is done by using the developed LabVIEW front panel as illustrated in Figure 3.4. This illustration of the graphical user interface collects the user input and displays the program output that the measurement system provides.
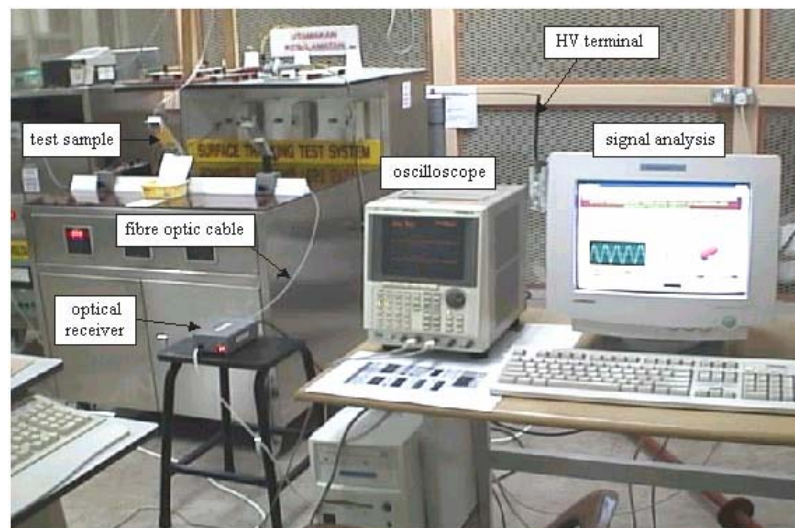
Figure 3.3 : Computer-based LC monitoring system
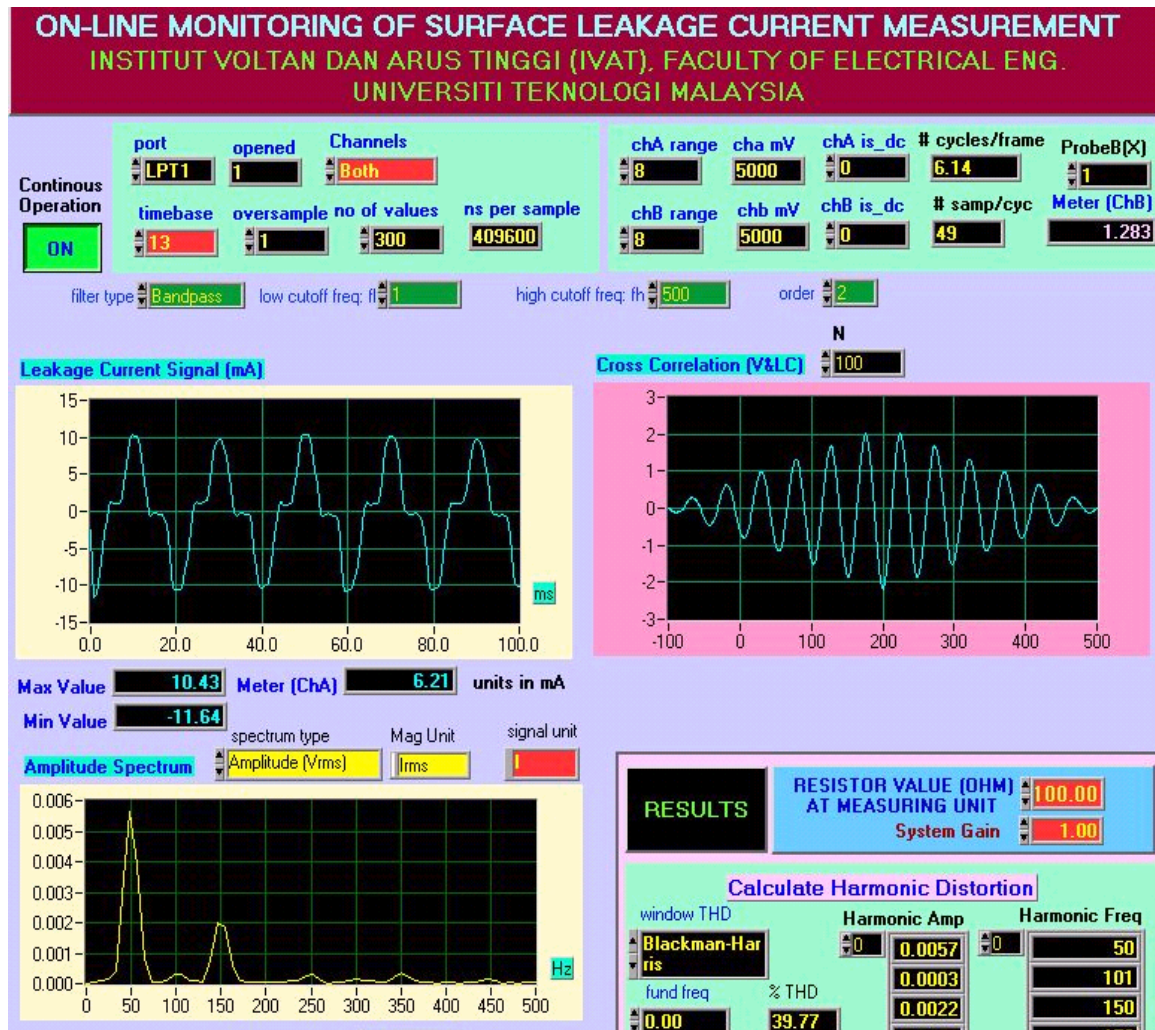
Figure 3.4 : LabVIEW front panel

3.4 Materials Preparation

Four different weight ratio of base polymer with different loadings of ATH were used throughout this work. The LLDPE injection molding grade with specified melt flow index of 50 g/10 min, manufactured by Titan (M) Sdn Bhd and natural rubber (NR) of SMR-CV grade, obtained from Rubber Research Institute of Malaysia (RRIM) were used as base polymer. The powder grade of ATH filler produced by BDH Ltd was supplied by Excelab Technology Sdn Bhd. This filler was mixed with the base polymer in order to improve the electrical surface tracking and erosion resistance. Table 3.1 shows the formulation of the compounds for the tracking test.

Table 3.1 : Compound formulations

Sample Description	Blend Components		Filler*	Sample Code
	Base polymer ratio (%)			
	LLDPE	NR	ATH	
LLDPE1:NR4	20	80	0	A1
	20	80	50	A2
	20	80	100	A3
	20	80	150	A4
LLDPE2:NR3	40	60	0	B1
	40	60	50	B2
	40	60	100	B3
	40	60	150	B4
LLDPE3:NR2	60	40	0	C1
	60	40	50	C2
	60	40	100	C3
	60	40	150	C4
LLDPE4:NR1	80	20	0	D1
	80	20	50	D2
	80	20	100	D3
	80	20	150	D4

* pph (part per hundred) of LLDPE/NR weight

The LLDPE and NR with ATH were blended in a Brabander Plasti-Corder at 160°C for 13 minutes at a rotor speed of 40 rpm. The samples of blends were then compression moulded into a slab-shaped with a dimension of 120x50x6 mm in an electrically heated hydraulic press at 160°C. The total moulding time was 15 minutes at a pressure of 100-120 kg/cm^2.

To study the microstructure of the material surface before and after the tracking test, a morphological analysis was conducted. The surface morphology of the compound was investigated by using a scanning electron microscope (SEM) of model JEOL JSM-5610. Before scanning, the samples were sputter-coated with platinum to minimise charging effect. A 20 mA sputtering current with 70 seconds coating time was used to obtain 6 nm deposited platinum film thickness. The electron gun of SEM was energised at 10 kV in order to avoid any possible damaged to the material surface if the higher voltage is used. The micrograph of the compound surface was recorded at 200 magnifications for clearer observation.

CHAPTER 4

ELECTRICAL TRACKING PERFORMANCE OF THE NEWLY FORMULATED LLDPE-NATURAL RUBBER (NR) BLENDS

4.1   Surface Tracking and Erosion Resistance

The surface tracking and erosion properties of the insulating material are very much related to the development of LC. The levels and the characteristics of the LC significantly influence the carbon tracks development from the electrical discharge activity. For this reason, the observation of LC is taken into consideration when analysing the surface tracking and erosion properties. The LC properties could provide useful information on determining the performance of polymer insulating materials.

Figure 4.1 shows the box-plot of LC data for each composition, which is recorded every minute until the end of the experiment. The value of LC within the box-plot shows that the data lies between the first and third quartile of a set of data collected. For all blend formulations, a range of 2-6 mA of LC is observed throughout the experiment. The same results are also found in the case of silicone rubber, polyethylene vinyl acetate and polyolefin (Chang, 2000; Gorur, *et.al* 1997b). The low-level of measured LC indicates that the compounds of NR/LLDPE have a

mechanism on suppressing the LC development. It is also believed that the blends are probably acquired a good hydrophobicity property due to the lower LC flow.

Figure 4.1(a), 4.1(b) and 4.1(c) show that at 50 pph ATH loading in the compounds, the surface tracking and erosion properties improve due to the lowest LC but start to decrease the tracking properties at higher level of ATH. Other study on EPDM compound has shown that with the presence of 40-80 pph ATH, the erosion of the surface sample is minimised (Costa, 1991). Xuguang, (2000) has reported that the capability of tracking and erosion resistance of high temperature vulcanized silicone rubber is optimized with approximately 50 pph ATH filler content. It is believed that the ATH filler plays an important role in improving surface tracking by allowing an endothermic dehydration and thus decreases thermal decomposition products. The heat generated at the temperature of >200 °C due to the high intense dry-band arcing has been reported by Kumagai, (2001) using infrared thermovision camera. High temperature spots induce a dehydration of ATH by way of endothermic reaction. The released water vapor from the endothermic reaction then cools the surface, thus limiting the thermal degradation and prevents the formation of continuous track.
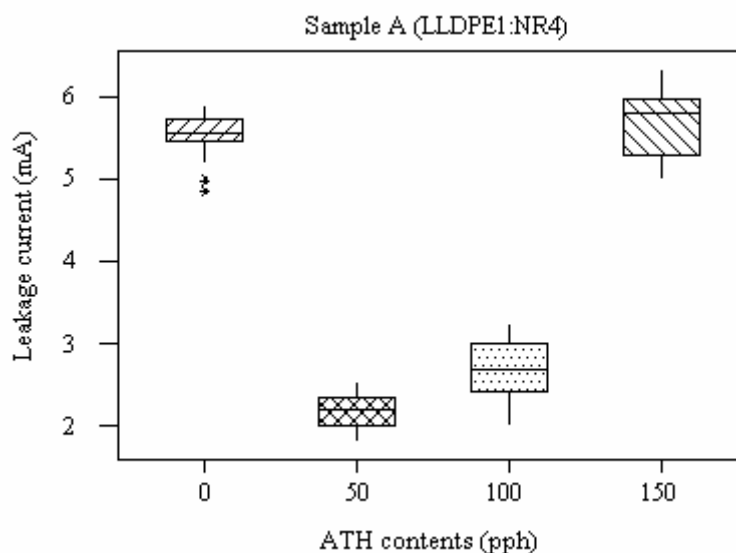
(a) Compound of 20% LLDPE and 80% NR
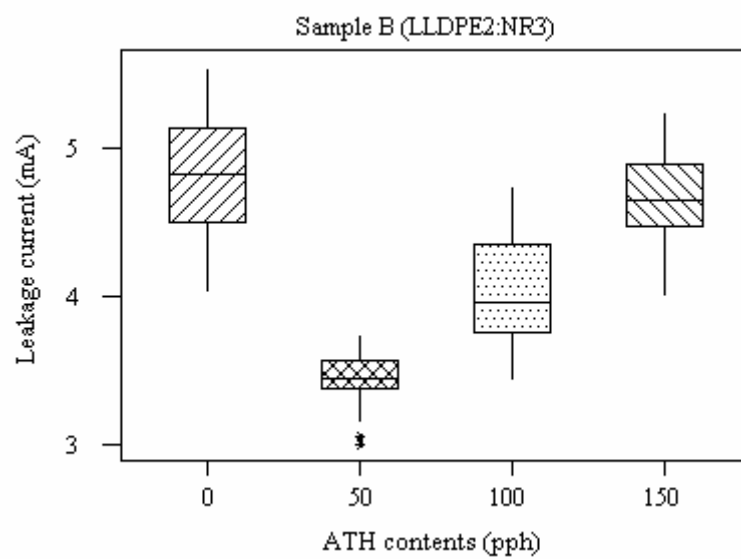
(b) Compound of 40% LLDPE and 60% NR
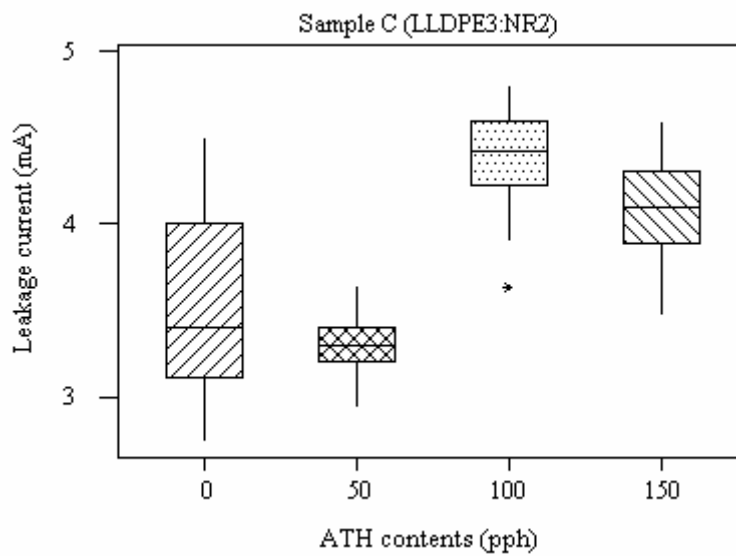
(c) Compound of 60% LLDPE and 40% NR
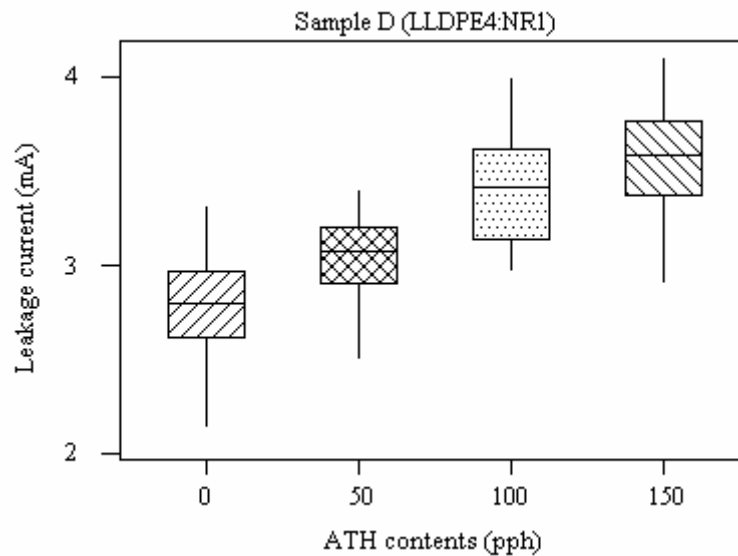
(d) Compound of 80% LLDPE and 20% NR

Figure 4.1: Leakage current magnitude of blends with different contents of ATH

At very large levels of ATH, the fillers are difficult to compound and thus resulting in rougher surface due to the difficulty of dispersing it uniformly in the compound, which leads to an increase in the surface LC. Meanwhile at small amount of ATH (< 50pph), the filler does not give sufficient protection against the damage during surface discharge and tracking activity.

On the other hand, Figure 4.1(d) indicates an interesting result with the LC at its lowest value for the compound without ATH (compound D1). This result that seems to be in contradiction with the other compounds (A1, B1 and C1) is probably due to the higher contents of LLDPE in the compound, which could impart high electrical tracking and flame retardance. It is believed that the LLDPE used in this compound might contain suitable fire retardance additive during manufacturing. Chang, *et al* (1997) has demonstrated that a specially formulated polymer compound with no ATH can achieve the optimization of tracking and erosion resistance. It is shown that the ATH filler is not necessary for certain compositions for improving

tracking properties. Therefore, compound formulation is more important than the generic polymer type for outdoor insulation materials.

Furthermore, the development of carbon track (CT) propagation is taken into consideration when analysing the tracking properties as depicted in Figure 4.2. The CT propagation is determined in terms of the CT rate development, which is the ratio of CT length to the time taken of the test period. Comparing between the magnitude of LC (Figure 4.1) and the rate of CT (Figure 4.2), it shows no correlation between the LC magnitude and the rate of CT. Some observations exhibit higher CT rate with low LC and vice versa. However for the compounds A (LLDPE1:NR4) and C (LLDPE3:NR2), both the LC value and CT rates are proportional to each other with increasing ATH filler.
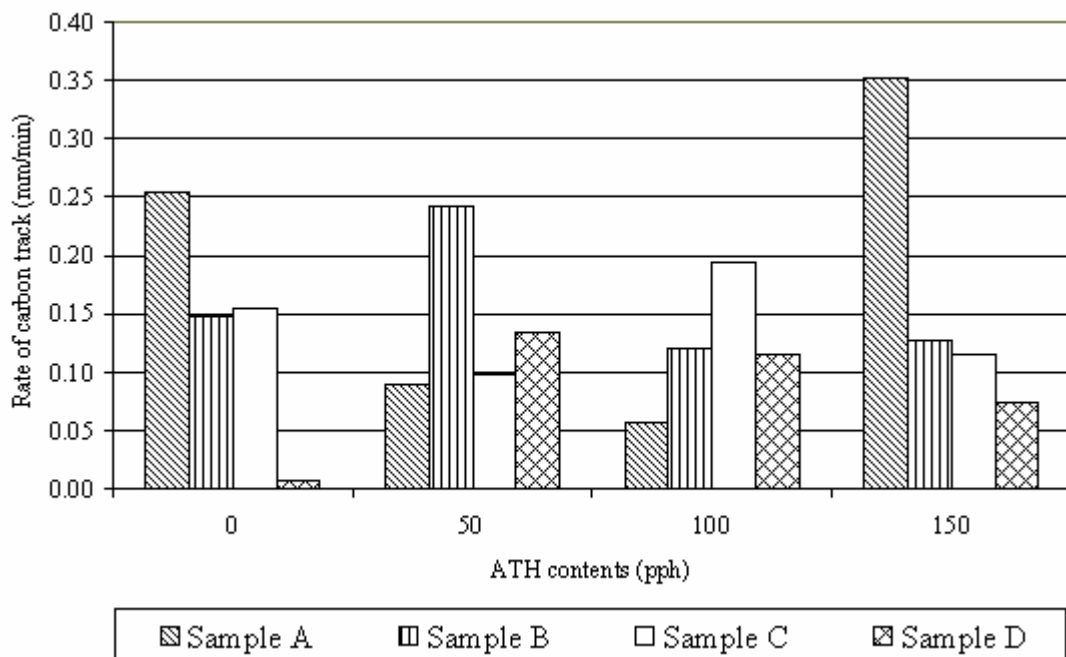
Figure 4.2: Rate of carbon track propagation at different contents of ATH

It is well mentioned by IEC 587 test procedure, that the length of CT development determines the degree of degradation of the polymeric insulating materials. A less degradation shows the capability of the insulating material to withstand the stress from the electrical discharges. From Figure 4.2, it is observed that

the sample D (LLDPE 80% and NR 20%) indicates a less degradation compared to other formulations. As a whole, sample D1 with the formulation of 80% LLDPE, 20% NR and no ATH is found to be the best formulation compound for resistance the tracking and erosion. For the compound filled with ATH, sample A3 (LLDPE 20%, NR 80% and ATH 100 pph) shows less degradation even though its LC is slightly higher compared to the compound filled with 50 pph ATH of the same group. This observation indicates that the effect of ATH filler is more of concern from the aspect of LC suppression rather than CT development.

4.2 Morphological Analysis

To study the blends compatibility under low and high level of ATH contents as well as to investigate the surface degradation due to the surface tracking phenomenon, the surface micrograph of compound A2, B4 and D1 are selected for discussion. Figure 4.3(a) and 4.5(a) exhibit the micrograph for the compounds filled with low level and no ATH respectively, while Figure 4.4(a) shows the surface microstructure for the compound with high contents ATH loading. Meanwhile the effects of electrical discharges on surface degradation are shown in Figure 4.3(b), 4.4(b) and 4.5(b).
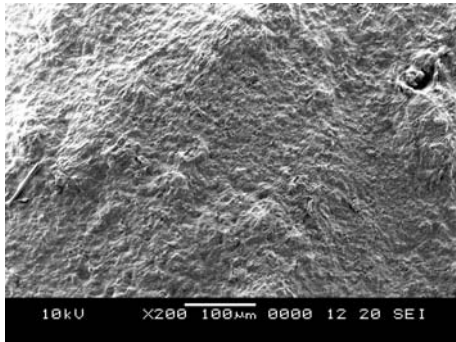
(a) before test
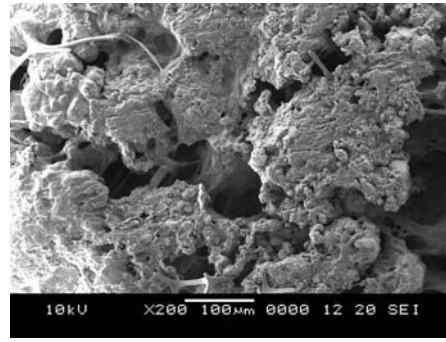
(b) after test

Figure 4.3 : SEM micrograph of sample A2
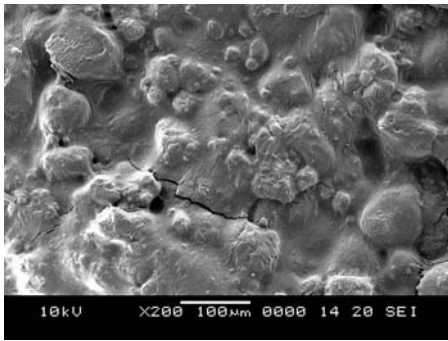
(a) before test
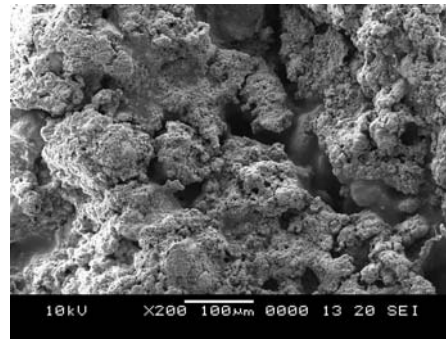
(b) after test

Figure 4.4 : SEM micrograph of sample B4
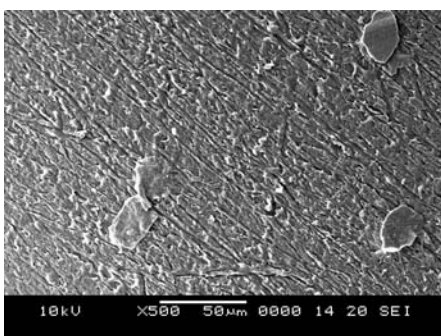
(a) before test
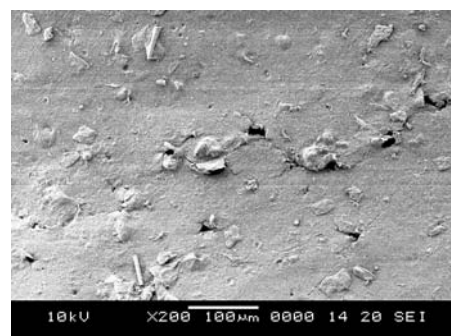
(b) after test

Figure 4.5 : SEM micrograph of sample D1

The micrographs of the compounds with less content of ATH (Figure 4.3(a)) and no ATH contents (Figure 4.5(a)) reveal a good miscibility of the blends. It is found that the basic components of the blend are well mixed and dispersed uniformly. Observation from other compounds filled with low ATH shows that the basic components in the compound are homogeneously dispersed and only small agglomeration of the fillers occurs. This shows that the interaction between fillers and the polymer matrix is strong.

However for higher contents of ATH fillers (Figure 4.4(a)), the material surface become rougher due to difficulty of dispersing it uniformly in the compound, where the particles of ATH filler appear on the surface. The ATH filler used in this compound seems to be irregular in their size. Some particles diameter can reach up to 100 μm and this bigger size of particles could decrease the surface tracking and erosion resistance and contribute to a less smooth surface (Deng, 1995).

When the compounds are subjected to high voltage stress, the surface structure is damaged due to the dry-band arcing. The SEM micrograph of Figure 4.3(b), 4.4(b) and 4.5(b) show that the material surface is porous and some cracks appear. The degree of surface damaging depends on the level of LC as well as the characteristics of electrical discharge. Sample D1 (Figure 4.5(b)) shows the least damaged compared to the rest of the compounds. A little damaged with less contents of carbon residue are observed on the surface. This observation agrees with the minimum rate of CT as well as lower LC that recorded from sample D1. It is also observed that the compounds with less concentration of ATH are less damaged compared to the compound with higher level of ATH (100-150 pph).

4.3   Leakage Current Waveforms Analysis

Different stages of the LC behavior are recorded from the experiment, as illustrated in Figure 4.6. For the insulator that preserves the hydrophobic properties best, its LC waveform is very small and practically not detectable. But, when the insulator surface is completely wet, the LC appears to be sinusoidal and resistive with higher magnitude as shown in Figure 4.6(a-i). The value of LC suddenly increases due to the drastically dropped of surface resistivity.

In order to determine the linearity of the waveform, a sampled of LC waveform signal is fed into the subprogram of total harmonic distortion component from the LabVIEW program. This subprogram (THD.VI) provides the on-line calculation of the total harmonic distortion (*THD*) of the signal. To display the amplitude spectrum of the signal, a subprogram of spectrum analyser is used accordingly.

From the frequency spectrum of Figure 4.6(a-ii), almost no harmonic components are recorded at the condition of completely wet insulator and the *THD* of the waveform is about 1.67%. The cases in which a weak dry-band activity is started or the condition where the partially lost of hydrophobic properties occur, the LC pattern becomes resistive and slightly non-linear as depicted in Figure 4.6(b-i). Small spikes are observed at the crests of the waveform due to the corona effect. At this stage, the LC is dropped to a lower value because of the high resistance from the existed dry-band. The frequency spectrum of the waveform in Figure 4.6(b-ii) indicates slightly increase in the harmonic components with a *THD* of 8.04%.

LC waveforms (*y-axis*: mA, *x-axis*: ms)	Frequency spectrums (*y-axis*: mA, *x-axis*: Hz)
(a-i)	(a-ii)
(b-i)	(b-ii)
(c-i)	(c-ii)
(d-i)	(d-ii)
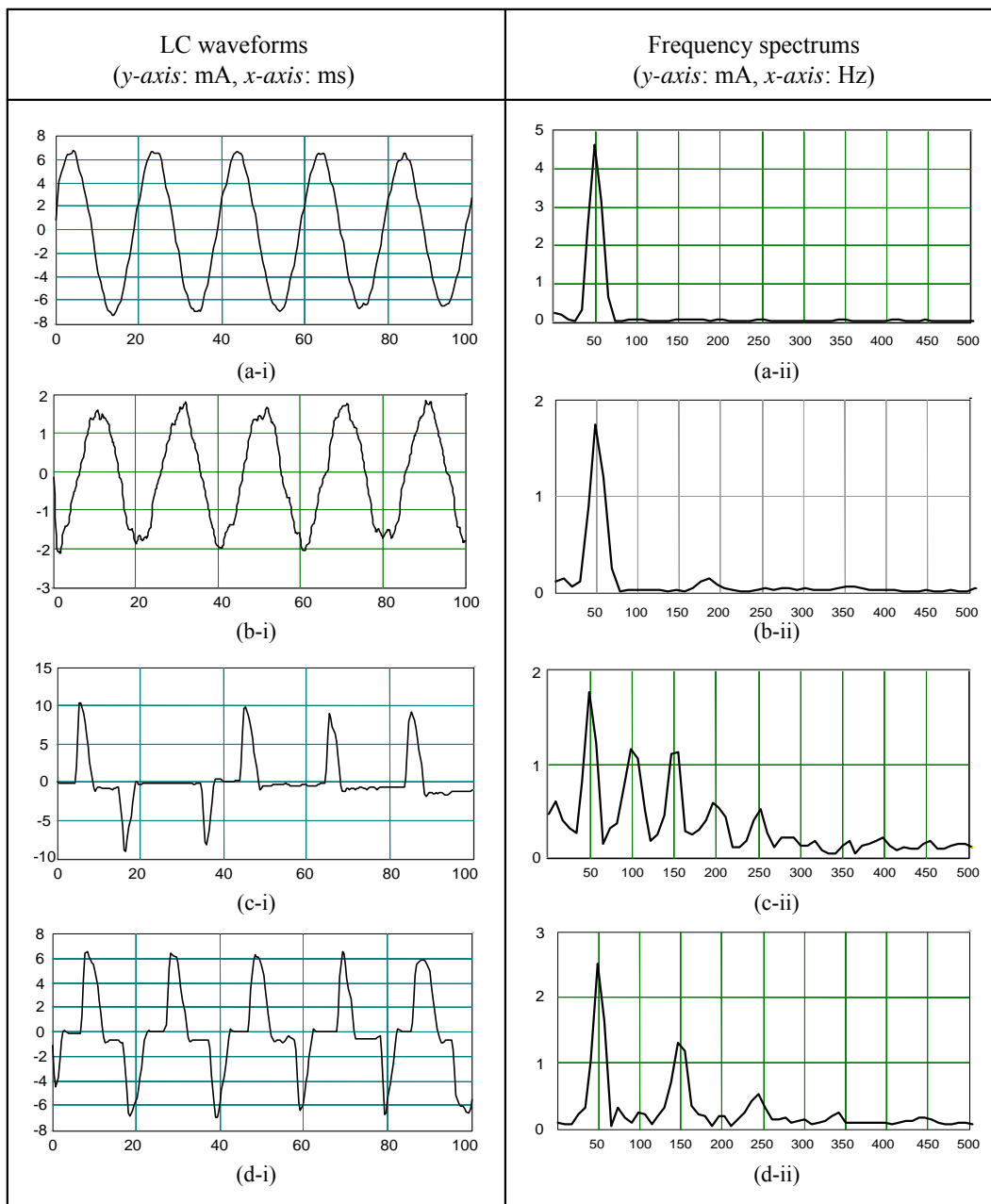
Figure 4.6 : Typical LC waveform and frequency spectral

The LC waveform in Figure 4.6(c-i) is based on the condition when several short discharges are observed at a certain time. These discharges move rapidly from one location to another location without causing any degradation on the insulator surface and would only occur in the very early stages of wetting. At this condition, the discharge current waveform appears as a series of pulses with non-symmetrical pattern, and hence reflected by the high value of the *THD*, which is recorded as 109.48%. Due to the unsymmetrical waveform, the frequency spectrum in Figure 4.6(c-ii) shows all the harmonic components.

Meanwhile, in the presence of intermittent, strong as well as continuous local arcs, the recorded LC waveform is illustrated in Figure 4.6(d-i) with a THD of 57.5%. The stable and continuous discharge results in the waveform pattern to be symmetry and contains odd harmonic components only as depicted in Figure 4.6(d-ii). The electrical discharges stay rooted in a particular spot much longer and the thermal degradation is initiated on the material surface.

Based on the recorded LC waveform as well as voltage waveform across the sample, the surface energy dissipated from the single discharge can be calculated using the following equation (Risino, 1994);

$$W_D = \frac{A \cdot x \cdot I_p^{1-n} \cdot \Delta t}{\sqrt{2}} \tag{4.1}$$

where, *A* and *n* are arc constants, I_p is a peak of the discharge current, *x* is a discharge length and Δt is a discharge period.

4.4   Conclusions

The electrical tracking performance and morphological properties of the newly formulated LLDPE-Natural Rubber (NR) blends under environmental and electrical stress are investigated by analysing leakage current and carbon track development. Experimental results show that different compositions as well as the surface physical conditions affect the characteristics of leakage current and discharges. Generally, compounding with 50 pph ATH filler gives good surface tracking resistance for the compounds filled with ATH. However, the compound of 80% LLDPE and 20% NR without ATH seems to be the best compound due to the least damaged and have a good mechanical strength.

Based on the results, the good formulation of LLDPE-NR blends that to be used as a high voltage insulating material can be suggested as follows;

1) For the formulation without ATH loading, the weight of LLDPE component to the weight of natural rubber must be at least of ratio 4:1 (LLDPE:NR)

2) For the compound with a weight ratio of LLDPE to NR contents less than 4:1, an extending filler of alumina trihydrate (ATH) is proposed to be incorporated in the polymer blends. In order to improve the surface tracking and erosion properties, the optimum amount of ATH in the compound is found to be in the range of 50-100 part per hundred of polymer weight.

3) Based on the results of leakage current level as well as the resistance to carbon track development, the weight ratio of LLDPE to NR must be at least of 2:3 (LLDPE:NR). In fact, a higher contents of NR compared to LLDPE in the compound could reduce the mechanical strength properties drastically, and this is not good to be used as an insulating material in high voltage applications. The physical inspection of the compounds with higher contents of NR than LLDPE has proved that a final product of this

compound showed bad quality and experienced a difficulty during processing and molding.

In comparison to other polymer materials from previous works, it is observed that the use of LLDPE blended with natural rubber is reliable as an alternative high voltage insulating materials in the future. It is hoped that this newly developed thermoplastic elastomer can be made more desirable or valuable if the compound uses suitable crosslinking agents or compatibilizers for optimizing the tracking performances.

A practical on-line monitoring system at a reasonable cost has been designed and evaluated for surface leakage current under Inclined-Plane Test method. The use of such measuring technique permits a better understanding on the performance study of the insulator materials. The higher the total harmonic distortion of the leakage current waveform, the higher the probability of hydrophobic properties lost in the insulating materials. In addition, the characteristics of surface discharge have significantly influenced the on set of material degradation. The results suggest that the combination of leakage current magnitude and waveshapes analysis can provide a reliable indication on the status of insulating materials. The feature of data storage in the designed system could facilitate the researchers to extend the study for further analysis without conducting the test again.

4.5   Future Work

Some of the recommendations for future work are listed as follows:

- *Improve the compatibility of LLDPE/Natural Rubber blends*. Adding a suitable crosslinking agent or compatibilizer into the blend could make the blend more homogeneous as well as strengthen the interaction between the polymer phases. This will ensure the quality of the final product of a compound, thus improving the tracking performance.

- *Conduct further electrical and chemical tests*. A complete data base of electrical properties such as breakdown voltage, hydrophobicity, loss tangent and dielectric properties could provide useful information for the researcher to investigate the overall performance of the LLDPE/NR compounds in the applications of high voltage engineering. Furthermore, from the chemical tests such as energy dispersion x-ray (EDX) or infrared spectroscopy, the changes of molecules structure of the compound before and after the tracking test can give an idea on identifying which atomic components or chemical elements that will probably dominate the molecular structure of the compounds.

- *Test the compound under the different and multiple stresses.* In outdoor application, the insulator will expose to the many environmental stresses. These stresses are humidity, ultra-violet radiation, water absorption, ozone generation, acid rain, thermal, etc. In actual service, several stresses happen simultaneously on the insulator material and will contribute more degradation to the material. By conducting a test under these conditions, the environmental stresses that give more defects to the insulating performance of a newly formulated material can be identified. Hence, an improvement on weathering resistance of the proposed material can be achieved by adding into a compound with the suitable antidegradant or stabilizer additives.

- *Expand the features of the developed LC signal analysis measurement.* The many advantages of the LC signal characteristics can be better seen and the correlation between the LC parameters can be made. This way, a broad and detail information of the signal characteristics can be used as an indicator to identify the on-line performance as well as to classify the degradation level of the insulating material into different stages. Thus, better reliability of the developed LC monitoring system can be achieved.

- *Use a non-electrical detection technique to detect electrical discharge signal.* At certain condition especially during weak dry-band activities or the hydrophobic properties are partially lost, detecting of the very small current discharge signal is quite difficult using a direct electrical detection technique. The use of non-electrical technique such as optical or acoustic detection method is practical to be used when investigating the pre-discharge activity and therefore the phenomena in the early stage of ageing can be assessed.

PART TWO

CHAPTER 5

D-DOT PROBE BASED SENSOR
DESIGN AND CONSTRUCTION

5.1   Introduction

D-Dot probes are field-coupled sensors, which are used to measure impulse voltages; they have attractive features including a non-intrusive installation, simplicity of construction and potentially wide bandwidth. Measurement of fast voltage transients by conventional dividers introduces inductive overshoots superimposed on the actual voltage waveforms. Moreover, this inductive effect slows the front of the waveform. For fast transient studies, such inductive and slow response problems are critical due to the fast rate of voltage rise involved. In this chapter, the design of a new D-dot based sensor which overcome the problems of voltage overshoot and slow response as observed in conventional voltage dividers is described.

5.2   Theory and Equivalent Circuit

The measurement of voltage transients can be better achieved by using a coaxial arrangement. In a typical D-dot based sensor as shown in Figure 5.1, an axial

rod is energized or connected to the high voltage source and the outer toroids which function as stress modifying shileds are grounded. The voltage sensor is basically a capacitive divider, with the high voltage arm made by the capacitance between the high voltage conductor and the signal toroid, and the low voltage arm made up by precision capacitors introduced between the signal toroid and ground. A coaxial cable picks-up the voltage signal from the low voltage arm. For improvement of signal immunity from noise, a triaxial cable, instead of a coaxial cable, was also used in this work.

The equivalent circuit for the capacitive divider is given by the circuit shown in Figures 5.2. C_1 is the capacitance between the inner toroid and the axial high-voltage rod, C_2 is the capacitance between the inner toroid and ground, and R_m is the matching resistance of the cable.
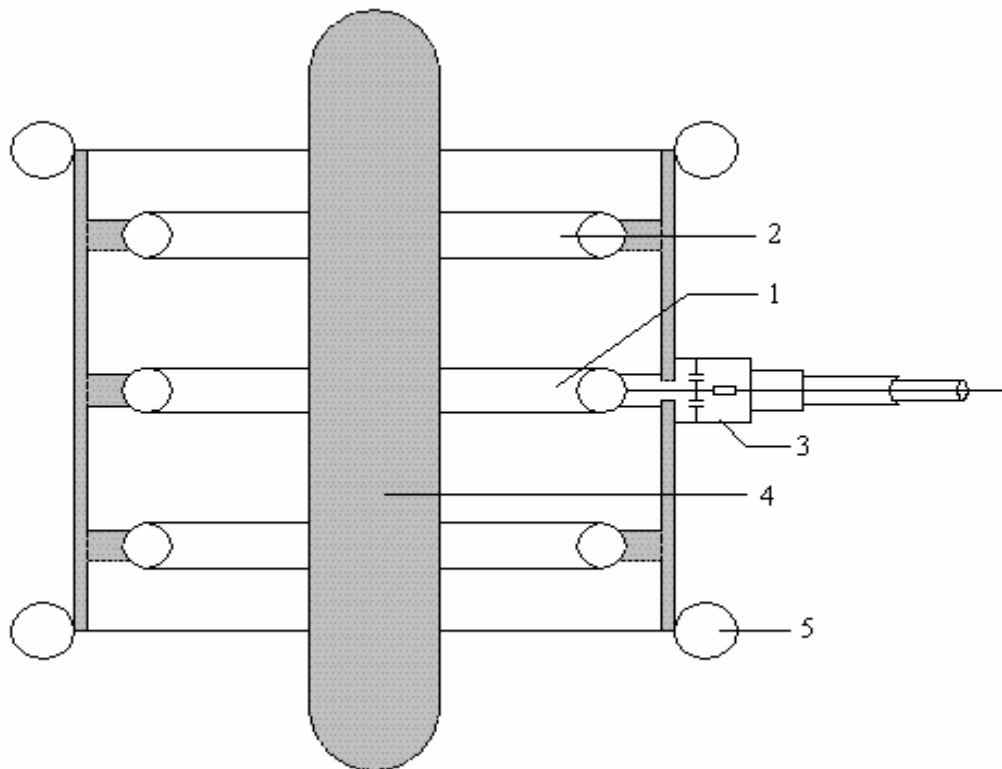
Figure5.1:- Schematic of the D-dot probe assembly

1: Signal toroid, 2: Grounded shielding toroids, 3: Low-voltage attenuator,

4: High-voltage conductor, 5: Stress-modifying toroids.
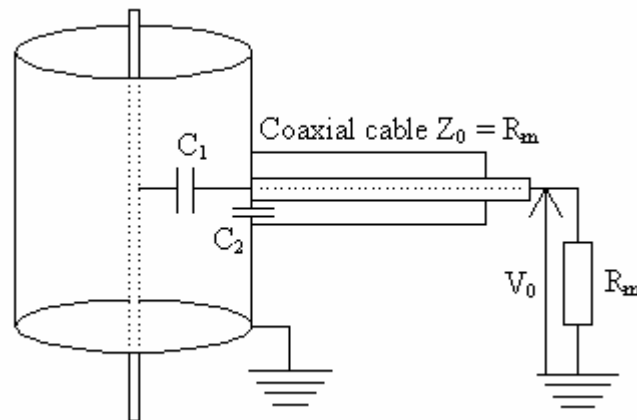
Figure 5.2: Equivalent circuit of the D-dot probe.

5.3 Probe Description and Design Criteria

The D-Dot probe design proposed in this work (Figure 5.2) essentially comprises three similar aluminium toroids (main outer diameter 407 mm, minor diameter 38 mm) placed coaxially around a cylindrical high voltage conductor. The three toroids are supported within a cylindrical aluminium tube. This facilitates easy removal and interchange of the probe to and from other test arrangements.

The outer toroids are equally spaced above and below a central sensor toroid. The outer toroids are electrically connected to ground and serve to shield the inner sensor toroid from extraneous fields/flux lines and provide a degree of field modification. The central toroid is electrically isolated from earth and forms the capacitance to the high voltage conductor. Two plates with rounded edges are fixed on the axial high-voltage rod to minimize the external electrostatic coupling with the toroid system and to reduce the maximum electric field along the axial rod. A means

of connecting a coaxial signal cable (and if required an externally connected capacitor to ground) to the central toroid ia also provided.

The capacitance C_1 between the high voltage conductor and the central toroid forms the high voltage arm of the divider, and the stray capacitances between the toroid and ground C_g, the capacitance of the measuring cable C_c and the capacitance of the recording equipment C_r form the low voltage arm C_{lv}. An additional precision capacitor C_{ext} connected in parallel with C_g, C_c and C_r may be required to give a total low voltage arm capacitance of C_{lv} and hence giving the desired attenuation $C_{hv}/(C_{lv} + C_{hv}$ (Figure 5.3).
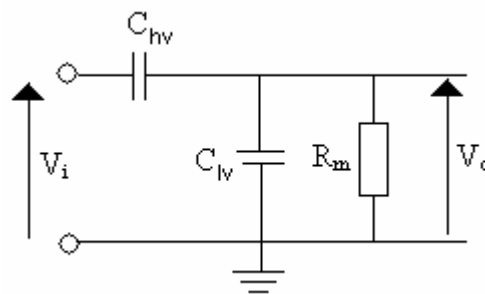
Figure 5.3: Simplified equivalent circuit of the D-dot probe.

One of the most important criteria in the design is to ensure that the highest local electric field at the maximum prospective arrester surge voltage of 50kV is of a sufficiently low value so as to ensure that neither partial (corona) breakdown nor complete flashover will occur. An adequate safety factor is needed because the magnitude of the electric field which could give rise to partial or complete breakdown can be significantly lowered by the roughness of the conducting surfaces and by the accumulation of dust on those surfaces.

Secondly, any electric flux lines terminating on the signal toroid must originate only from the high voltage conductor and not, for example, from the test object. Finally the capacitance between the high voltage conductor and the signal toroid must be of sufficient value (very low) to provide an adequate signal ratio

$C_{hv}/(C_{lv} + C_{hv})$. Due to mechanical consideration of the whole system the outer diameter of the toroids was fixed. Further modification in the capacitance value of the high voltage arm (once the diameter of the high voltage conductor was fixed) could be achieved by altering the spacing between the signal toroid and the shielding toroids. Increase of the spacing would tend to increase C_{hv} and decrease C_g and therefore C_{lv}.

5.4   Computer Simulation of the Probe

In order to verify the design of the D-dot probe in terms of its electrical field characteristics, the finite element SLIM application was used to determine the electrical field and potential distribution.

5.4.1   SLIM Application

SLIM is a professionally engineered, fully integrated collection of software modules that provides facilities for the generation and solution of electromagnetic finite element models. SLIM has been continuously developed over the last 30 years by the ALSTOM Research & Technology Center and provides a state of the art design environment supported by professional engineers, mathematicians and computer scientists.

SLIM can improve product design and reduce development costs and has a satisfied customer base that includes major power transmission, distribution and generation companies, electrical machine manufacturers and R&D centers throughout the world. SLIM is the only electromagnetic finite element package that is

commercially available from a manufacturer of electrical equipment and its development is driven by the requirements of experienced product designers.

5.4.2   Determination of the Maximum Electric Field

A lot of practical high voltage design requires knowing what the maximum E-field is, for insulation design, corona reduction, etc. The exact field can, of course, be calculated numerically by solving Laplace's equation over a suitable field with appropriate boundary conditions. As complicated and time consuming as this is, it is necessary when performance is critical, in integrated circuit design, designs for absolute minimum cost, and so forth. However, for more run of the mill experimentation and use, where a little overdesign can be tolerated, approximations to the field are just as useful.

In order to meet the above criteria computer modeling of the probe was conducted using the finite element program. The first consideration was to find a design, which would yield the lowest electrical field value (in particular at the point and the high voltage conductor adjacent to the signal toroid).

Simulation was necessary both to ensure that the electrical fields within the probe assembly were safely below the corona level at the maximum prospective voltage and to determine the optimum configuration for the desired probe capacitance. The effects of high voltage conductor profile and spacing of the shielding toroids were investigated. The potentials contours for the final design configuration are shown in Figure 5.4 and the electrical field along the high voltage rod is shown in Figure 5.5.
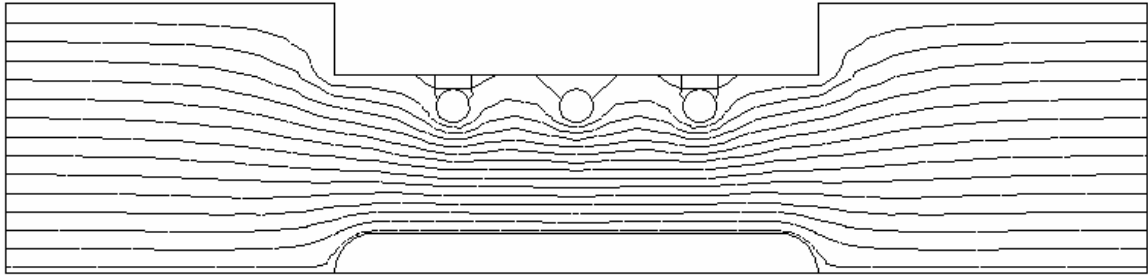
Figure 5.4:   D-Dot probe equipotential contours at intervals of 1 per-unit.
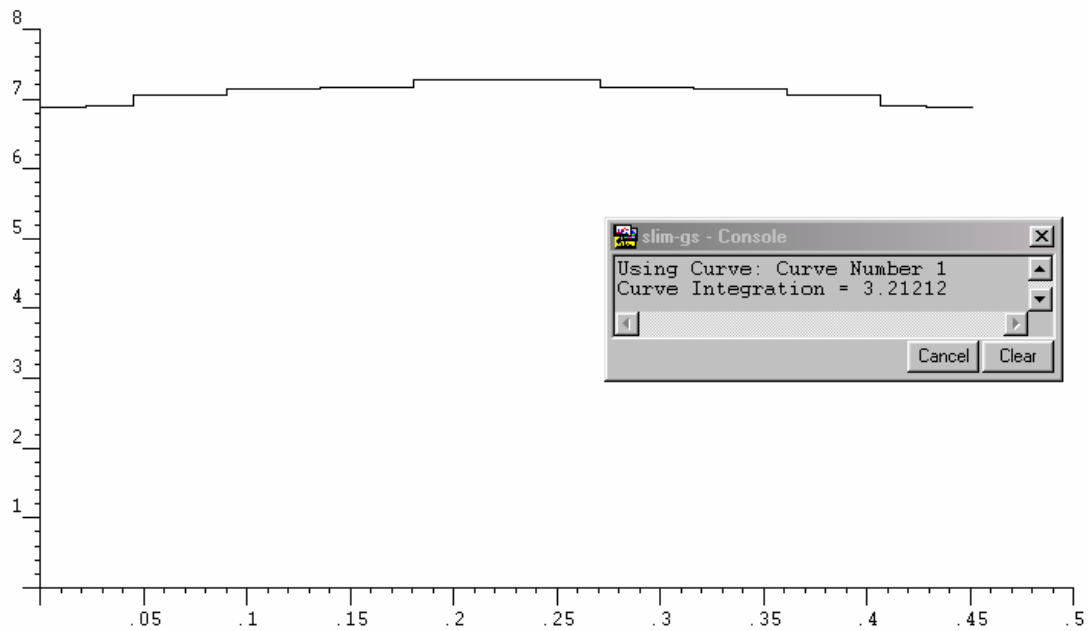
Figure 5.5: Electric Field along High Voltage Rod

With careful construction to eliminate any unnecessary roughness of the conductors surface and judicious profiling the maximum local field values predicted can be seen to be satisfactory.

5.4.3   Effect of Shielding/Field Modifying Toroids

The effect of spacing between the signal toroid and the shielding/field modifying toroids was studied. It was found that with increased spacing the capacitance between the high voltage conductor and the signal toroid increased. However, increased spacing results in a decrease in the effectiveness of the shielding/field modifying toroids to prevent spurious signals being induced in the signal toroid. A compromise between the two criteria (maximum high voltage capacitance and maximum shielding) was chosen to be a spacing of 10cm between each shielding/field modifying toroids and the signal toroid.

5.4.4   Calculation of the Probe Ratio

The groups of three similar toroids having minor/major-mean diameters of 38/405 mm respectively, are modeled. The group is axially arranged in a coaxial test rig. The middle toroid is fixed and electrically isolated from the main cylinder, while the other two toroids are movable up and down to control the value of C_2 by changing the gap (δ) as shown in Figure 5.8. The axial high voltage rod has 45mm in radius while the inner diameter of the main cylinder is 422mm.

The value of the capacitance between the high voltage conductor and the signal toroid (at $\delta = 100$mm) was calculated within the finite element program by applying unit potential to the signal toroid, and zero potential to the remaining toroids, high voltage conductor and outer shielding (Figure 5.12). Then by integrating the flux over the surface of the high voltage conductor the capacitance between the signal toroid and high voltage conductor can be determined. The value of the high voltage arm capacitance was computed to be 3.63pF find from D*2πrL (2 * 3.142 * 0.045 * 1.2856 x 10^{-11}), (Figure 5.13). Figure 5.13 to Figure 5.14 shows a spacing of 100mm

between the signal toroid and the shielding/field modifying toroids. Figure 5.15 to Figure 5.16 shows a spacing of 210mm between the signal toroid and the shielding/field modifying toroids.
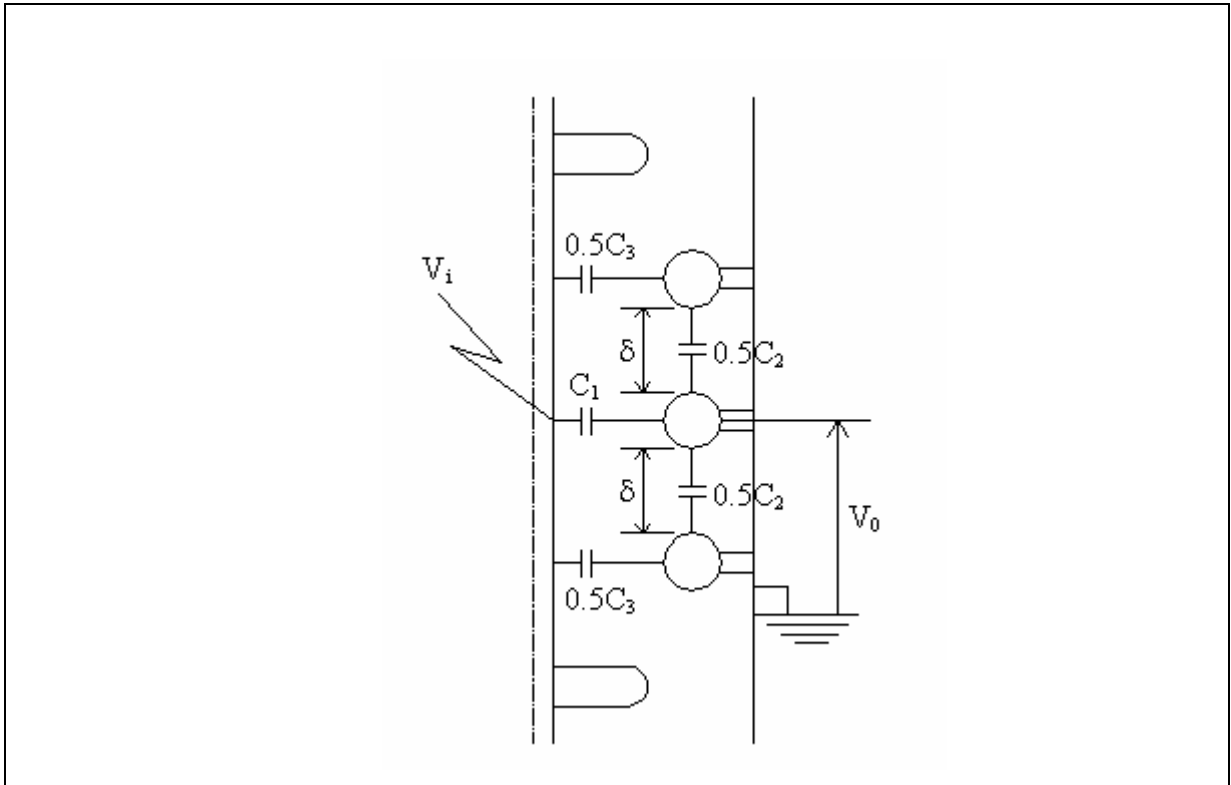
Figure 5.8: Definition of the probe capacitances.
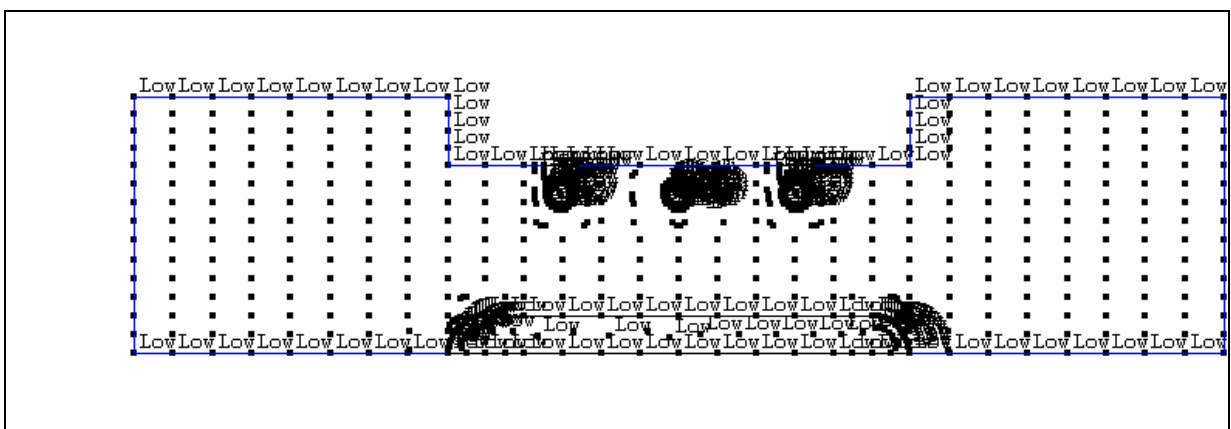
Figure 5.9:   2D Mesh Generation
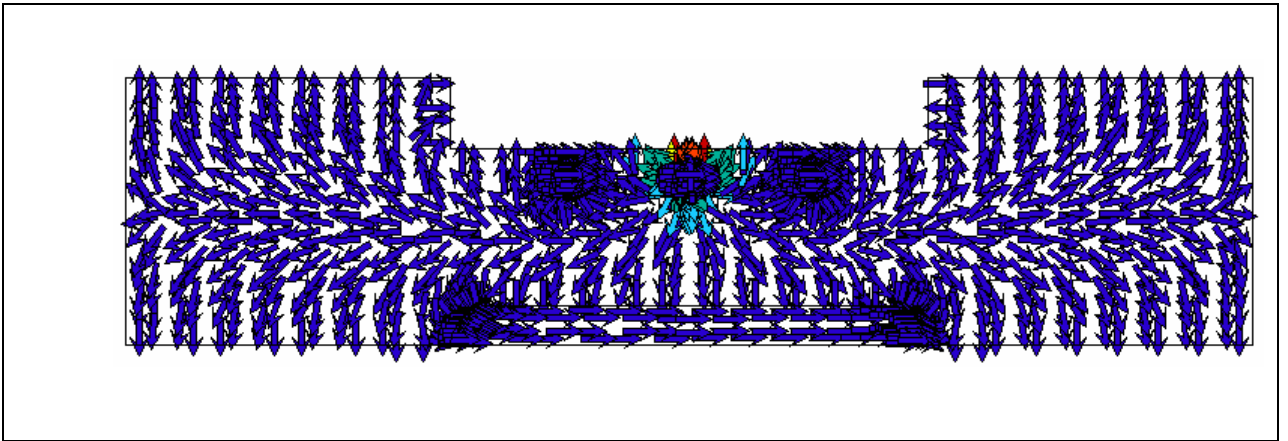
Figure 5.10: Vector Display (Color Mode)
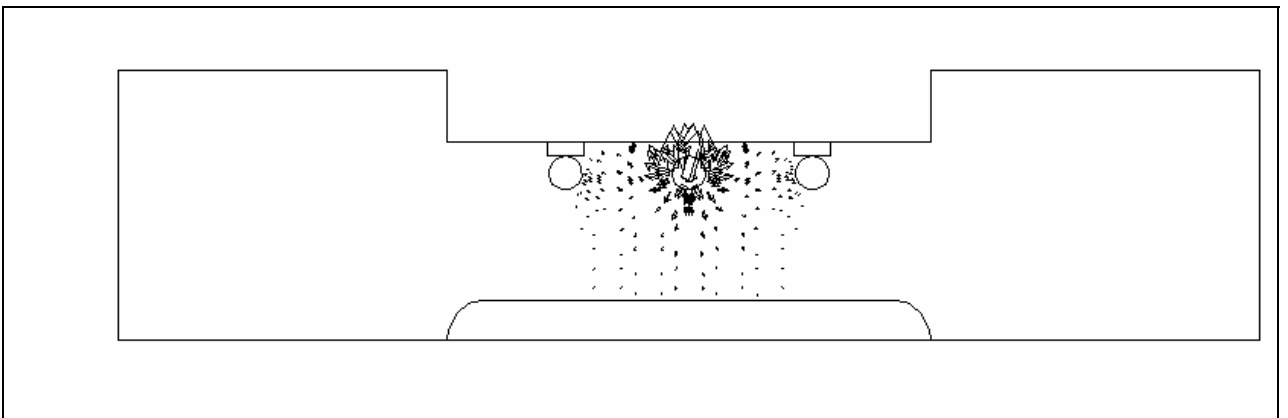
Figure 5.11:   Vector Display (Scaled Mode)
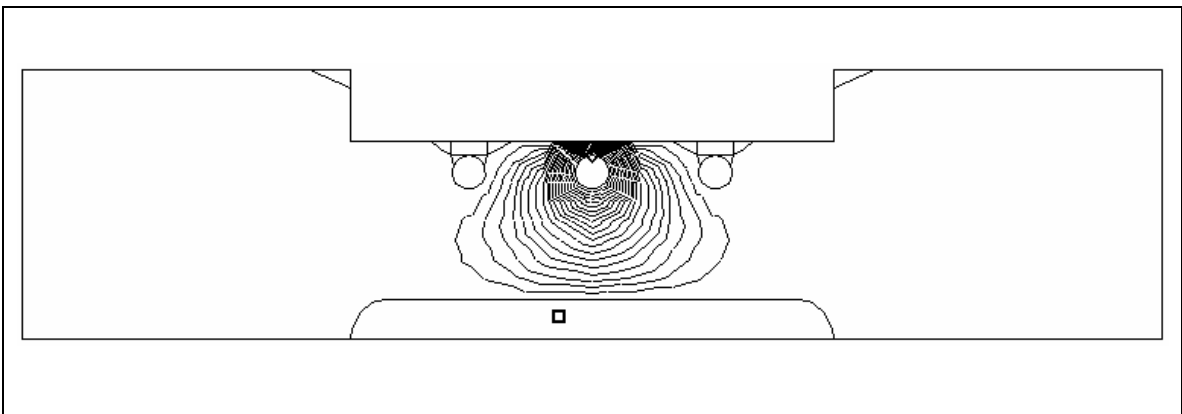
Figure 5.12: D-Dot probe equipotential contours at intervals of 1 per-unit.
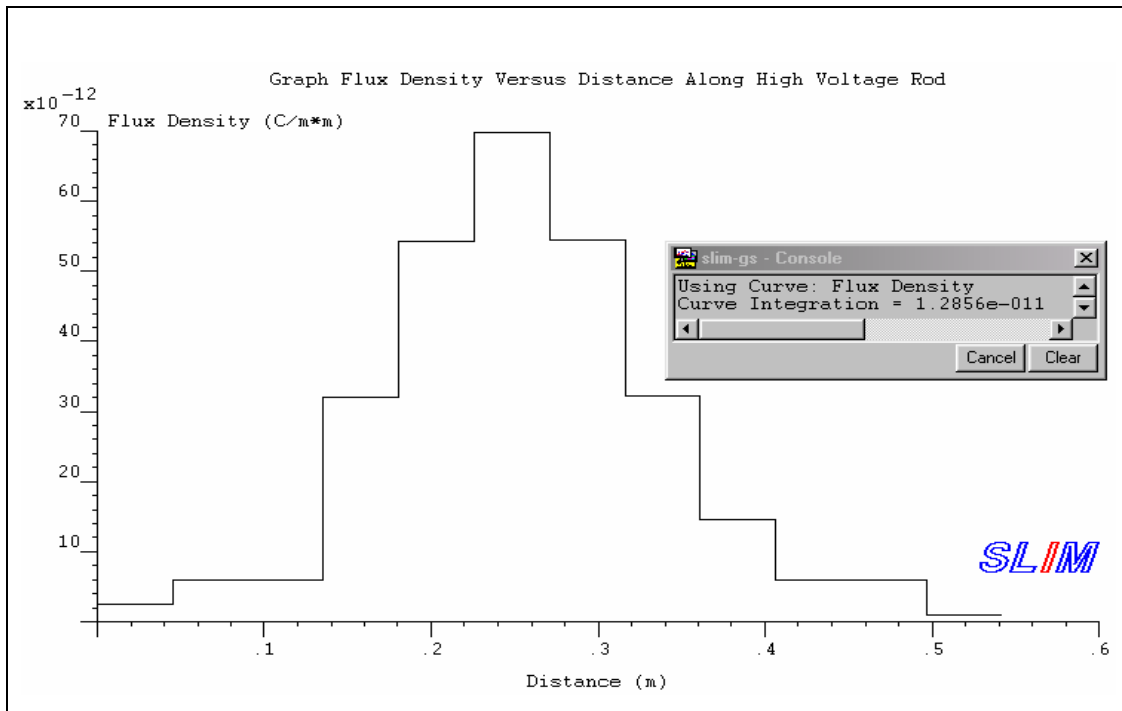
Figure 5.13: Flux Density over the Surface of the High Voltage Conductor
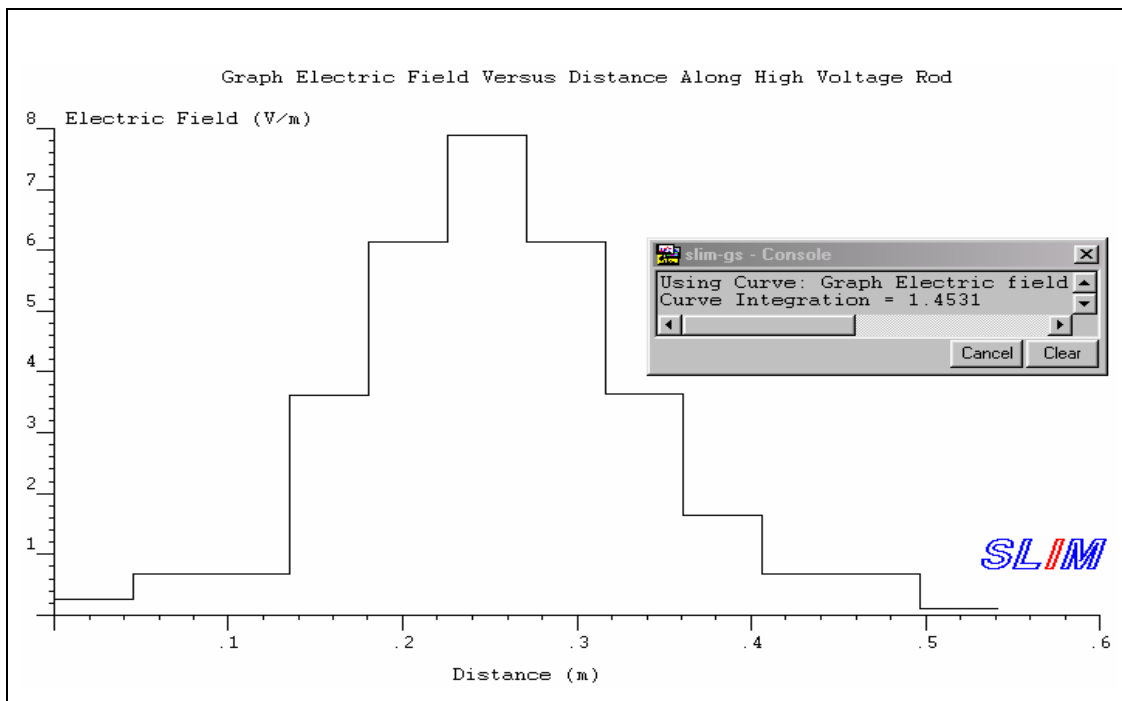
Figure 5.14: Electric Field over the Surface of the High Voltage Conductor
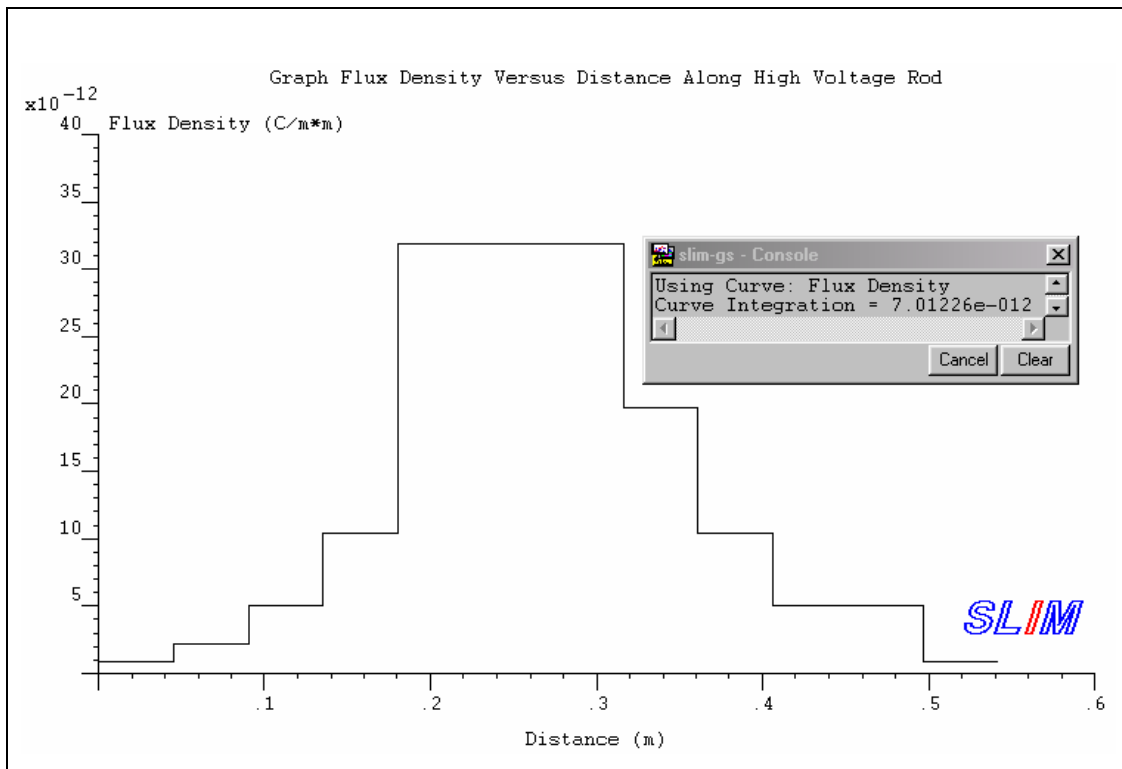
Figure 5.15: Flux Density over the Surface of the High Voltage Conductor
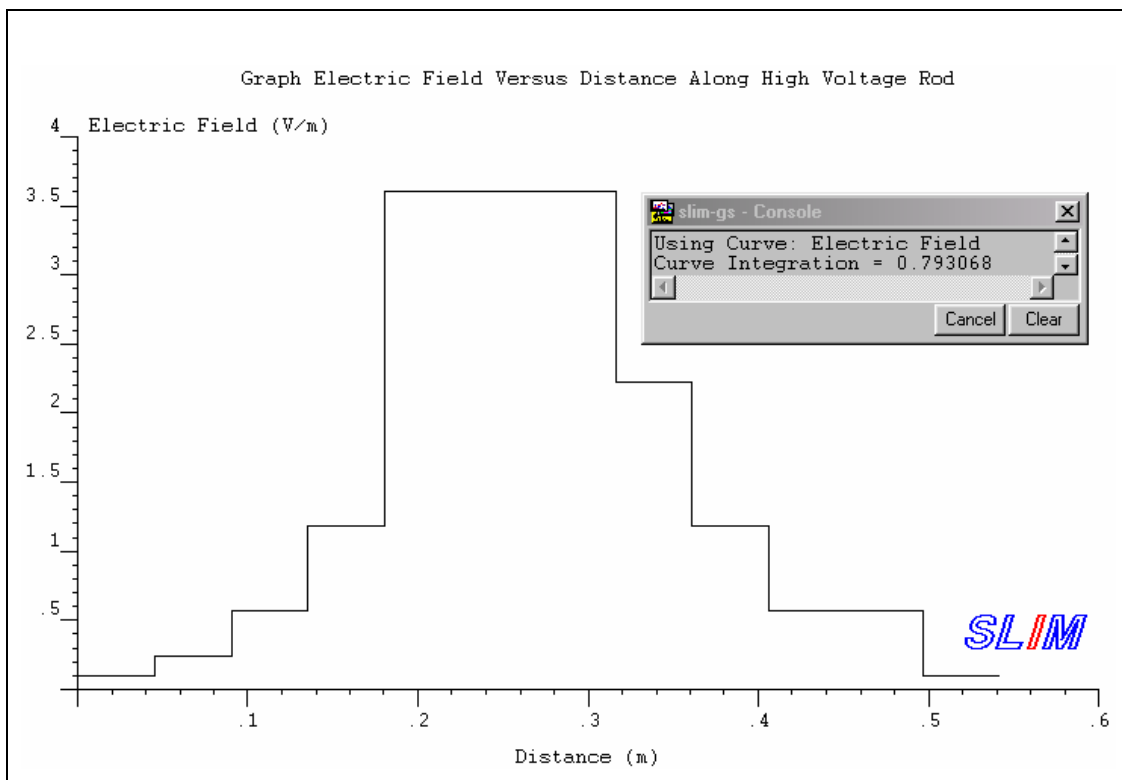
Figure 5.16: Electric Field over the Surface of the High Voltage Conductor
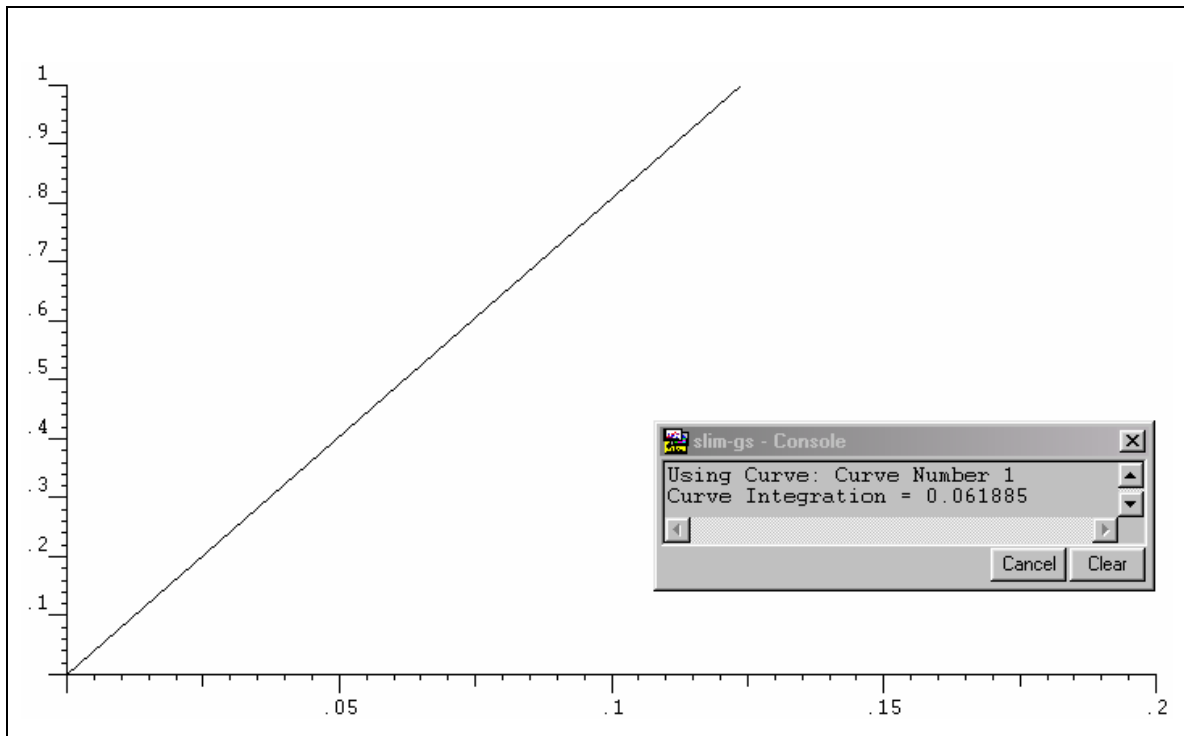
Figure 5.17: Voltage Potential at Signal Toroid versus Distance

A low voltage arm comprising four 8.2nF high precision low-inductance capacitors connected in a radial manner together with a series damping resistor (5.5Ω) and a cable matching resistor (75Ω) is required to achieve a satisfactory output. Based on these values, the D-Dot probe divider ratio is then estimated as

$$\frac{V_H}{V_L} = \frac{C_L + C_H}{C_L} = \frac{3.63 \times 10^{-12} + (4 \times 8.2 \times 10^{-9})}{3.63 \times 10^{-12}} = 9.04 \times 10^3$$

The low-voltage arm is housed within an aluminium shielding enclosure. This is due to the fact that without the additional attenuator the capacitance of the signal cable would represent the bulk of the low-voltage arm capacitance is distributed nature then distorting the recorded output. The low-voltage attenuator along with the capacitance formed by the signal toroid forms the low-voltage arm capacitance. The capacitance of the triaxial cable is merely 2% of this attenuation capacitance.

5.5   Materials

5.5.1   Aluminium

Aluminium is an important commercial metal possessing some very unique properties. It is very light (density about 2.703) and some of its alloys are very strong, so its strength weight ratio makes its very attractive for aeronautical uses and other applications in which weight saving is important. Aluminium, especially in the pure form, has very high electrical and thermal conductivities, and is used as and electrical conductor in heat exchangers, etc. aluminium has good corrosion resistance, is nontoxic, and has a pleasing silvery white color; this properties make it attractive for applications in the food and container industry, architectural, and general structural fields.

Aluminium is very ductile and easily formed by casting and mechanical forming methods. Aluminium owes its good resistance to atmospheric corrosion to the formation of a tough, tenacious, highly insulating, thin oxide film, in spite of the fact that the metal itself is very anodic to other metals. In moist atmospheres, this protective oxide may not form, and some caution must be taken to maintain this film protection. Although aluminium can be joined by all welding processes, this same oxide film can interfere with the formation of good bonds during both fusion and resistance welding and special fluxing and cleaning must accompany welding operations.

Pure aluminium melts at 660 ^{0}C (1220 ^{0}F). Aluminium has relatively high thermal and electrical conductivities. The metal is always covered with a thin, invisible film of oxide, which is impermeable and protective in character. Aluminium therefore, shows stability and long life under ordinary atmospheric exposure.

Exposure to atmospheres high in hydrogen sulfide or sulfur dioxide does not cause severe attack of aluminium at ordinary temperatures, and for this reason aluminium or its alloys can be used un atmospheres which could be rapidly corrosive to many other metals.

Aluminium parts should, as a rule, not be exposed to salt solutions while in electrical contact with copper, brass, nickel, tin, or steel parts, since galvanic attack of the aluminium is likely to occur. Contact with cadmium in such solutions results in no appreciable acceleration in attack on the aluminium, while contact with zinc (or-zinc-coated steel as long as the coating is intact) is generally beneficial, since the zinc is attacked selectively and cathodically protects adjacent areas of the aluminium.

Most organic acids and their water solutions have little or no effect on aluminium at room temperature, although oxalic acid is an exception and is corrosive. Concentrated nitric acid (about 80% by weight) and fuming sulfuric acid can be handled in aluminium containers. However, more dilute solutions of these acids are more active. All but the most dilute (less than 0.21%) solutions of hydrochloric and hydrofluoric acids have a rapid etching action on aluminium.

The outstanding characteristics of aluminium and its alloy are their strength-weight ratio, their resistance to corrosion, and their high thermal and electrical conductivity. The density of aluminium is about 2770 kg/m^3 (0.10 lb/in^3), compared with 7550 kg/m^3 (0.28 lb/in^3) for steel. Pure aluminium has a tensile strength of about 90 MPa (13 kpsi), but this can be improved considerably by cold working and also by alloying with other materials. The modulus of elasticity of aluminium, as well as of its alloys, is 71 GPa (10.3 Mpsi), which means that it has about one-third the stiffness of steel.

Solutions of the strong alkalies, potassium, or sodium hydroxides dissolve aluminium rapidly. However, ammonium hydroxide and many of the strong organic bases have little action on aluminium and are successfully used in contact with it.

Aluminium in the presence of water and limited air oxygen rapidly converts into aluminium hydroxide, a whitish powder (Brody & Clause, 1986).

5.5.2   Physical Structure

5.5.2.1 Coaxial Arrangement

Figure 5.3 shows the arrangement. The outer aluminium cylinder is 625mm high and has a diameter of 550mm. The D-Dot probe assembly comprises a signal toroid (1) and two similarly dimensioned shielding toroids (2) placed coaxially around the high voltage conductor. The whole probe assembly is contained within a cylindrical aluminium tube which has a diameter 422mm with stress toroid (5). The high voltage conductor is centered by an insulating spacer (Perspex). A low voltage arm (3) for the D-dot probe sensor is made radially connected capacitors and is contained within an aluminium shielding enclosure. The large aluminium cylinder, which encloses the transducers, provides electrostatic shielding in addition to providing a current return path to ground. The low voltage signals from the voltage transducers are transferred to the recording equipment via trixial cables of approximately 28m in length. Connection from the high voltage conductor to the capacitor bank is made via the high pressure SF_6 spark gap which is pneumatically triggered.

5.5.2.2 Hollow (expand) Conductors.

Hollow conductors are used in high voltage conductor when, in order to reduce corona loss, it is desirable to increase the outside diameter without increasing the area beyond that needed for maximum economy. Not only is the initial corona voltage considerably higher than for conventional conductors of equal cross section, but the current carrying capacity for a given temperature rise is also greater because of the larger surface area available for cooling and the better disposition of the metal with respect to skin effect when carrying alternating currents.

5.5.3   System Characteristic Parameters

5.5.3.1 Skin Effect

Is a phenomenon, which occurs in conductors, carrying currents whose intensity varies rapidly from instant but does not occur with continuous currents. It arise from the fact that elements or filaments of variable current at different points in central or axial filament meets the maximum inductance, and in general the inductance offered to other filaments of current decreases as the distance of the filament from the axis tends to produce unequal current density over the cross section as a whole; the density is a minimum at the axis and a maximum at the periphery. Such distribution of the current density produces an increase in effective resistance and a decrease in effective internal inductance; the former is of more practical importance than the latter. In the case of large copper conductors at commercial power frequencies, and in the case of most conductors at carrier and radio frequencies, the increase in resistance should be considered.

5.5.3.2 Corona Effect

Corona is caused by the electric field next to an object exceeding the breakdown value for air (or whatever it is immersed in). Since the magnitude of the field is inversely proportional to the radius of curvature, sharper edges break down sooner. The corona starting voltage is typically 30 kV/cm radius. Dust or water particles on the surface of the object reduce the corona starting voltage, probably by providing local areas of tighter curvature, and hence higher field stress.

The easiest case to analyze is that of a sphere. The magnitude of the electric field at the surface of a sphere in free space is simply the voltage/radius. Note that if the sphere is near another conductor, the field is no longer uniform, as the charge will redistribute itself towards an adjacent conductor, increasing the field.

Since corona is fundamentally a breakdown phenomenon, it follows Paschen's law: the voltage is a function of *pd*. Double all the dimensions and halve the gas pressure, and the corona voltage will be pretty much the same.

5.5.3.3 Conductor Losses

Conductor loss depends somewhat on frequency. This is because of an action called skin effect. When current flows through an isolated round wire, the magnetic flux associated with it is in the form of concentric circles. The flux density near the center of conductor is greater than it is near the surface. Consequently, the lines of flux near the center of the conductor encircle the inductance and cause the inductance near the center of the conductor to be greater than at the surface. Therefore, at radio frequencies, most of the current flows along the surface (outer skin) rather than near the center of the conductor. This is equivalent to reduce the cross sectional area of the conductor and increasing the opposition to current flow (that is, resistance). The additional opposition has a 0^0 phase angle and is, therefore resistance and not a reactance. Therefore, the ac resistance of the conductor proportional to the square root of the frequency. The ratio of the ac resistance to the resistance of a conductor is called the resistance ratio. Above approximately 100MHz, the center of a conductor can be completely removed and have absolutely no effect on the total conductor loss.

5.5.4   Complete Design

5.5.4.1 Materials for D-Dot Probe

Table 5.1 gives the details of materials used.

5.5.4.2 Engineering Drawing

Figures 5.18 – 5.36 gives the details of all parts and the dimension of the D-dot probe. The construction and the arrangement of the probe were designed using the AutoCAD program. All dimensions are in millimeter (mm).

Table 5.1 Materials used for D-dot Probe Assembly

Component Name	Materials	Quantity
Aluminium Cylinder	Thin Pure Aluminium	2
Stress Modifying Toroids	Flexible Aluminium	2
Cylinder Spacer	Pure Aluminium (Solid)	8
Perspex Support	Perspex	2
Grounding Toroid	Pure Aluminium Toroid	2
Signal Toroid	Pure Aluminium Toroid	1
High Voltage Conductor (with screw threads)	Pure Aluminium (Hollow)	1
High Voltage End (Solid with screw threads)	Pure Aluminium (Solid)	1
High Voltage End (Solid)	Pure Aluminium (Solid)	1
Signal Toroid Spacer	Insulator (e.g. Perspex)	3
Attenuator	Pure Aluminium (Body). Insulator (Between Signal Conductor & Grounding Body)	1
Grounding Toroid Spacer	Pure Aluminium (Solid)	8
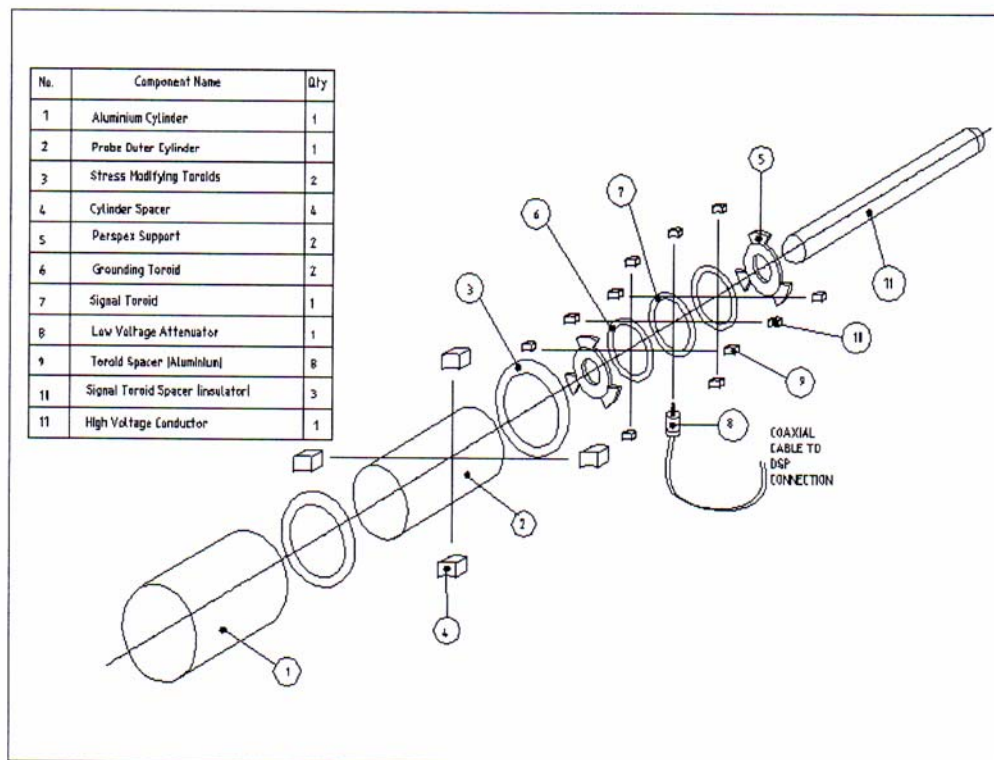
Figure 5.18:   Component in the D-dot probe

No.	Component Name	Qty
1	Aluminium Cylinder	1
2	Probe Outer Cylinder	1
3	Stress Modifying Toroids	2
4	Cylinder Spacer	4
5	Perspex Support	2
6	Grounding Toroid	2
7	Signal Toroid	1
8	Low Voltage Attenuator	1
9	Toroid Spacer (Aluminium)	8
11	Signal Toroid Spacer (Insulator)	3
11	High Voltage Conductor	1
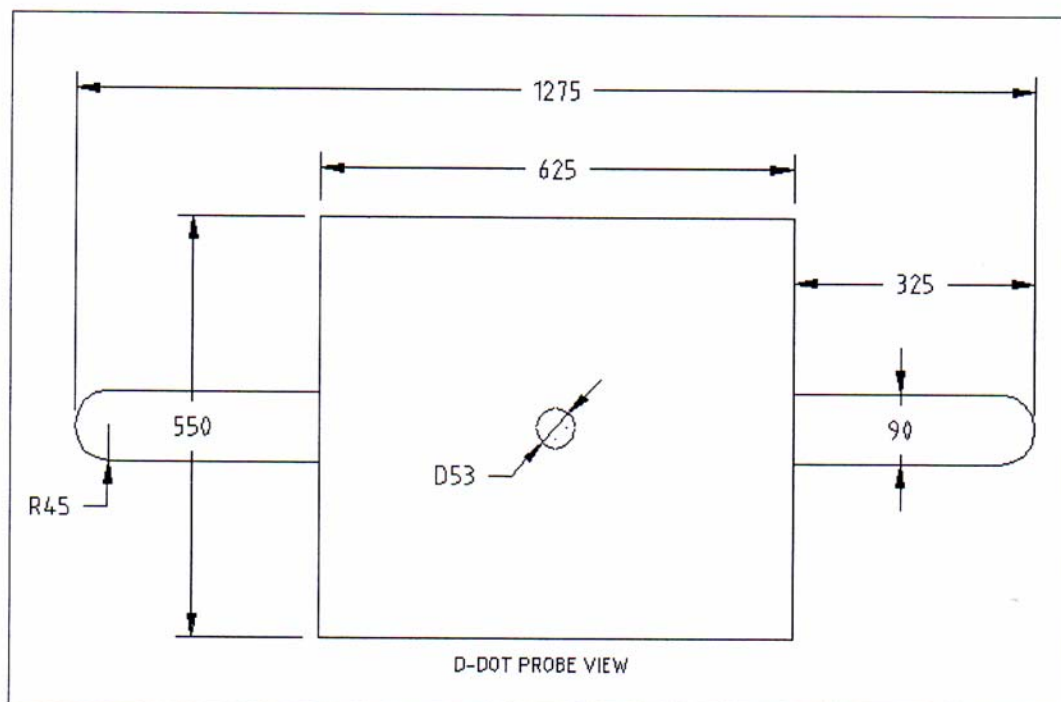
Figure 5.19:   D-dot probe view from one side
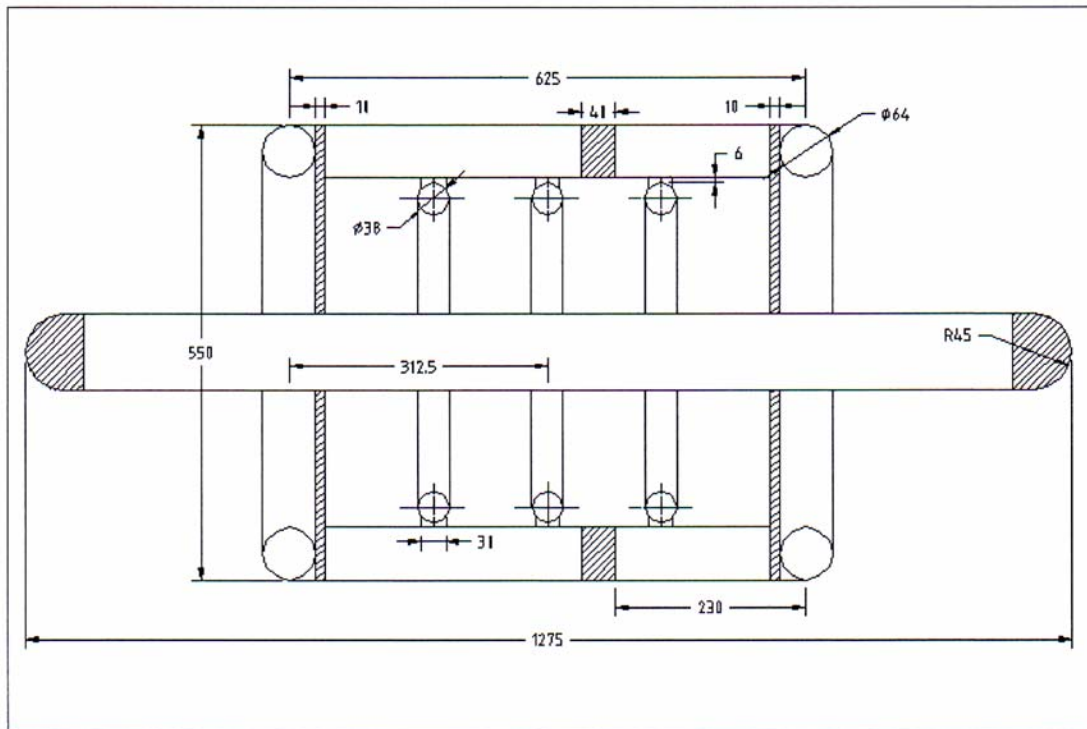
Figure 5.20: Dimension of D-dot probe (slice at the middle)
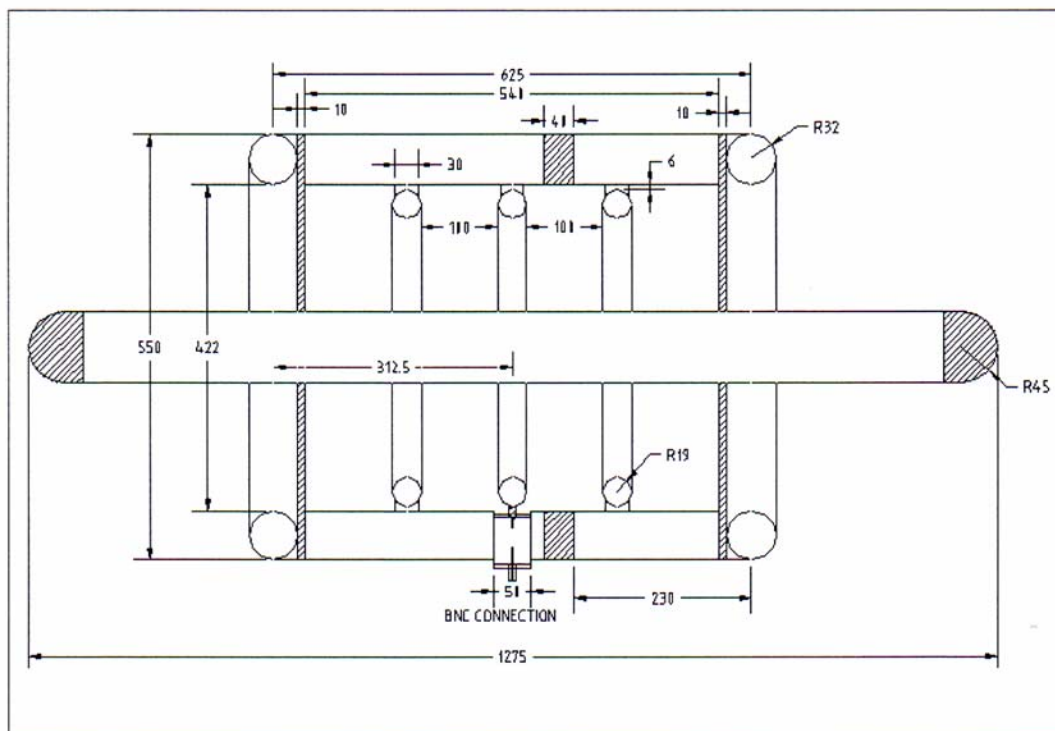
Figure 5.21: Dimension of D-dot probe with attenuator
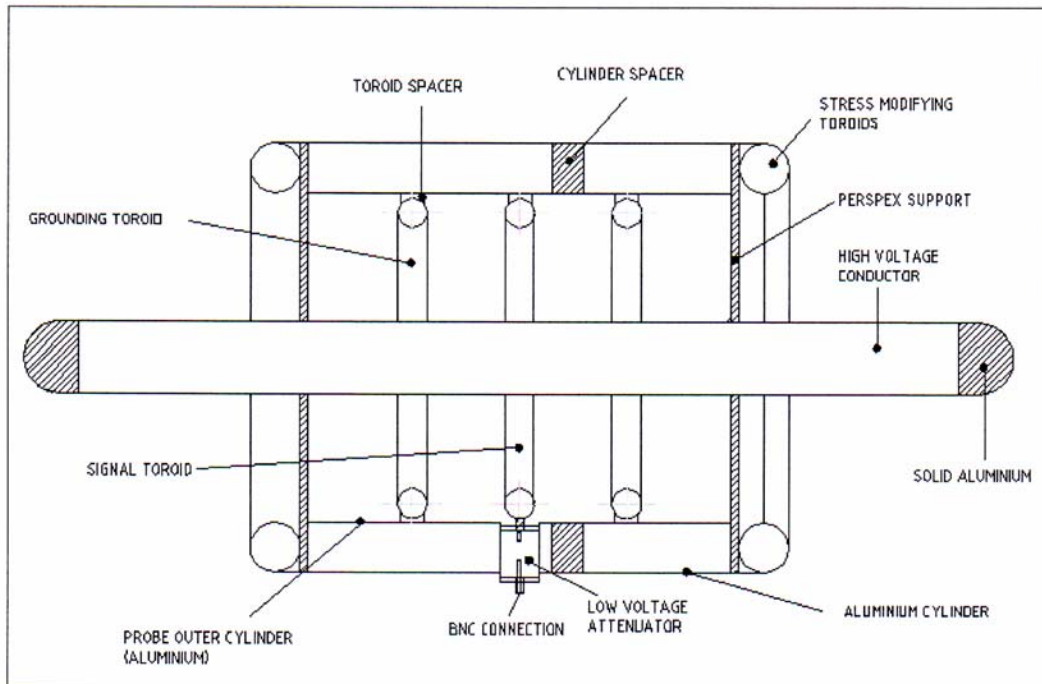
Figure 5.22:   Schematic diagram of D-dot probe arrangement
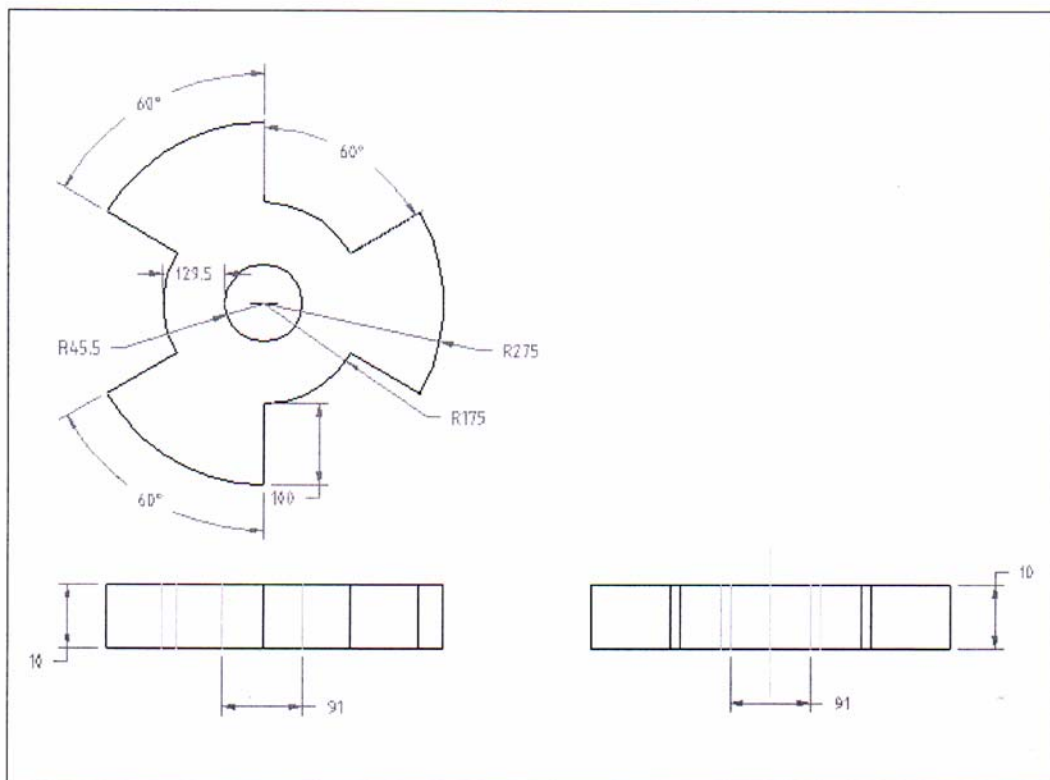
Figure 5.23:   Perspex support for high voltage rod
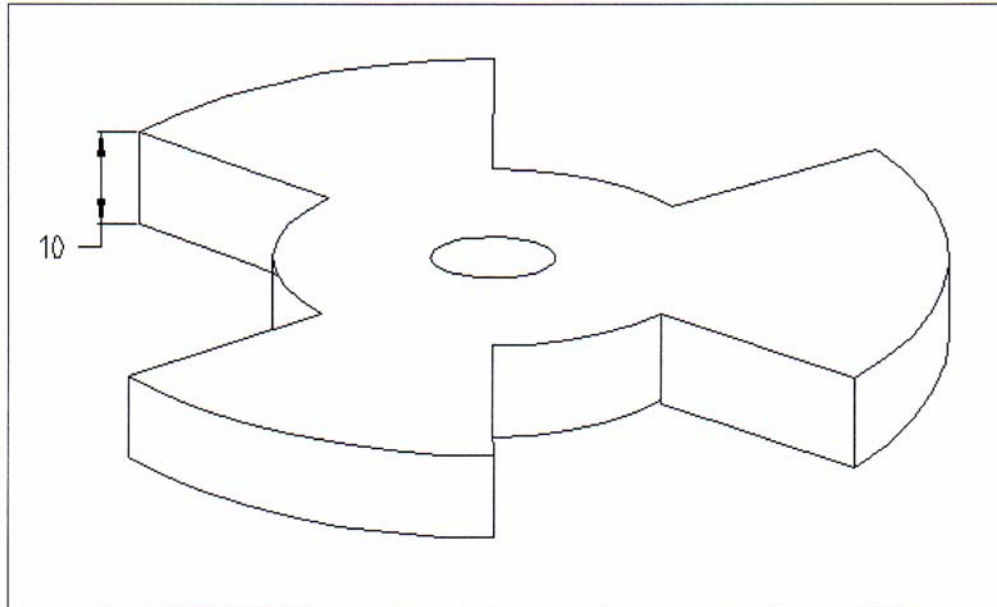
Figure 5.24:   Perspex support for high voltage rod (3 D view)
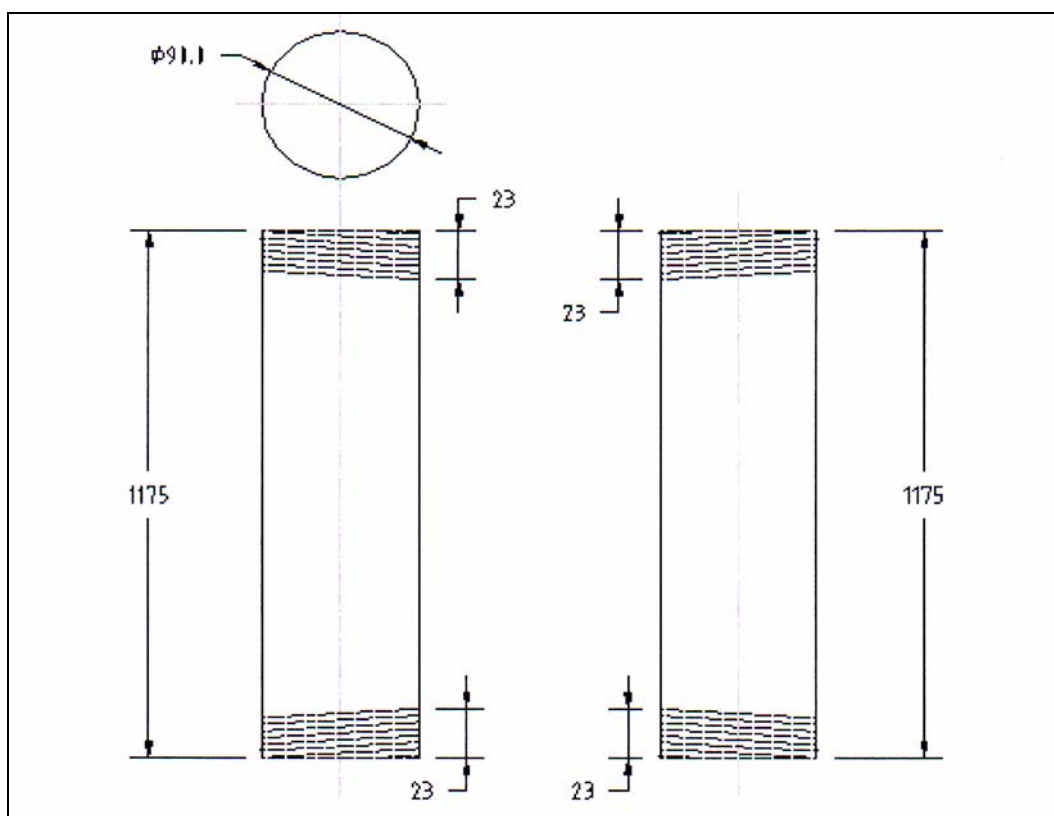
Figure 5.25:   High voltage rod without ending screw
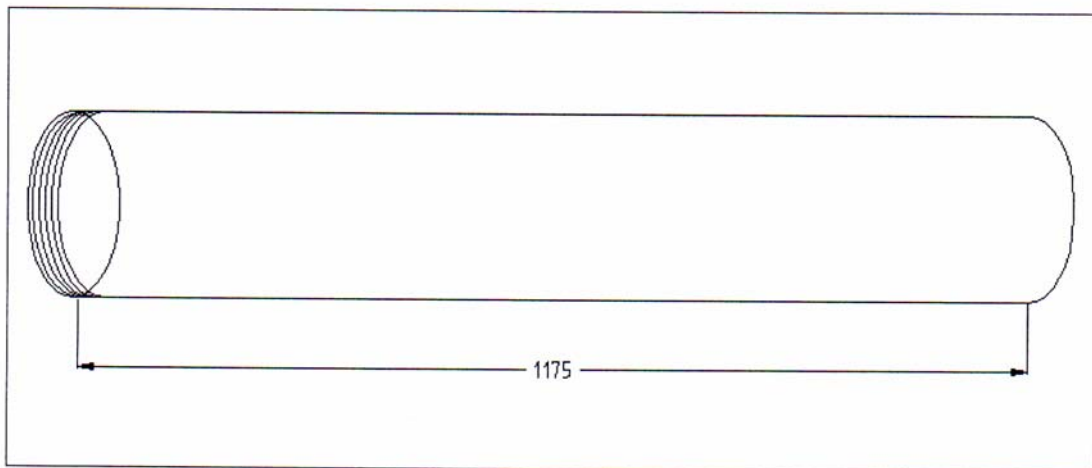
Figure 5.26:   High voltage rod without ending screw (3 D view)
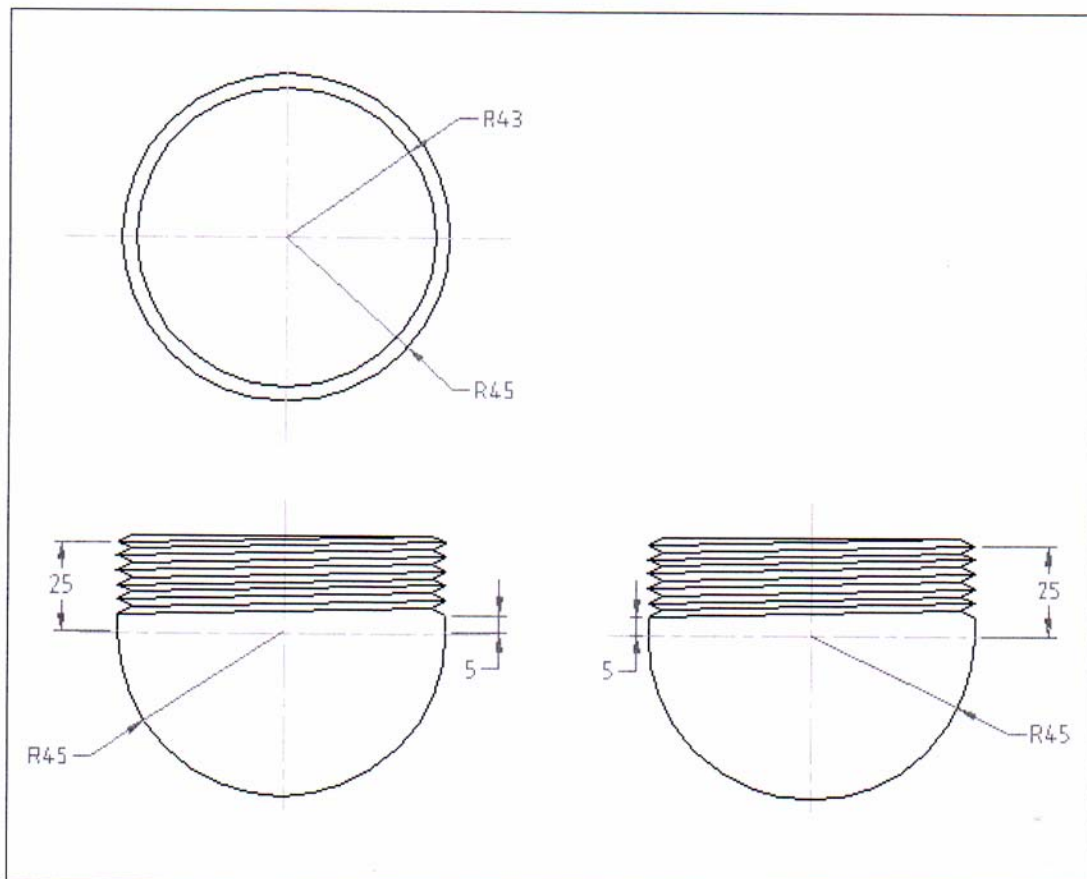
Figure 5.27:   Solid ending screw for high voltage rod
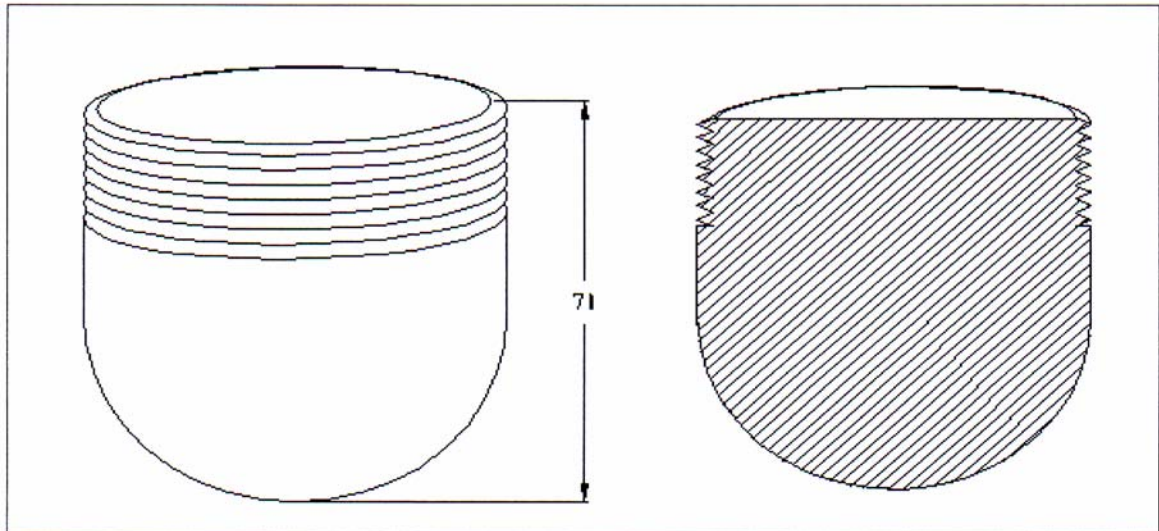
Figure 5.28:   Solid ending screw for high voltage od (3 D view)
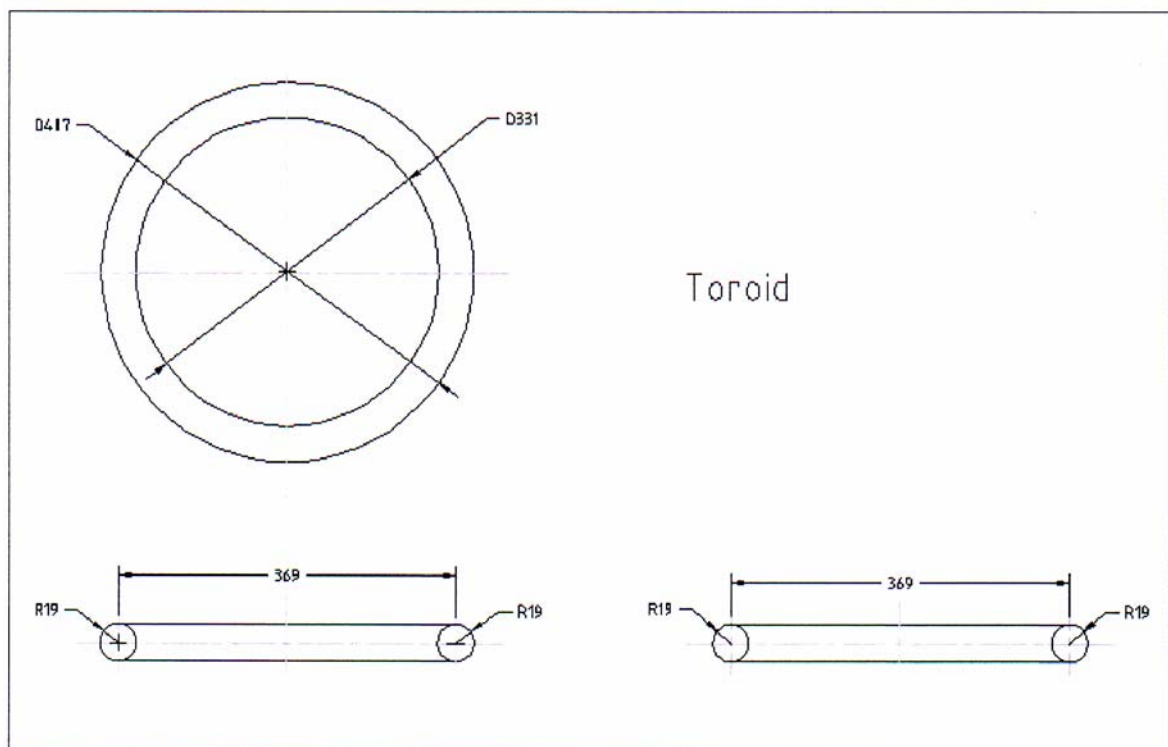
Figure 5.29:   Signal and grounding toroids
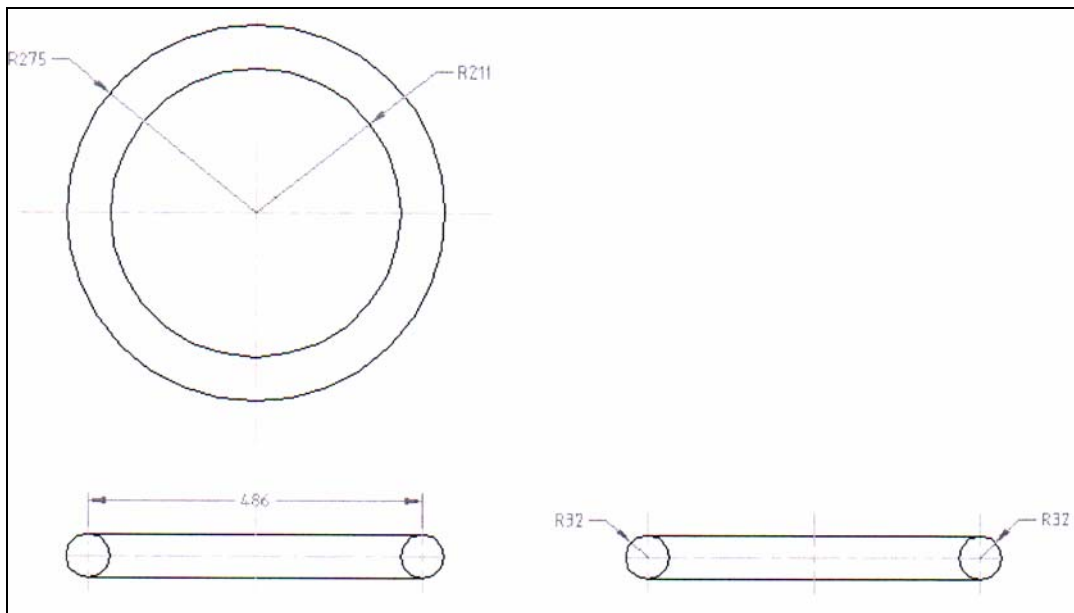
Figure 5.30:   Stress modifying toroids
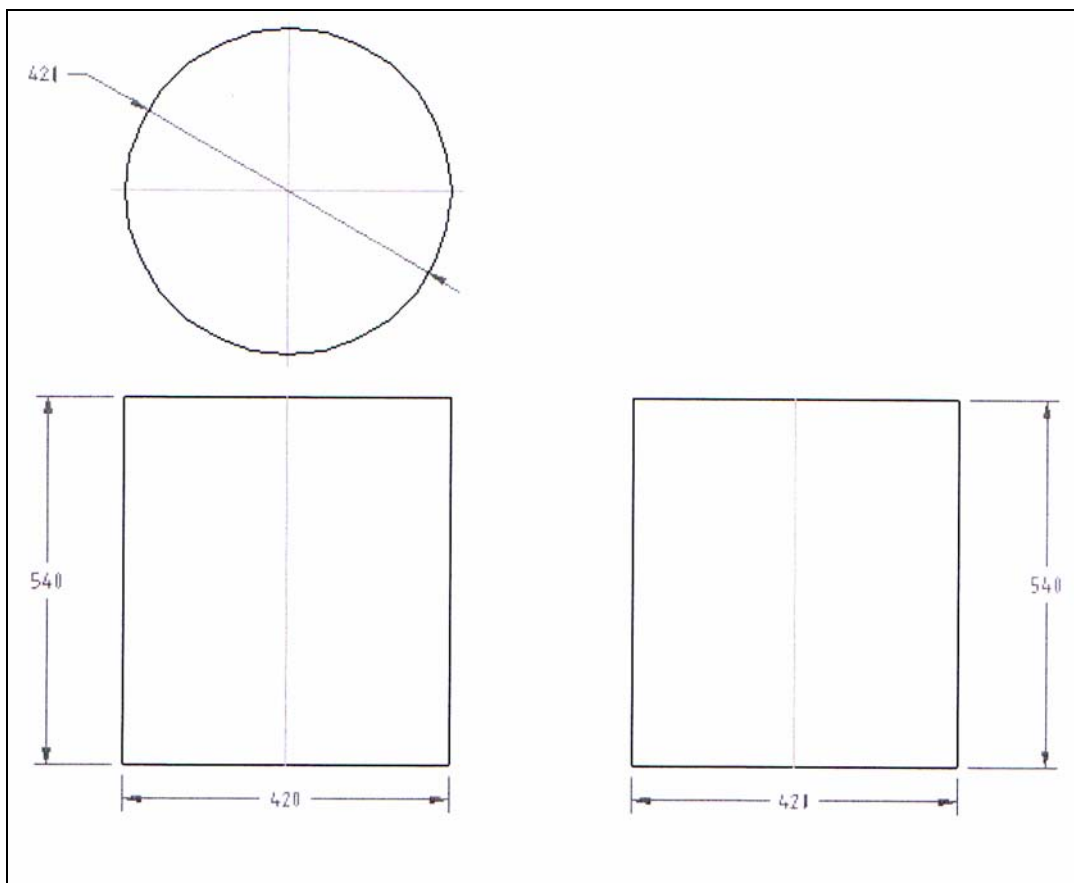
Figure 5.31:   Thin cylinder aluminium (inner)
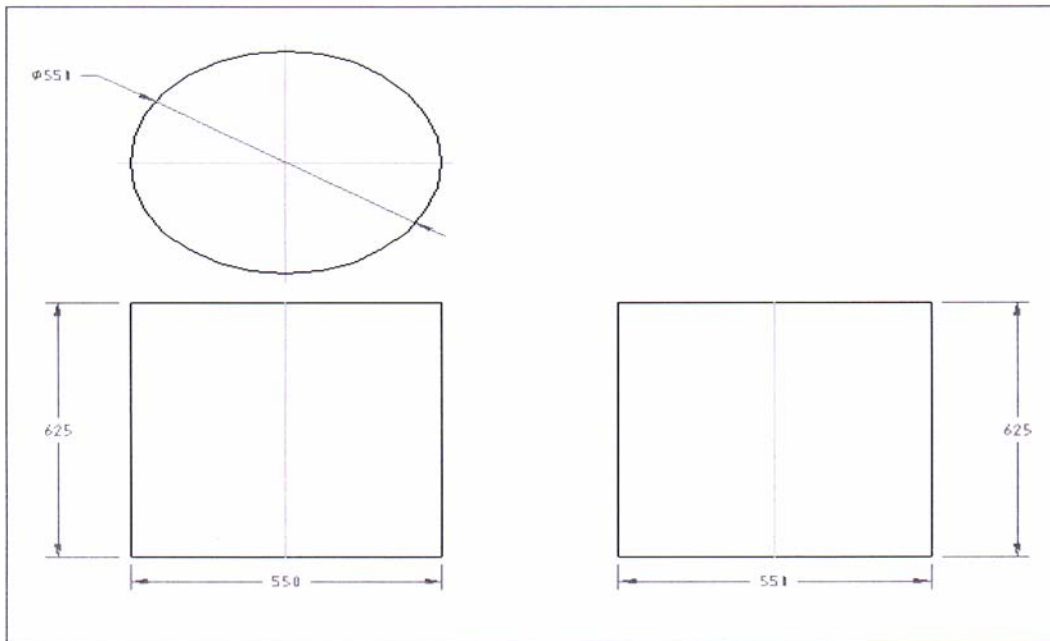
Figure 5.32:   Thin cylinder aluminium (outer)
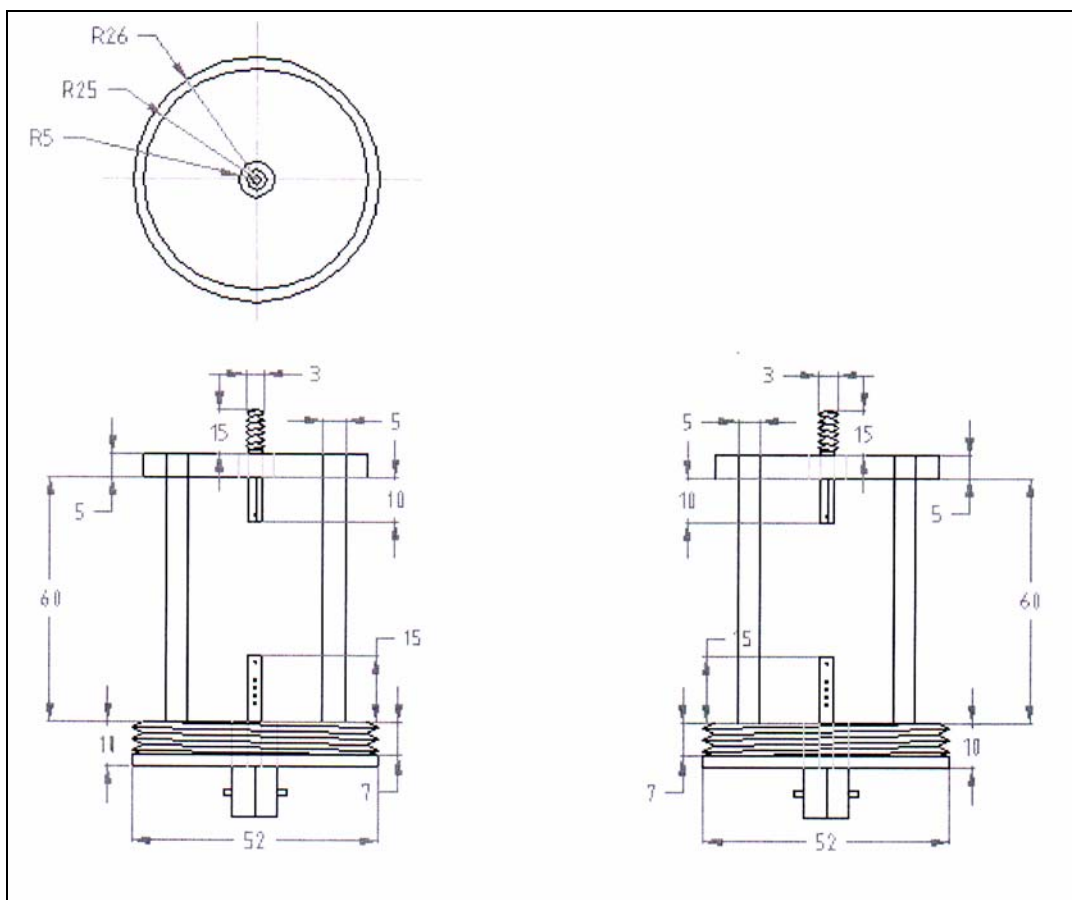
Figure 5.33:   Attenuator
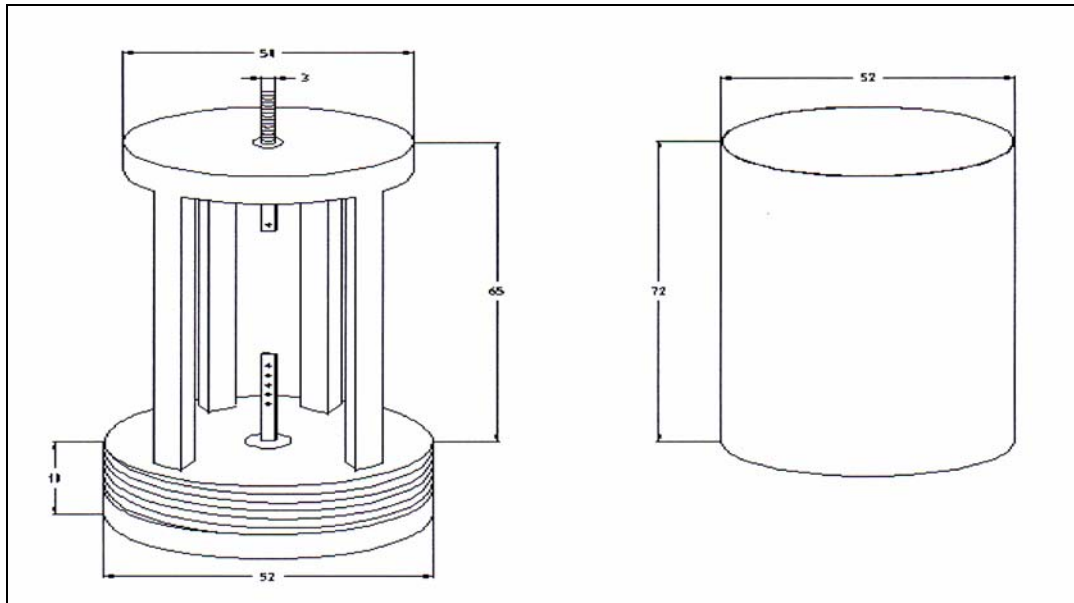
Figure 5.34:   Attenuator (3 D view)
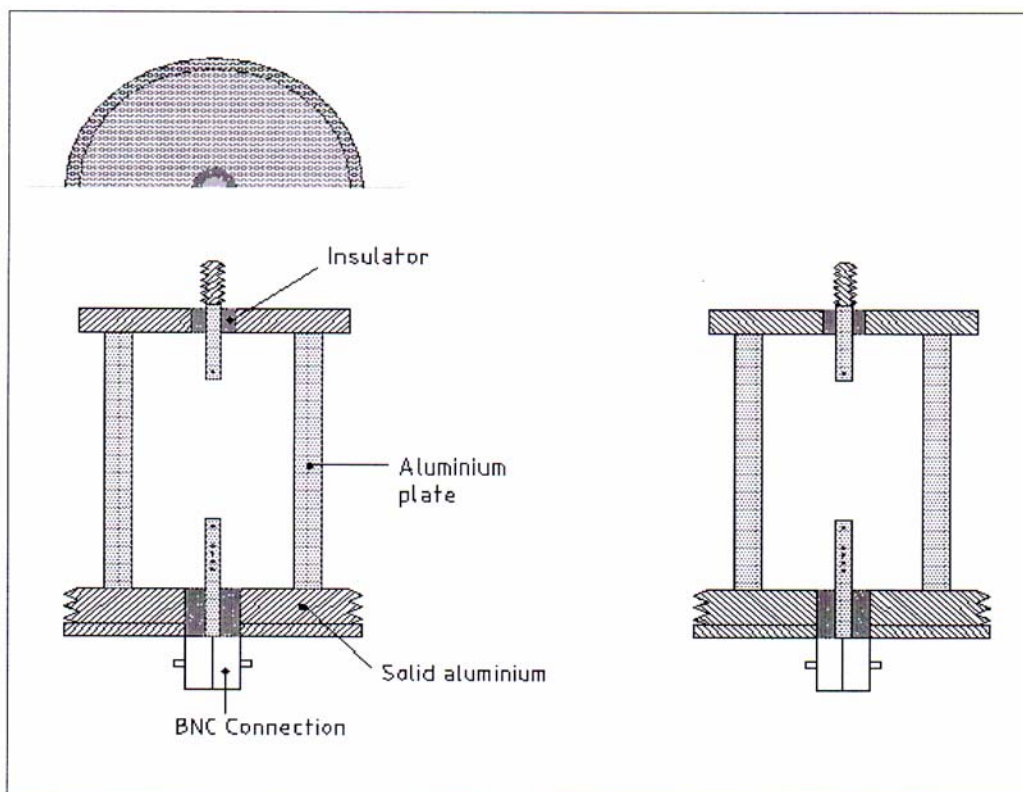
Figure 5.35:   Attenuator schematic arrangement
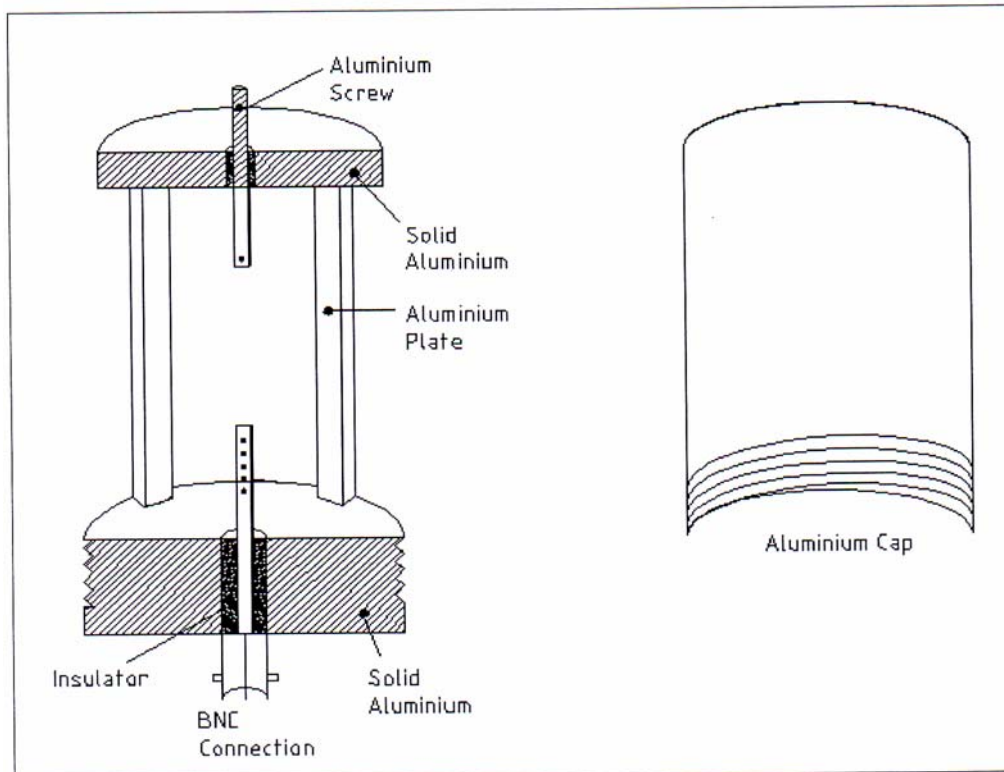
Figure 5.36: Attenuator arrangement

5.6   Discussion

Within this project, voltage measurement concept was developed using the electrical field measurements performed by the D-Dot probe, instead of the normal voltage measurements using voltage dividers. By comparing some results of simultaneous measurements for impulse voltage transients made on different kinds of HV equipment it is apparently demonstrated that such electrical field measurements can significantly improve this difficult and specialized measurement technique.

Due to the very well-known theory and practice of impulse voltage dividers, the development of which has quite a long history, the limitations concerned with the voltage transfer characteristics of such dividers are well known. The most advanced

theory of voltage dividers is based upon traveling wave or transmission line theory, i.e., by taking the propagation of electromagnetic waves in one dimension into account. It should also be well known that this theory has a fundamental limitation for proper application in the definition of an input voltage of any transmission system that is simulated by this theory. This input voltage can o be defined by the condition that an electrostatic field exists for which $\oint_c E.ds = 0$, within a plane of limited extension in both directions. This condition, however, is not fulfilled for all high voltage impulse measurements, for which the distance between two points of different potentials V, i.e., between an HV terminal of any piece of equipment and ground potential, becomes larger than some fraction of the wavelength, λ, of the transient voltage, assumed to be sinusoidal or harmonic, with frequency $f = I/\lambda$. A quite optimistic interpretation of "some fraction" would be a factor of 1/10 and assuming that the electrical field is built up within a plane or space, for which vacuum conditions can be assumed ($\varepsilon = \varepsilon_0$, $\mu = \mu$) the velocity of light, c_0, will govern the most optimistic assumption for electrostatic conditions, for which the definition of any voltage, i.e., the difference of potentials, is still possible. If, therefore, a voltage pulse to be measured between terminals being separated by some distance d contains frequencies f_u higher than about $c_0(10d)^{-1}$, the definition of a "voltage" becomes questionable. Note that even a distance of only 1 m restricts f_u to 30 MHz.

At this point one should consider that the most difficult problems concerned with voltage dividers, i.e., the problems related to the connection between voltage divider and terminals of test objects ('lead to divider'), or the bandwidth of the best possible divider structures, can be related to this fundamental problem. But as far as the application of voltage dividers is concerned, it is quite possible to achieve a bandwidth f_B which may well be in agreement with the above-mentioned limitations, if the dividers are carefully built and constructed. This was demonstrated by calculations as well as by measurements in the original publication concerned with "damped capacitive voltage divider" There it was shown that f_B can be as high about $f_B \approx (2h\sqrt{L'C'_e})^{-1}$, where L' is the inductance per unit length (p.u.l.), C'_e is its stray capacitance p.u.l. to ground, and h is the height or length of the divider column. It is unnecessary to show that this expression is related to the travel time of the voltage

transient necessary to reach ground potential. This high bandwidth can, of course, only be reached by an optimal design of the dividers.

Nevertheless, the application of field sensing device as has been done at ground or at HV potential for a long time is certainly a good tool to supplement high voltage impulse measurements, if it is done with care.

5.7   Conclusions

In most test-applications the full impulse voltage is a lightning or a switching impulse voltage. These impulse voltages can be measured quite accurately with voltage dividers. The present work has been directed towards the developments of a better understanding of the transient response measurements. Method for improved impulse voltage measurement techniques have been described and compared to the conventional voltage divider method. The technique is based upon the D-dot probe principle used in pulse-power applications. Its design and capacitance for voltage ratio determination has been derived from electric field computations. The D-dot probe has been designed as a portable unit enabling it to be incorporated in any suitable system.

According to the experimental results obtained from (Naylor P. 1995), the methods demonstrate unequivocally that there is no evidence of a voltage overshoot/spike on the front of the residual voltage waveform. Such observations can still be made even when the rate-of-rise of voltage at the arrester terminals is in the order of I kV/ns. The rate-of-rise is comparable to those that can be anticipated for an unattenuated lightning strike close to the arrester terminals. Such overshoots that have been reported in the literature may be ascribed with the voltage divider measurements.

It has been shown that charge simulation modeling by SLIM analysis gives the capacitive equivalent circuit and the best arrangement of the probe. Good linear calibration curve is obtained for the probe against the conventional capacitive divider.

Also faster response and less inductive overshoot are achieved from the calibration of the D-dot probe.

It can be concluded that the D-dot probe based sensor will improve the impulse voltage measurement. The high accuracy necessary for the measurement of amplitude of an impulse voltage will be performed with voltage dividers, but the waveshape of the impulse voltage will additionally be evaluated from measuring systems, like the D-dot probe based sensor.

The constructed D-Dot probe based divider need to be tested and calibrated against a standard divider. It is suggested that this is done in the next phase of the research where a complete test system consisting the high current generator, surge arrester load and the transducer are assembled. The performance of the D-Dot probe based sensor can therefore be ascertained.

CHAPTER 6

TUBULAR CURRENT SHUNT
DESIGN AND CONSTRUCTION

6.1   Introduction

The measurement of impulse current can be carried out by a calibrated low-ohmic resistor in series with the circuit under test. We have discussed earlier that if the resistor has a purely ohmic resistance, its voltage drop is proportional to the current. But for low-ohmic resistor used to measure high currents, it is difficult to satisfy the above assumption. The time domain voltage drop is affected by non-ideal properties of the measuring resistor, as represented by self and mutual inductances as well as the skin effect.

Currents flowing through ohmic resistor may cause surrounding magnetic and electric fields. These stray fields can be modeled by an inductance place in series with the resistor. The tubular shunt resistance has already been decided to be as low as possible. So we need to limit the inductance value to be less or equal to zero. This can be achieved by appropriate design and suitable choice of geometrical dimensions.

6.2   Tubular Shunt Design Procedure

Tubular current shunt resistor operation can be described as follow (see Figure 6.1). The tubular current shunt is connected in series with the circuit under test. The impulse current generated enters the resistor at the current input terminal (1). The current flow through the inner cylinder (2) made of non-magnetic material foil. The resistive foil is soldered at both ends namely the input terminal and the earth terminal (5). The voltage drop across the inner cylinder is measured by using potential lead (4) placed between the input terminal and the outer case of the coaxial shunt which is connected to the earth terminal. The potential lead is extended to the cathode ray oscilloscope for signal reading. The space between potential lead and the inner cylinder is free from any electric and magnetic fields. So this design resistor should act as a pure ohmic resistor. The current returns through outer cylinder (3) made from conducting material that encloses the shunt and provide the current path to ground.
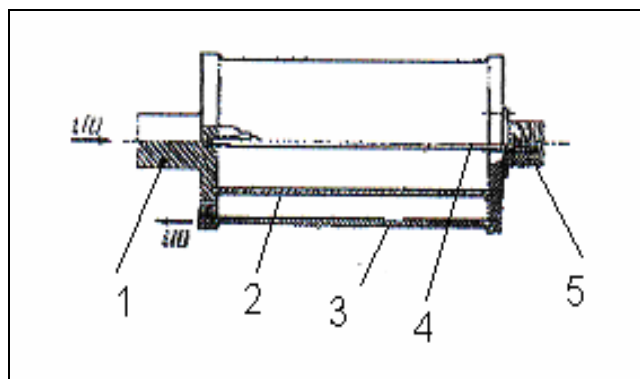
Figure 6.1: Tubular Shunt

The impulse rating of low-ohmic resistors depends solely upon the thermal capacity of the resistive element. Because the standard impulse current is of short duration, it is possible to assume that no heat being transferred to the surrounding. At the same time the impulse current is heating the resistive material. This means that the electrical energy is converted into thermal energy and then stored in the resistive material. This can be shown in mathematical equation as,

$$\int R\, i^2\, dt \;=\; m\, c\, \Delta T \qquad\qquad\qquad (6.1)$$

where   m   = specific weight in g/cm^3

      c   = specific heat of the resistive material in Cal/g°C

      ΔT = the temperature rise in °C

According to the above equation the impulse rating is related to the weight of the resistive material. The above equation when divided by the resistance value yields the limit load integral $\int i^2\, dt$, which is often used as a specification for the thermal impulse rating of current shunts.

The main purpose in designing the shunt resistor is to determine the prospective peak current amplitude to be measured, (I_{max}) and the limit of the recording equipment (V_{max},). After the two parameters have been determined, the resistive value can be calculated based on the following equation,

$$V_{max} = R_{sh}\,.\, I_{max} \qquad\qquad\qquad (6.2)$$

The next step to be considered is to determine the maximum acceptable relative change in resistance of the resistive material. This value should be as low as possible so that the resistance change at high temperature is slightly lower. The value should be selected such that the relative change in resistance is within 0.1%.

When the relative change in resistance has been determined, the maximum allowable temperature rise can be calculated. By knowing this, we can determine the volume of resistive material required to construct the resistive shunt that has an adequate thermal capacity. The material must be capable to withstand the heat due to

the conversion of the electrical energy into thermal energy. The maximum allowable temperature can be calculated, by using the following equation

$$\Delta R_{sh} = \gamma \, \Delta T \tag{6.3}$$

where ΔR_{sh} =   the maximum relative change in resistance

           γ =   the temperature coefficient of the material

           ΔT = the maximum acceptable relative change in temperature

When the maximum relative change in resistance and the maximum acceptable relative change in temperature have been determined, the resistance of resistive material can be calculated as below

$$\Delta R_{sh} = \frac{(R_{sh}\,\theta - R_{sh})}{R_{sh}} \tag{6.4}$$

where $\Delta R_{sh}\theta$ = the resistance at the maximum acceptable temperature.

The volume of the resistive material, V, can be determined based on Equation 6.5.

$$V = \frac{m}{\delta} \tag{6.5}$$

where δ = the density of the material. Then the physical dimensions of the shunt can be determined as

$$V = d\,w\,l = A\,l \tag{6.6}$$

where

$$d \quad = \quad \text{the thickness of the material,}$$

$$w \quad = \quad \text{the width of the material,}$$

$$l \quad = \quad \text{the length of the material, and}$$

$$A \quad = \quad \text{the cross-sectional area of the material}$$

Table 6.1 shows the properties of the chosen resistive material namely nickel chromium.

Table 6. 1: Nickel Chromium Properties.

Definition	Symbol	Value
Density	δ	8.4 g/cm^3
Resistivity	ρ	108 $\mu\Omega$.cm
Thermal coefficient	γ	0.00005 C^{-1}
Specific heat	c	0. 107 cal/ g°C
Max. relative change in R_{sh}	ΔR_{sh}	0.1%
Max. permissible relative temperature rise	ΔT	20 °C

6.3 Calculation for Nickel Chromium Dimension

The first step to be taken is to determine the impulse current waveform flowing through the shunt resistor. An example of the impulse current waveform is shown in Figure 6. 2.
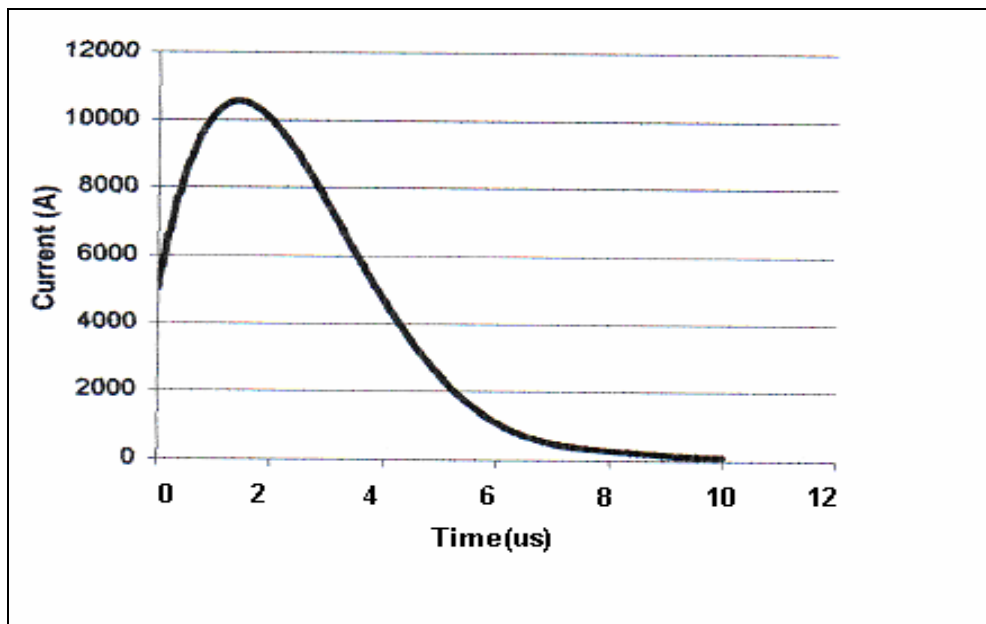
Figure 6.2 Impulse current waveform (1/4 shape)

Referring to equation 6.1, $\int i^2$ dt represent the area below the squared current waveform. The corresponding squared waveform current is shown in Figure 6.3.
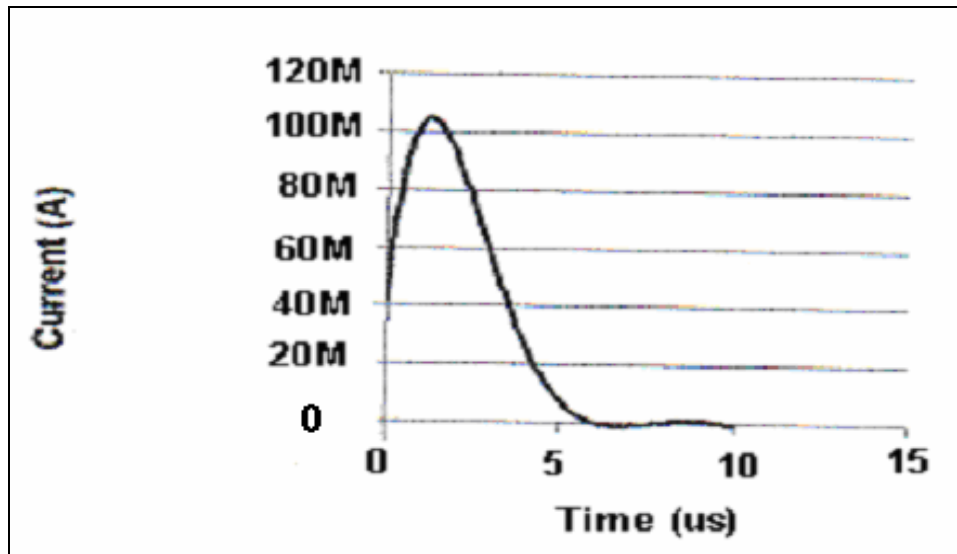
Figure 6.3: Squared impulse current waveform

Refer to equation 6.1, $\int i^2$ dt represent the below area of the squared current waveform. So, the next step is to produce squared waveform current. This is shown in figure 6.3.

To calculate the area below the waveform of Figure 6.3, the 3/8 Simpson Method was applied. The value of the area is 31344.26 A^{2}s. Substituting the above value in Equation 6.1, the mass of Nickel Chromium required to form 51mΩ resistance is obtained. The calculation is shown as below.

(5mΩ) x (31344.26μA^{2}s) = m (0. 107 cal/g°C) x (20°C)

m = 73.2342g

Now we need to calculate the volume of the shunt resistor. This volume is

needed to confirm the dimension of Nickel Chromium required to achieve 5mΩ resistance. By using the equation 3.5, the volume is calculated as

V = 8.718363373 cm^3

We also know that the resistance of a material is given by

$$R_{sh} = \frac{\rho l}{A}$$ (6.7)

While cross sectional area of foil, A can be obtained by

$$A = \sqrt{\frac{\rho V}{R_{sh}}}$$ (6.8)

and

$$l = \sqrt{\frac{V R_{sh}}{\rho}}$$ (6.9)

The relationship between the area and the thickness of the foil is geven by

$$A = d \cdot w$$ (6.10)

To calculate the foil width, we need to consider the thickness of the NiCr foil. This is because the thickness of the foil will affect the risetime of the shunt. The risetime of the shunt is given as

$$T_r = \frac{\mu d^2}{k \rho}$$ (6.11)

It can be clearly seen from the above equation that the thickness of the foil should be as thin as possible so that the risetime can be reduced. The coefficient k being in the region of 4<k<6. In this work, the coefficient k was chosen to be equal to 8. This is because the response time is determined more accurately when the coefficient k equals to 8(Naylor P, 1995).

By reducing the foil thickness, it can reduce measurement errors associated with the skin effect. The reduction of the thickness of the resistive material is limited by the product available in the market. Furthermore, the price of a thinner resistive

material will cost much higher due to the difficulties in the production process. In this project the thickness of NiCr foil is 0.125mm. Therefore, from equations 6.9 and 6. 10 we obtain the foil width of 34.7172cm.

6.4   Alternative Resistive Material

Consideration of other resistive materials in constructing the shunt resistor was also carried out. One of the important properties is that the shunt material must be non-magnetic. The material must also have high specific heat coefficient to withstand the high temperature rise. The other characteristics such as the density, resistivity and thermal coefficient of the chosen material must be equal or nearly equal to those of the NiCr.

Initial investigation showed that the properties of the NiCr are largely dominated by the nickel element. Therefore other nickel based alloys should be studied as alternatives. The main objective in this sub-topic is to evaluate the maximum allowable energy absorption of the various available alternative materials.

Evanohm and nikrothal L are the most preferable nickel based alloys to be used as alternatives to NiCr. The resistivity, density and specific heat of these materials are almost equal to those of NiCr. But the evanohm's temperature coefficient is much lower than that of NiCr. Constantan and manganese are the least suitable alternatives. This is because their resistivity and specific heat are much lower than evanohm and nikrothal L but their density is equal to the density of NiCr. The detailed properties of these alternatives resistive materials are shown in Table 6.2.

Table 6.2: Properties of various resistive materials

Alloy	Nikrothal L	Evanohm	Constantan	Manganese	Nickel Cromium
Resistivity at 20° C ($\mu\Omega$.cm)	133	118	49	43	108
Temperature Coefficient (1/°C)	20×10^{-6}	5×10^{-6}	30×10^{-6}	20×10^{-6}	50×10^{-6}
Density (gcm^{-3})	8.1	8.8	8.9	8.4	8.4
Specific Heat at 20°C (cal/g°C)	0.11	0.1	0.098	0.097	0.107

Using the data in Table 6.2 and applying equations 6.1 to 6.10, the dimension of the resistive material required to give a value of 5mΩ in resistance can be calculated. Table 6.3 shows the dimension required for all the resistive materials considered.

Table 6.3: Calculated dimension of resistive materials required to give 5 mΩ value of resistance.

Alloy	Nickel Cromium	Nikrothal L	Evanohm	Constantan	Manganese
Thickness (mm)	0.125	0.125	0.125	0.125	0.125
Length (cm)	20.097	18.436	18.779	28.977	31.839
Width (cm)	34.717	39.232	35.453	22.718	21.916
Cylindrical radius (cm)	5.525	6.244	5.643	3.616	3.487

6.5   Materials Used in Constructing The Shunt Resistor

6.5.1   Aluminium

Aluminium is the abundant metal in the earth's crust and the third most abundant of all elements after oxygen and silicon. Alumina is made up of aluminium and oxygen. To produce aluminium metal, it is necessary to separate these two elements of the aluminia. The process which transforms alumina into aluminium is called smelting.

The aluminium, in a molten form, sinks to the bottom of the pot. It is siphoned out in a process known as tapping and is transparented to a holding furnace being cast as pure aluminium (better than 99.7%) or small amounts of other elements such as magnesium, silicon or manganese are added to form aluminium alloys. Different alloys give different properties to the metal, such as extra strength or greater resistance to corrosion.

Primary aluminium can be rolled, extruded or cast to make aluminium end products. Rolling involves a block of aluminium being 'squashed' between large rollers to make product such as aluminium plates, sheets or foils.

Extruding is a process in which round logs (billet) of hot aluminium are forced through a pattern cut into a steel die. Casting occurs when molten aluminium is poured into moulds to manufacture specific shapes. Aluminium is a non-rusty metal type that is commonly used as a replacement of copper. Pure metal aluminium has high tensile characteristic which is about 90MPa (13 kPsi), good resistivity and has high temperature withstand. Aluminium of 6061 type was used to to build the coaxial shunt component in this work.

6.5.2   Nylon

Nylon has a high coefficient of thermal expansion (about three times that of aluminium) and low heat conductivity. The family of nylons consists of several types. Nylon 6/6, nylon 6, nylon 6/10, nylon 6/12, nylon 11, nylon 12, and nylon 6-6/6 copolymer are the most common. Of these, nylon 6/6 and nylon 6 dominate the market. The numbers refer to how many methyl units ($-CH_2-$) occur on each side of the nitrogen atoms (amide groups). The difference in number of methyl units influences the property profiles of the various nylons. Moisture absorbance is decreased due to reduced polarity with further separation and less regular location of the very polar amide groups.

Resistance to thermal deformation is lowered due to more flexiblity and mobility in these methyl unit sections of the main chain. As these units increase in length, making the molecules appear more like polyethylene, the properties of the nylon shift slightly toward those of polyethylene. Not considering the effects of moisture, nylon 6/12 has lower modulus, higher elongation, lower strength, lower thermal distortion temperature, lower hardness and lower melting point than nylon 6/6. Nylon 6/12 is more expensive than nylon 6/6. The property which gives nylon 6/12 its utility is moisture absorption which is approximately half of that of nylon 6/6. This means the properties are much more consistent and experience less fluctuation due to ambient humidity levels in the end application.

Another dominant feature of nylons is crystallinity. As with most crystalline polymers, the molecular chains are uncluttered by large substituent groups. They are flexible and regular in group spacing and crystallize readily. As with acetals, this crystallinity is responsible for properties of wear resistance, chemical resistance, thermal resistance, and unfortunately, higher mold shrinkage. The overall excellent profile of nylons results in their probably having the most diverse range of applications of all thermoplastic polymers.

6.5.3   Acrylic

Acrylic is a type of plastic product. It only has half the weight of glass. Acrylic has a great impact resistant and also unaffected by sun or salt spray. Temperature range of the acrylic plastic is around -30 to 1600°F for continuous service.

Before this material being process to end product, it needs to be washed with mild soap or detergent, with plenty of lukewarm water, dry with soft cloth or chamois. Grease, oil or tar can be removed with hexane or kerosene. Solvent residue should be removed by washing immediately. Window-cleaning sprays, scouring compounds, acetone, gasoline, benzene, carbon tetrachloride or lacquer thinner should not be used.

When working with the material, the paper masking film needs to be left on the sheet as long as possible. Except for intricate detail work, the masking should only be removed when the project is completed. All tools should be sharp. Water or drilling oil need to beused as a coolant when cutting sheets over 1/8" thick or drilling sheets over 3/16" thick. The material needs to be wet before cleaning process.

Acrylic sheet up to 3/16" thick may be cut by a method similar to that used to cut glass. A scribing knife, a metal scriber, an awl, or a utility knife can be used to score the sheet. The scriber need to be drawn several times (7 or 8 times for a 3/16" sheet) along a straight edge held firmly in place. Then the sheet needs to be clamped or held rigidly under a straight edge with the scribe mark hanging just over the edge of a table. A sharp downward pressure need to be applied to break the sheet along the scribe line. The edges can be scaped to smooth any sharp comers. This method is not recommended for long breaks or thick material.

Acrylic can be heated to make it pliable. It will become rigid. A strip heater is the best tool to form acrylic. This tool will only form straight. The sheet can be heated until it begins to sag at the bend line. The bend should be made away from the side exposed to the heating element. Sheet thicker than 3/16" should be heated on both sides for a proper bend. For best results forming jigs or clamps should be used, and heavy cotton gloves should be worn when handling heated acrylic.

6.6   Technical Drawings of Coaxial Shunt Resistor

After the dimension of the core material (Nickel Chromium foil) is determined, the next step is to design the whole structure of the tubular shunt resistor. The design process using AutoCAD software is described extensively in this section.

Figure 6.4 show the overall view of the shunt resistor designed and constructed. Figures 6.5 to 6.24 show the complete design with all relevant parts of the whole current shunt.

Some consideration must be taken before the designing process of the outer part is started. Detailed information of the standard size and dimension for the materials used must be known first. Availability of these required materials also need to be considered. Aluminium sheet with the thickness of 1 mm was used to build hollow cylinder for the outer casing part of the shunt resistor to reduce the influence of power circuit on the distribution of current in the resistive tube. Rivet connection were applied to achieve the desired geometry (cylindrical shape). This part should have at least three levels of screw holes for the assembly process of the input terminal, earth terminal and earth base. All of these parts were made from solid aluminium 6061.

The upper shielding (Figures 6.5 – 6.7) was placed on the top part of the shunt. This part was also made from solid aluminium 6061. The input terminal (Figure 6.10) and the upper shield need to be insulated to prevent short circuit of the current path. So the insulator applied here is made of perspex (Figure 6.8), which is an acrylic clear plate. This material has been chose because of its high temperature withstand characteristic.

Nylon cylinder (Figure 6.17) was placed on the inside of the Nickel Chromium. The nylon provides support for the foil itself. Inside the nylon cylinder, a hollow path was made to place copper lead used for sending the impulse current signal to measuring devices such as a cathode ray oscilloscope.

The earth terminal was placed between the input terminal and the earth base. At the center of this part, a BNC connector was placed as a connector for the coaxial cable. There is a space between the earth terminal and the earth base as a place to connect the coaxial cable from outside the shunt resistor.
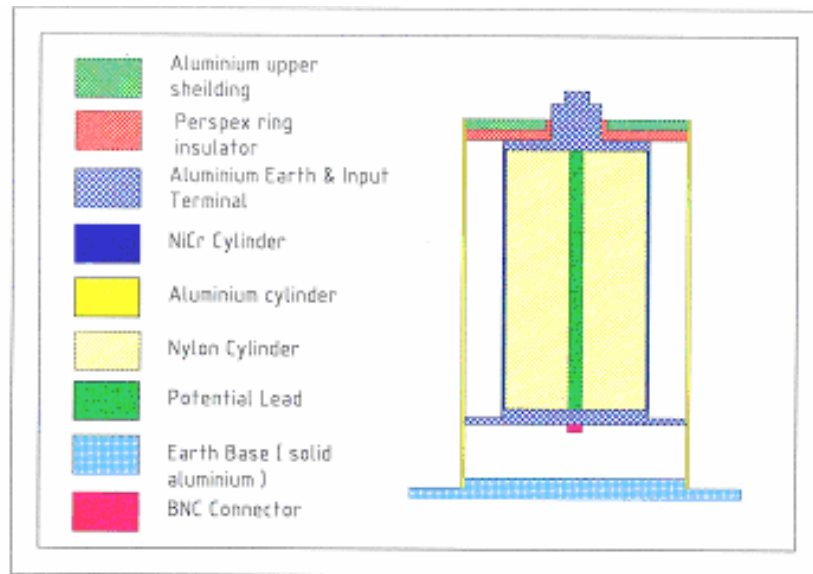
Figure 6.4: Overall view of Shunt Resistor
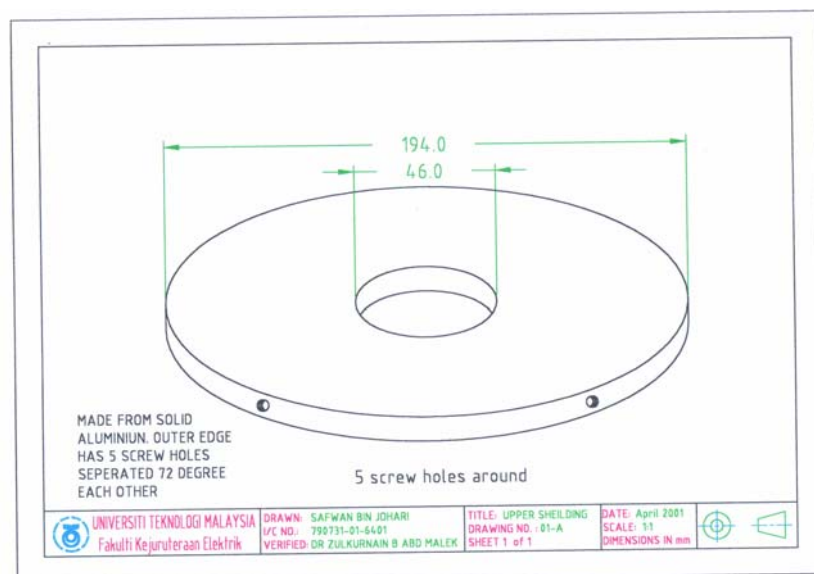
Figure 6.5: Upper Shielding 1
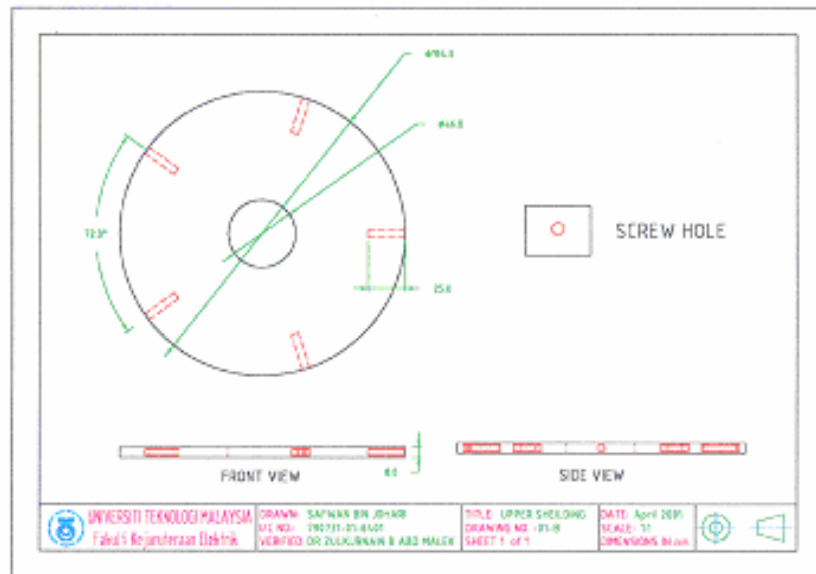
Figure 6.6 :   Upper Shielding 2
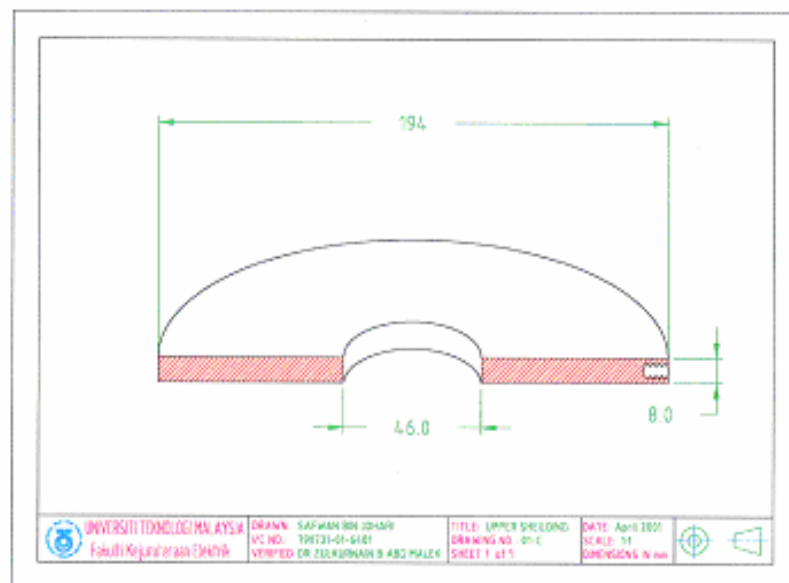
Figure 6.7   :   Upper Shielding 3
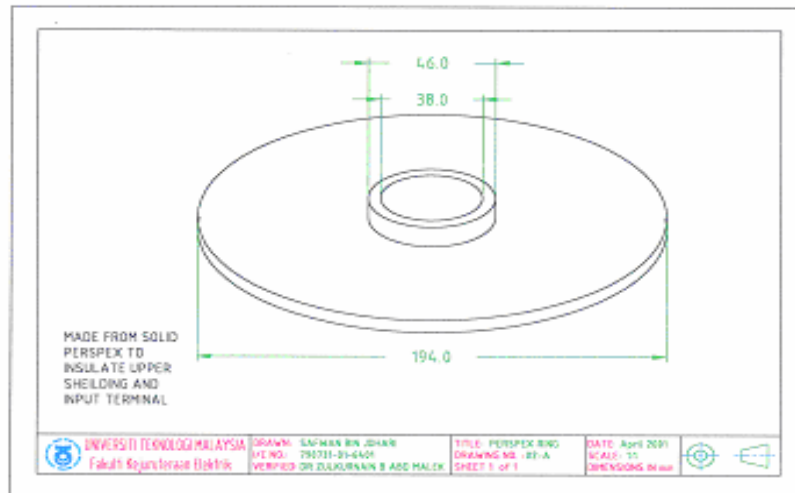
Figure 6.8   :   Perspex Ring 1
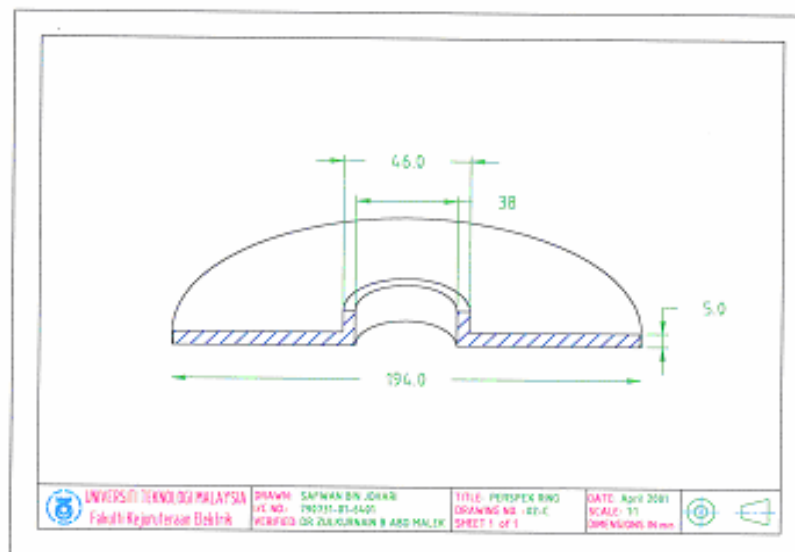
Figure 6.9   Perspex Ring 2
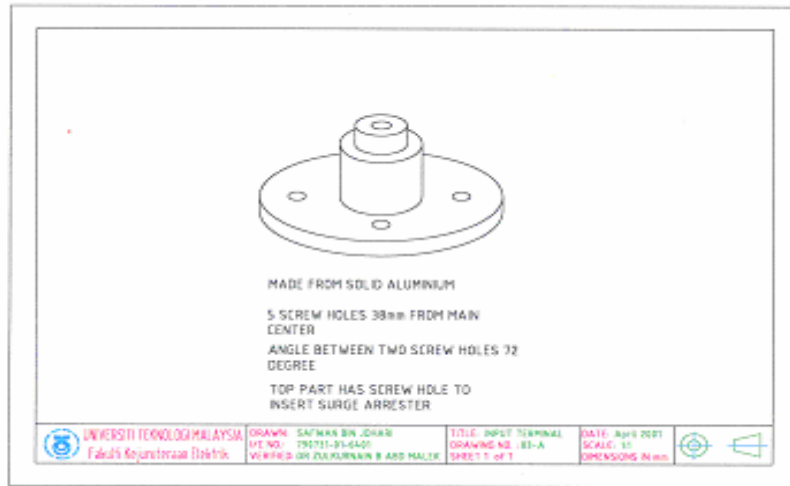
Figure 6.10   Input Terminal
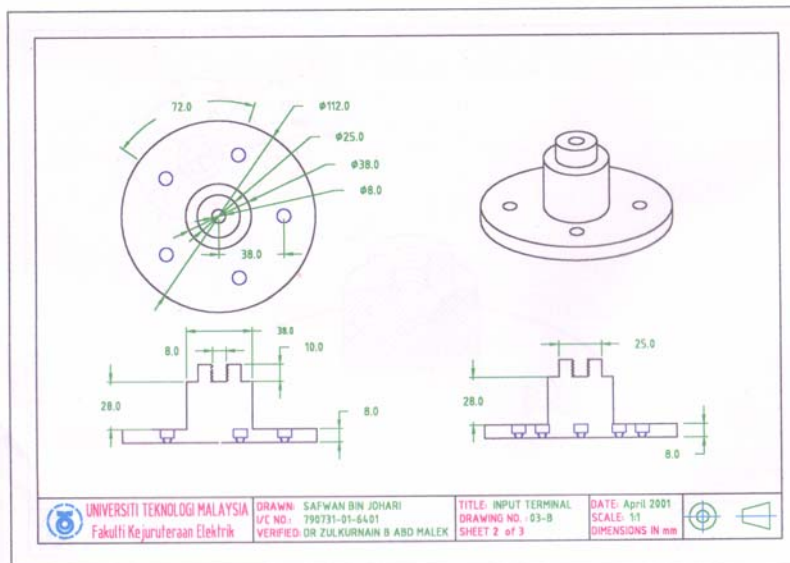
Figure 6.11   Input Terminal 2
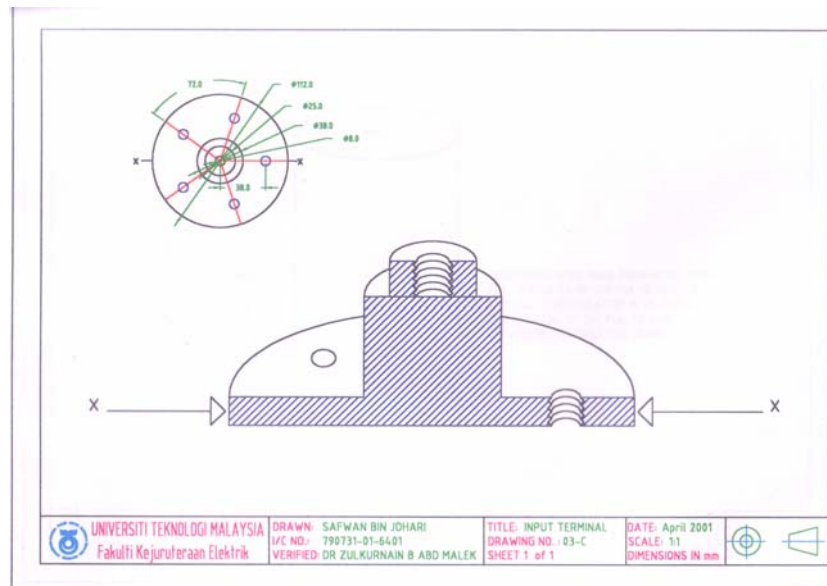
Figure 6.12   Input Terminal 3
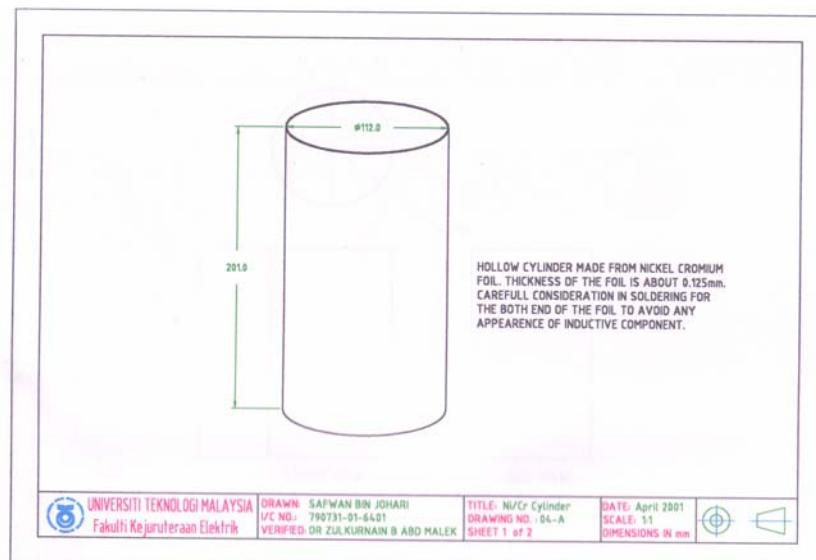
Figure 6.13   Ni/Cr Cylinder

90
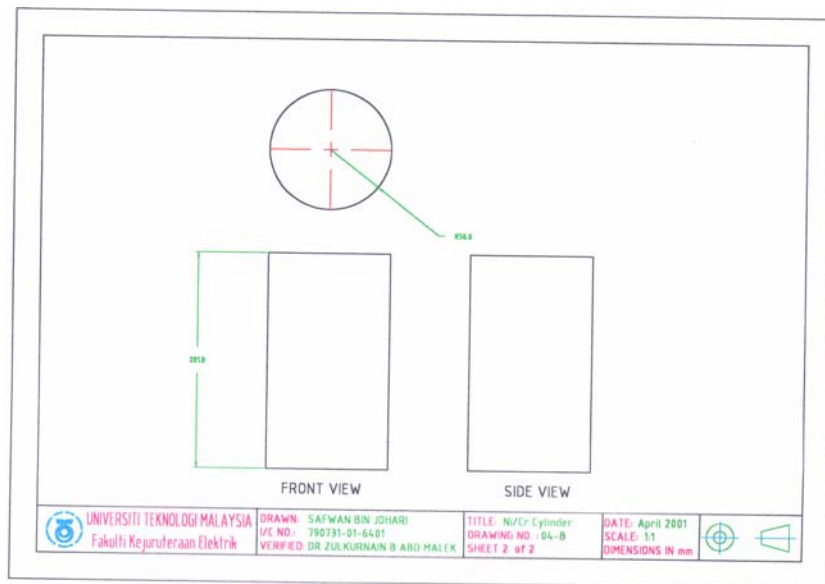
Figure 6.14   Ni/Cr Cylinder 2
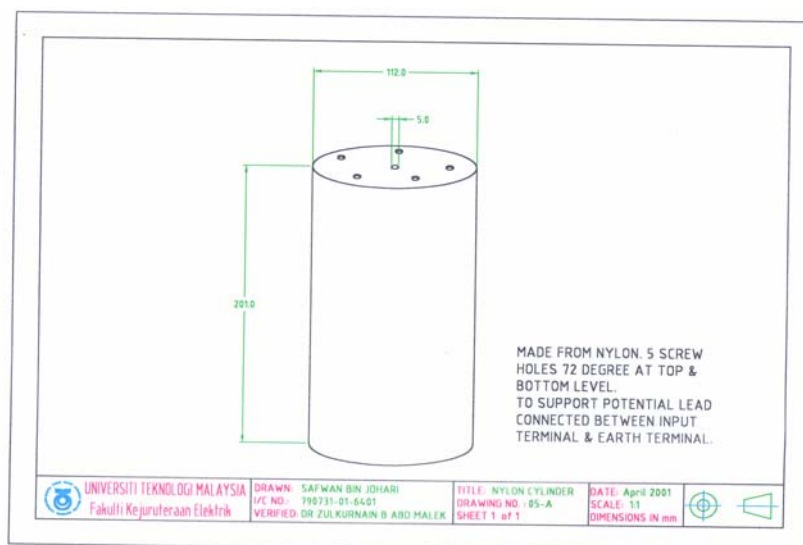
Figure 6.15   Nylon Cylinder
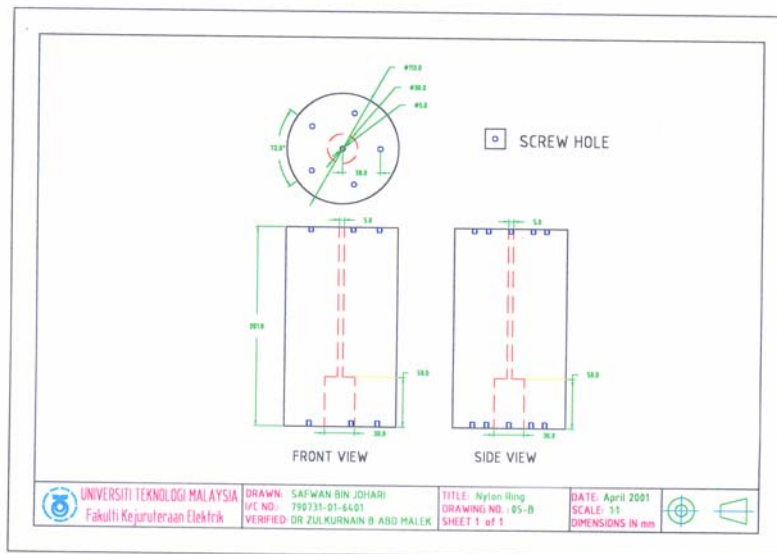
Figure 6.16   Nylon Ring
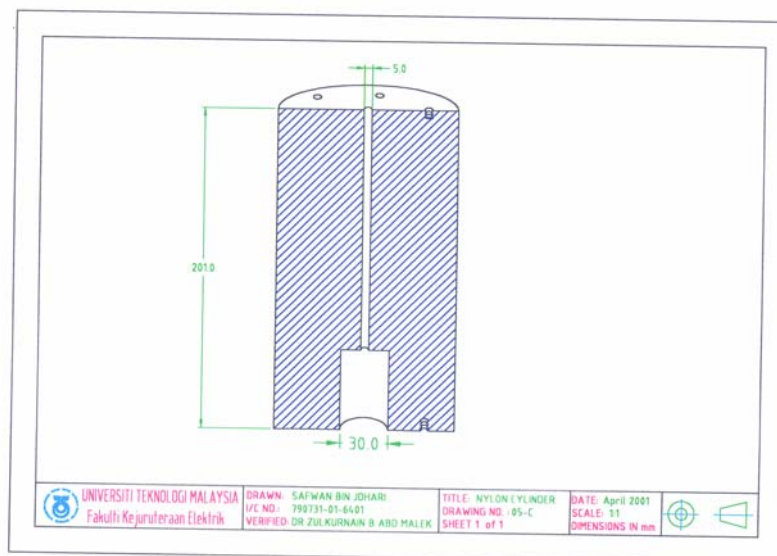
Figure 6.17   Nylon Cylinder
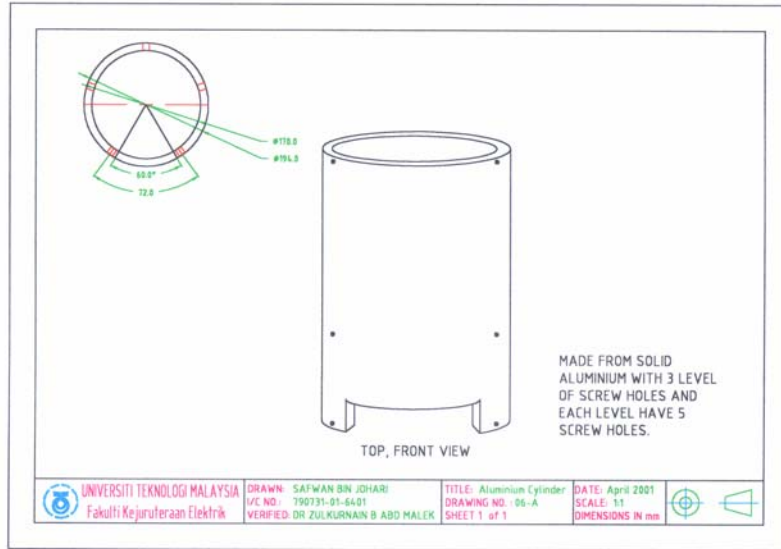
Figure 6.18   Aluminium Cylinder 1
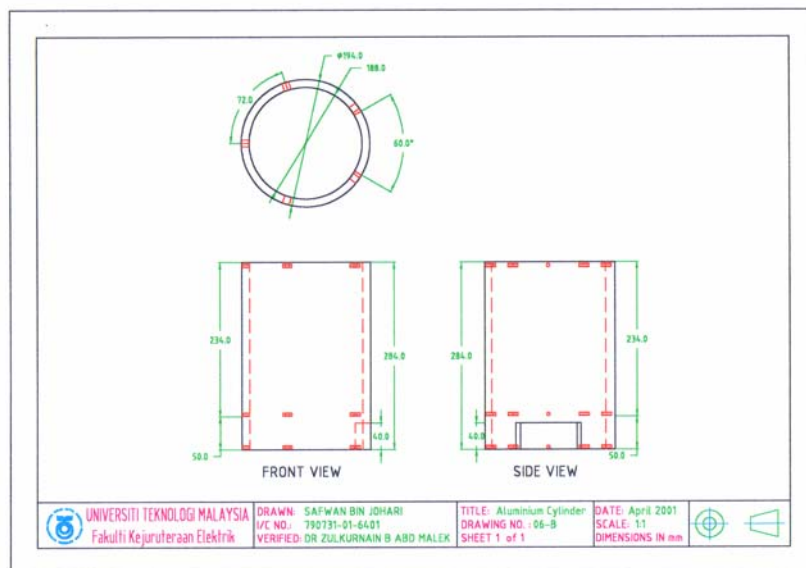
Figure 6.19 : Aluminium Cylinder 2
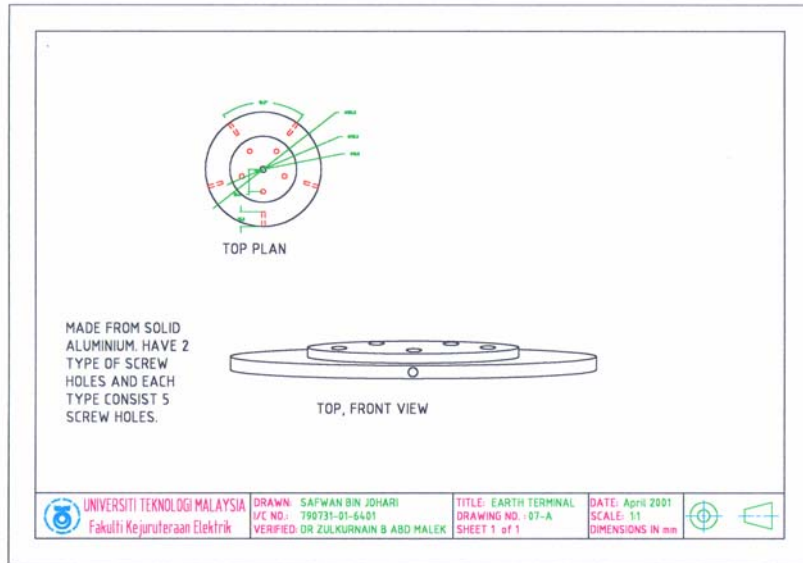
Figure 6.20 : Earth Terminal
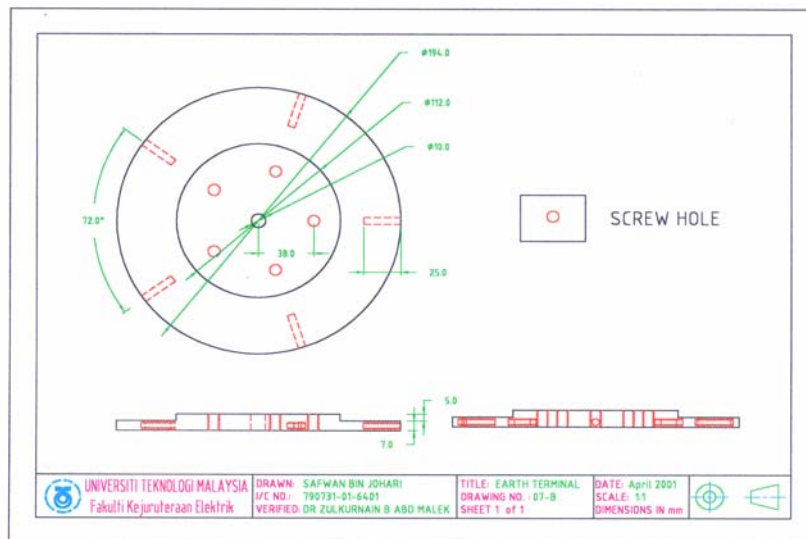
Figure 6.21 : Earth Terminal 2
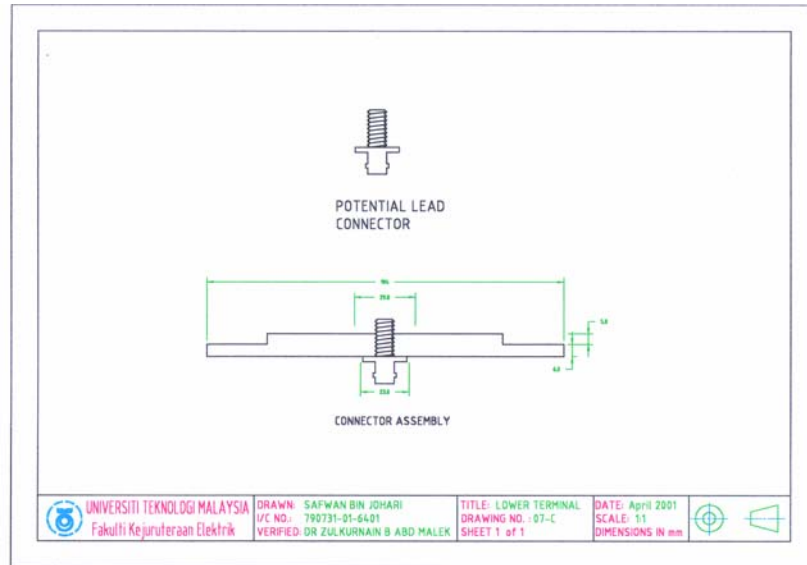
Figure 6.22 : Lower Terminal
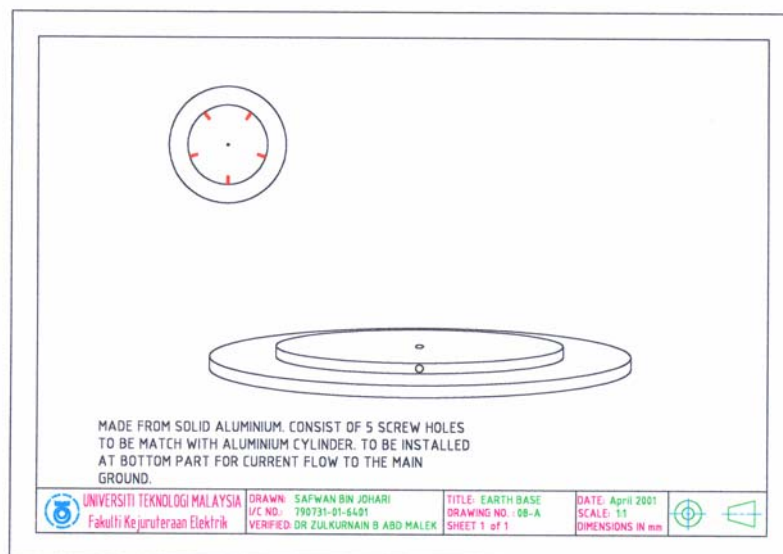
Figure 6.23 : Earth Base
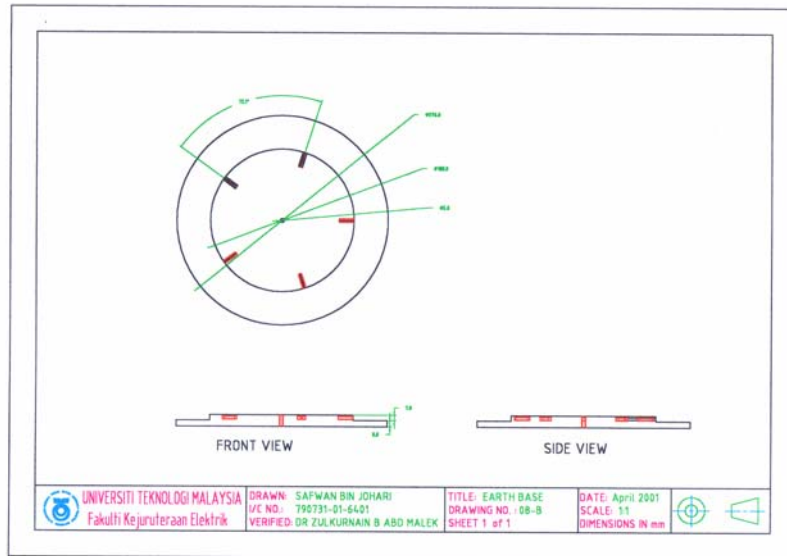
Figure 6.24 : Earth Base 2

6.7   Construction

The Mechanical Production Laboratory, UTM, had been chosen to construct the shunt. However, due to the long delay to get the job done, an outside of the university vendor was engaged. During the project, it was discovered that the Nickel Chromium material could not be obtained in a small amount. Nevertheless, the construction of the coaxial current shunt was carried out without the current shunt material. It is hoped that with future sufficient budget, this construction of the whole shunt can be completed.

6.8   Discussion

The resistance of the shunt needs to be measured using a direct voltage source. The slope of the measured voltage-current curve will give the value of the resistance. The load should be of two types, namely, a known load of linear response and a non-linear zinc oxide surge arrester.

A low inductance arrangement for current shunts is usually achieved by arranging a return current path close to that in the resistive material. A similar performance can also be obtained when the outer aluminium shielding cylinder shunt is earthed in a coaxial manner at the top (whilst isolating the bottom of the shunt from earth) as compared to the case when the shunt is earthed at the bottom via the aluminium supporting cylinder.

6.9   Conclusions

This chapter deals with the theoretical consideration in designing resistive tubular shunt for measurement of current impulse with peak magnitude approximately 10 kA and pulse duration approximately 10 µs. Most of the discussion has been how to design a 5 mΩ resistor suitable for high current measurements.

The chapter also describes the construction of the current shunt up to its completion except for the resistive foil. The resistive foil was unable to be obtained locally due to its unavailability locally. Due to this, the current shunt could not be used in the high voltage high current surge arrester test facility.

CHAPTER 7

HIGH CURRENT SWITCH
DESIGN AND CONSTRUCTION

7.1   Introduction

A high current switch is simply a spark gap switch. Spark gap switches are commonly used in trigger generators;

Pulse forming networks, Marx generators and other high-energy pulsed power systems. They are particularly well suited for applications that require switching of very high voltages and rather high currents. Triggered spark gap is a simple device. A high voltage trigger pulse is applied to a trigger electrode initiates an arc between the anode and cathode electrodes. Triggered spark gaps or triggered high current switch is more advantageous in means to control the switch activation. Trigger mechanism include field distortion, laser induced, UV illumination. Laser triggering is suitable for low jitter applications but the cost is much higher compared to other methods. However, other triggering mechanism is still relatively simple for most applications.

The spark gap may be filled with a wide variety of materials (gas). The most common are air, SF_6, argon and oxygen. It may also be left as vacuum. Often a mixture of gases is used. Solids may also be used but they are usually designed for single shot use (used only once).

The approach to design such a device requires knowledge on the desired operating voltage, the allowable current to flow, insulation strength, high voltage clearances and other skills such as ergonomics and manufacturability. In the application of the design, the knowledge in constructing an impulse current generator is vital as such to determine the ability of the switch and the current generator. This includes the capacitor bank, inductance of the circuit, resistance. They are predetermined in order to obtain the desired impulse shape of voltage and current.

In this chapter, first the methodology of the project is explained in detail. It describes the design consideration, design concept, fabrication, measurement and testing of the developed switch. Then the results of the test were displayed along with some discussions. The conclusion of the project is also described along with the recommendations for further works.

7.2   Design consideration

7.2.1   Size and shape of electrodes

The main component of the switch is the electrodes, which are made of brass. Deciding the dimension of the electrodes is based on the diameter of the uniform filed electrode and the thickness. A diameter of 50mm is chosen and thickness of 10mm.The dimensions is based on a previously designed triggered switch by (Naylor, P. 1995). The shape of electrode is of a disc type with a flat surface and a smoothened edge. It was intentionally shaped to a Rogowski profile, whereby the x and y coordinates of the edge of the disc is contoured to the equipotential line of the field. However, due to the difficulty of machining the electrode, only a simple curving surface that diminishes the edge is chosen.

7.2.2   Maximum gap setting

The maximum gap between the electrodes is chosen to be around 30mm. This is chosen as to enable the gap to withstand 100kV stress without self-breakdown. This can be referenced to the graph below.
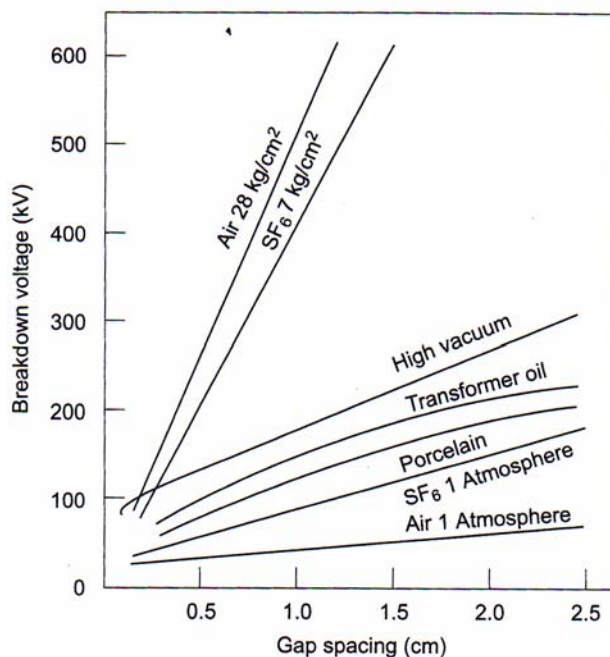
Figure 7.1 :   Breakdown voltage vs gap

It can be seen that from the graph, breakdown voltage of 175kV can be achieved at 1 atmosphere of SF_6 with a gap spacing of around 25mm.Adding a safety factor of 20% gives 30mm maximum gap setting.

7.2.3   Thickness of insulation (acrylic)

The thickness of insulation concerned is to insulate the HV electrode from any flashovers to the environment. This is chosen to be at least 10mm thick.

7.2.4 Electrode bolts and termination

The electrode discs will have to be terminated with the circuit to be used. Therefore, a threaded bolt specially made, to be connected to the discs was also designed. Then, as to terminate the cables, two flat washers and two nuts were provided.

7.2.5 Gap adjustment

To adjust the gap, the threaded bolt is shaped as to allow the use of a spanner to turn the bolt. This would then adjust the gap up or down.

7.2.6 Acrylic as the body of the switch

The acrylic is divided into two parts, top and bottom. The top part will house the HV electrode, while the bottom part will house the Earth electrode. The two parts will be joined uniformly using eight plastic bolts. The use of plastic bolts is required in order to avoid any interference on the field in the gap under high voltage stress

7.2.7 Spark plug as the trigger

The spark plug is embedded into the earth electrode and the tip of the spark plug is levelled of with the earth electrode's surface. This is because the body of the spark plug is also considered as the earth / ground of the switch and also the whole system.

7.2.8 Rubber rings and 'O' rings as seals to the gap

The gap will be injected with SF_6 gas at certain pressure. Therefore, it needs to be pressure sealed as to ensure the injected gas will maintain the pressure and not be lost to the environment. For this purpose rubber rings or 'O' rings have been placed at these particular points.

a)   Between the top and bottom casing

b)   Between the HV electrode and the top casing.

c)   Between the earth electrode and the bottom casing.

d)   Between the HV electrode bolt and the top casing

e)   Between the inlet valve and bottom casing.

7.3   Design concept - Ease of fabrication

To achieve this, all the dimensions are ensured not to be too small. This would cause a problem for fabrication. The tolerance provided is considered as up to +/-1mm. Even though most machines operate below this range, it would help in ensuring that the fabricated item will work well even there are some measurement errors involved in the process.

Furthermore, the other materials to be used such as rubber rings and plastic bolts are sourced prior to the design of the switch. This would give some guidance in designing process and also lead-time in fabrication stage.

7.4   Fabrication

The design was sent to NZZ Engineering in Taman Kobena. In this stage, the main consideration is the smooth finish of the electrode surface, smoothing of the edge and ensuring the gap is tight sealed so that no leakage of the gap medium to the environment will be present.

7.4.1 Electrode Surface finish

The surface finish was done using a lathe machine with electronic measurement of accuracy up to +/-0.5 mm. This will ensure that the surface is flat across it. The finish of the surface is polished with fine soft wool substituted with the lathe tool. Polishing is controlled by the machine to ensure that the surface remains flat.

7.4.2 Smoothing the electrode edge

Initially, a dimension of Rogowski electrode is provided for the electrode. However, since the diameter of the electrode is only 50mm, the Rogowski profile cannot be achieved with the lathing machine available. It is then decided that a simple curved profile be replaced for the electrodes.

7.4.3 Tight sealing of the gap

To ensure the gap sealing, 'O' rubber rings are used. This is referred to in section 7.1.1.8.

7.5 Testing

7.5.1 Circuit for testing of the switch

The circuit below is introduced in order to test the switch.
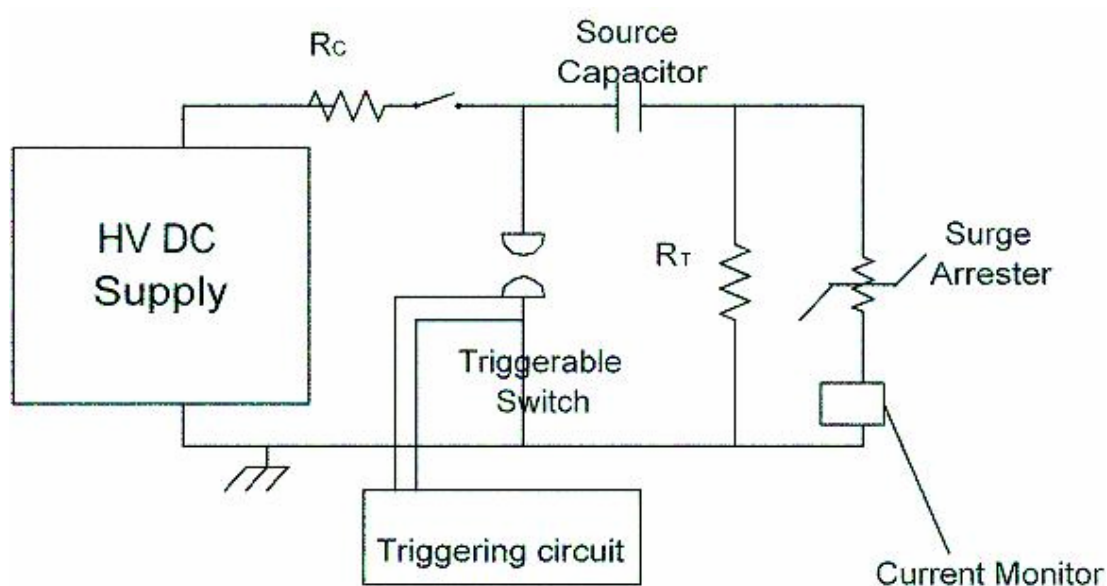
Figure 7.2 : Testing circuit

This circuit consists of

a. R_c: The charging resistor, 10 MΩ high voltage resistor. This resistor controls the charging rate of the Source Capacitor.

b. R_T : The tail resistor, 8.5kΩ high power resistor. This resistor provides the tail time of the impulse voltage produced by the switch.

c. Isolating switch: the isolating switch is located beside R_c. It isolates the supply after the capacitor has been fully charged.

d. Source Capacitor: The source capacitor used is a 1µF, 20kV capacitor. It will store the charge that will flow through the circuit once the high current switch is triggered.

e. Surge arrester: the surge arrester will provide a path for the high current to flow once the switch is triggered and the clamping voltage is

reached. It is rated at 440 volts and maximum current is 5kA. From the experiment, it is found that the clamping voltage is around 3kV.

f.   Current monitor: this device is actually a current transformer with the ratio of 0.001V/A. This means that for each volt recorded by the current monitor (through oscilloscope), there is 1kA of current flowing through the conductor that it monitors (in this case, current through the surge arrester).

g.   The connections between the components in this set-up uses copper strips with thickness of 2mm and width of 25mm. This will reduce the overall circuit inductance. However due to some material limitation, the connection of the circuit to the ground uses a common insulated stranded copper wire with diameter of 3mm.

h.   HV DC supply: This unit supplies the high voltage direct current supply to the capacitor. It consists of AC supply, step-up transformer, rectifiers, measuring resistors and a smoothing capacitor. The arrangement is readily available in Institut Voltan dan Arus Tinggi (IVAT). The circuit configuration is shown below:
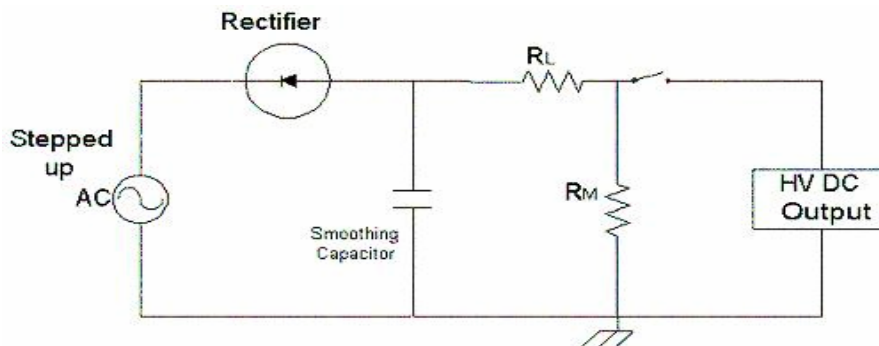
Fig 7.3:   **HVDC supply schematic**

7.6   Measurements

7.6.1   Current

The current is measured using a current transformer with 0.001V/A ratio. The equipment is placed in series and at the low voltage end of the surge arrester. In order to monitor the current flowing through the surge arrester only, the strip conductor connected after the surge arrester is passed through the current monitor. This ensures that if no current flows through the surge arrester, the current monitor will detect no current flow. The output voltage of the current monitor is fed into a digital oscilloscope.

7.6.2   Voltage

The measurement of the voltage across the surge arrester is done using a capacitive divider of ratio 360:1. The output is also fed into a digital oscilloscope. However, the result will not be displayed due to the signal captured by the oscilloscope is full of noise and distorted and may not be true for our purpose.

7.7   Results

7.7.1   Designed switch

The designed switch is shown in the 2-dimensional drawings in the Figure 7.2. With this drawing (information), the design is sent for fabrication.

7.7.2 Fabrication

The fabrication is done by NZZ Engineering. They take around a month from the receipt of the drawing till completion of job. They also include the supporting structure of the switch, which is not included in the drawing.

The fabricated switch is as shown in Figure 7.4 below:
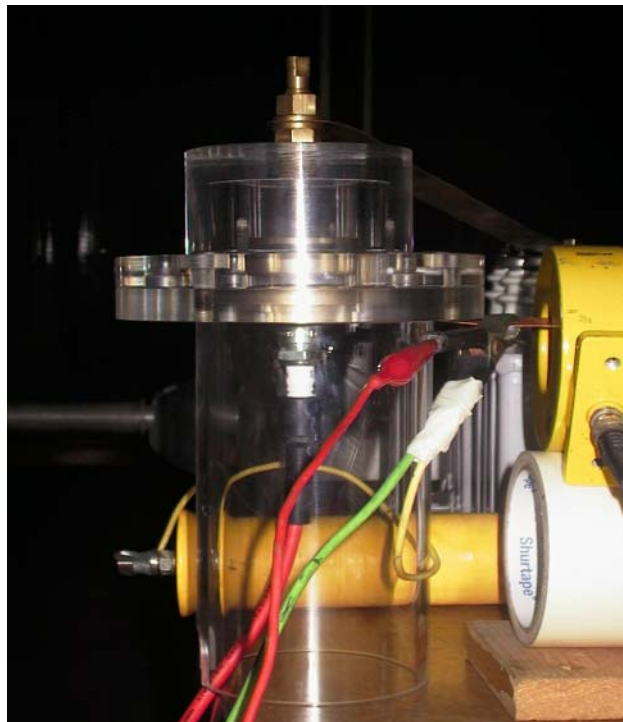
Figure 7.4 :   Photograph of the developed switch

7.7.3 Maximum Current

The maximum current that can be generated with the circuit and the high current switch is 5.4kA. This can be shown with the plot of the digital oscilloscope (from current monitor) as in Figure 7.5 below.
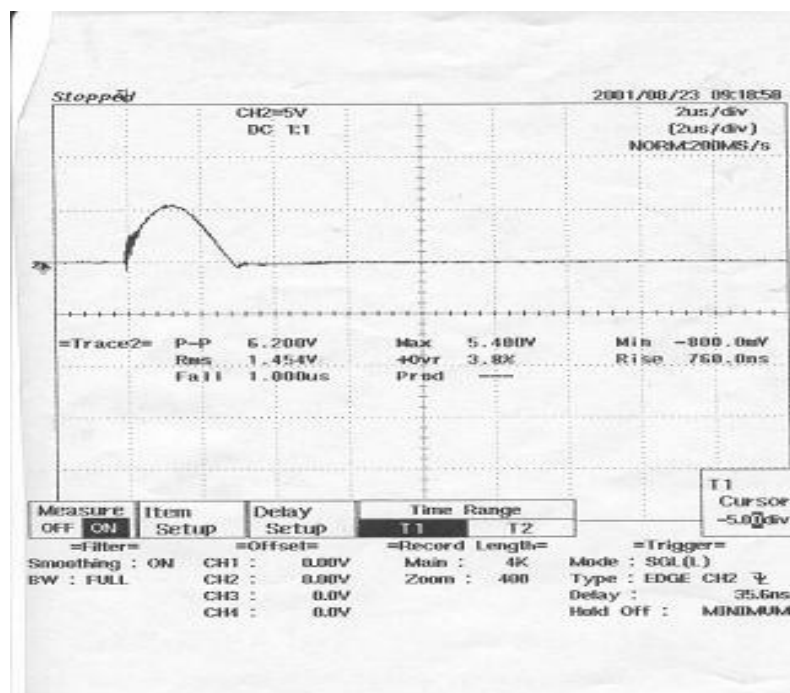
Figure 7.5 :   Output from Current monitor.

7.7.4   Risetime of impulse current

It can be noted from Fig 7.4 above that the risetime is approximately 1 μs. (As the time to peak takes half of the division scale, and with the time per division of 2 μs)

7.7.5   Voltage Applied

The voltage applied on the source capacitor to achieve the maximum current is around 8.4 kV, with a charging time of at least 2 minutes.

7.8   Discussion

7.8.1 Maximum Current

The maximum current in the circuit is not limited by the designed switch characteristics. It has been shown in chapter 2.1.7.4 that the maximum current depend on $\dfrac{W}{\omega L}$. The maximum current in the circuit is limited indeed by the impulse current generator circuit characteristics. They are the circuit's charging voltage, capacitance and inductance. It is also evident from equation (2.3) that in order for high peak currents, the inductance of the circuit should be low.

7.8.2 Risetime

The risetime of the impulse is also limited by the inductance of the impulse generator circuit. In the test, the risetime is found to be of approximately 1 μs. The inductance of the circuit is high and this is due to the source capacitor used and copper strip is not used to connect the whole test circuit to the ground.

7.8.3 Current flowing through spark

For a certain given characteristics of the circuit, the maximum current allowable through the gap will depend on how much current will flow during the breakdown process. This is similar to 7.3.1 whereby it is limited to factors other than the switch parameters.

7.8.4   Breakdown Process

The breakdown process occurring at the switch may be classified to uniform or non-uniform field breakdown.. This can be differentiated by the breakdown location across the electrode. If the breakdown occurs at the edge of the electrode, this can be classified as non-uniform field breakdown, which is usually preceded by corona. This type of breakdown occurs at voltages less than the withstand voltage of the gap and the current flowing should be much less. For breakdown occurring at the centre of the electrode, this can be considered as a uniform field breakdown.

7.8.5   Inductance of Circuit

The inductance of the impulse generator circuit may be calculated from equation (2.5) given that the other characteristics of the circuit such as the circuit's capacitance and resistance are known with the output fall time.

7.8.6   Uniformity of the electrodes

It is noticed that at very short distances (5 to 15mm) and very long distances (25 to 33mm), the spark (breakdown) occurs at the edge of the electrodes. This proves the non-uniformity of the electrodes, whereby the breakdown occurs at the higher stressed area of the electrode.

7.8.7   Test at Higher Voltages

The switch has not been tested to trigger at higher voltages of more than 9 kV. However, it has been tested with higher voltages to determine the gap withstand

voltage. With a maximum gap setting of 3.3cm, the highest withstand voltage of the gap is tested to be 33kV, whereby self-breakdown of the gap occurs. In order to achieve higher withstand voltage for the gap, pressured SF_6 as the gas medium must be used. The 100kV withstand should be achieved as addition of 30% of SF_6 into the air would increase the withstand voltage by 100%.(Kuffel, E. and Zaengl, W.S, 1984).

7.9   Conclusions

The developed switch is able to switch up to 5kA impulse current with the current impulse generator set up. The limitation is due to the circuit's inductance, capacity of the source and the charging voltage of the generator.

The risetime of the current is not up to the objective of 0.1 to 0.5 μs. This is due to some inductance present in the capacitor and also the grounding wire.The switch has not been tested to a 100kV DC stress with the medium of pressured SF_6 used.

Tests with pressured SF_6 should be conducted to determine the highest withstand voltage of the switch. The switch should be able to withstand up to more than 100kV, as the pressured SF_6 will increase the insulation level of the gap in the switch.

A low inductance capacitor should be sourced. This is to help minimise the characteristic inductance of the impulse current generator and thus increasing the peak current and the risetime of the impulse current.

The electrodes used should be profiled to a uniform field electrode. It is noted that the difficulty of producing the profile is due to the size of the electrode, which is small. In order to obtain the profile, increasing the size of the electrode would help as

the tolerance would then increase with the size. This would help in increasing the gap withstand voltage and also avoiding breakdown at the edges of the electrodes.

The edges present on the HV electrode bolt may cause corona when subjected to 100kV dc. They will need to be smoothened as they could create higher field stress at the edges. Alternatively, stress relieving corona rings could be used.

CHAPTER 8

HIGH CURRENT HIGH VOLTAGE
SURGE ARRESTERS TEST FACILITY

8.1   Introduction

The previous three chapters (Chapters 5, 6 & 7) describe the design of important elements in the high current high voltage test circuit suitable for distribution-level (11 kV) zinc-oxide surge arresters. The elements are the D-dot based voltage transducer, the current shunt, and the high current switch.

In this chapter, these elements are combined with the source capacitors and the charging circuit to complete the test circuit. The test circuit was used to carry out preliminary tests on five samples of zinc oxide surge arresters and a linear liquid resistor.

8.2   Experimental Set-up

The experiment was set up to produce a fast transient (1/4 µs) impulse current. For wave shaping, R_{front} was not used in this case whereas R_{tail} was connected in

parallel with the surge arrester sample. For DC charging voltage generation, two diodes were connected in series to cope with the high peak inverse voltage. A large copper plate was used as ground.

DC voltages were measured using the resistive potential divider. As noted in Chapter 6, the current shunt is yet to be completed and hence was not used in the test. Signals were channeled to the digital oscilloscope through suitable coaxial cables.

For safety, the earthing switch was installed. The high current switch or the spark gap consisted of two planes adjusted to a certain distance to obtain the desired flashover voltage. The complete experimental circuit is as shown in Figure 8.1.

The output voltage measured by the D-dot probe was calibrated using a commercial capacitive divider which as connected in parallel with the D-dot probe. The high current impulse was measured using a commercial current transformer instead of the designed impulse current shunt.
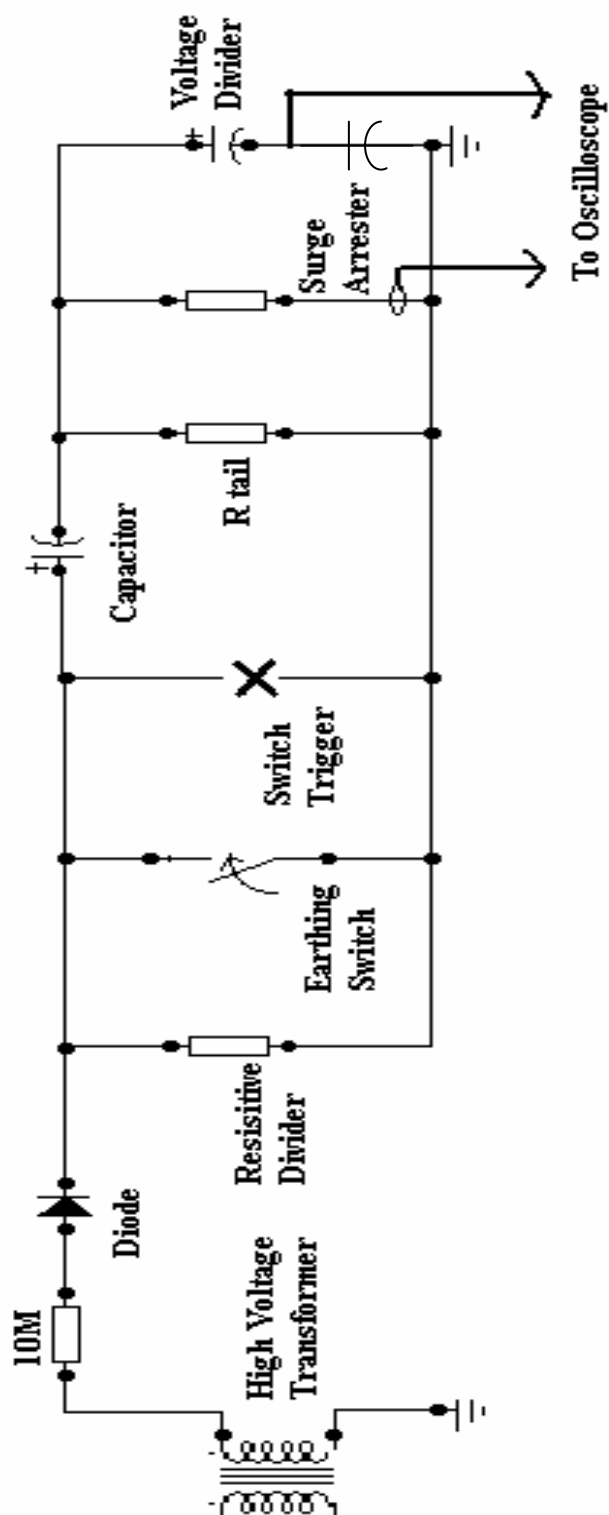
Figure 8.1: **Circuit of the Experimental Set Up**

8.2.1 Operation of the Test Facility

The high voltage transformer steps up the voltage. The alternating current is rectified to dc by the two half-wave diodes. More diodes can be used in series to produce a higher peak inverse voltage. The capacitor is then fully charged and when sparking takes place, the capacitor discharges through R_{tail} and the load. For higher breakdown voltages, the distance of the gap can be adjusted to larger spacing. It can also be done with the use of SF_6 gas. Table 8.1 gives the gap breakdown characteristics in term of the gap gas pressure.

Table 8.1: High Current Switch Gap Characteristic (Gap distance = 1cm)

Breakdown Voltage (kV)	Pressure (bar)
32	0.00
41	0.25
52	0.50
60	0.75
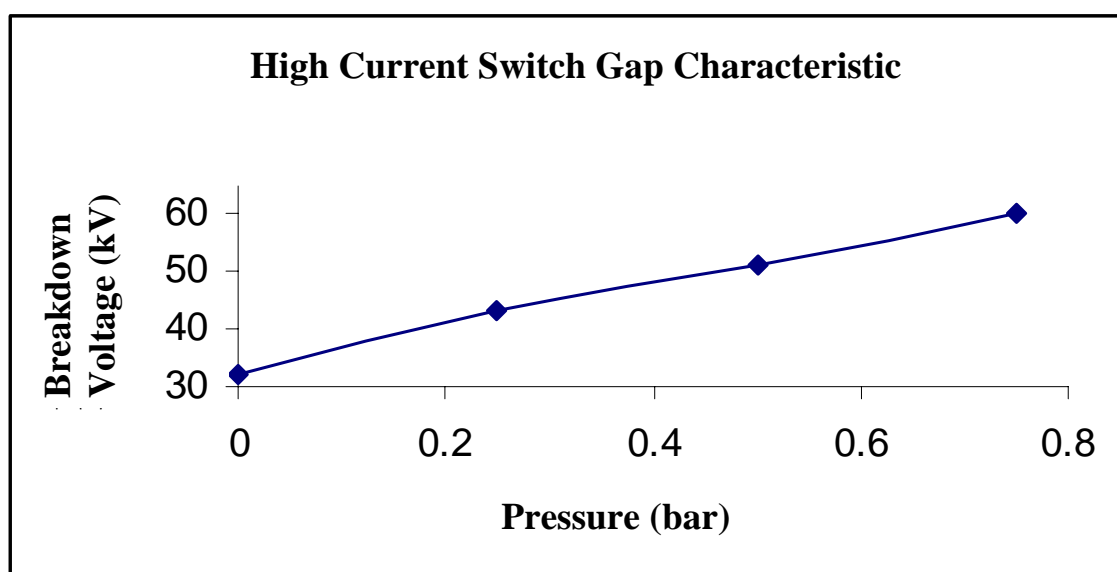
Figure 8.2: High Current Switch Characteristic in term of SF_6 Gas Pressure

Figure 8.2 shows the correlation between the breakdown voltage and gap pressure. From the graph, the breakdown voltage increases with the increase of pressure of the gas. In this case, SF_6 was used. The gas is an electronegative gas and the electron attachment is high, thus, with only a little pressure increase, the breakdown voltage increases significantly.

The resistive potential divider measured the dc charging voltage. The capacitive potential divider was used for impulse measurement and the Rogowski coil for impulse current measurement. A 20m (50Ω) coaxial cable was used for transmission of signals to the oscilloscope.

For safety, the earthing switch was installed. Every time the circuit was de-energised for modification, the switch is in close position.

8.2.2   The equipment

The following equipment was used in the test circuit.

High voltage transformer
Charging Resistor – 10MΩ, 60W
Diodes – 140kV, 500kΩ, 5mA, 8W
Resistive Potential Divider – 140kV, 140MΩ
Capacitor –0.15 μF
Spark Gap (Switching)
R_{tail} - 2400Ω
Capacitance Potential Divider – 1200pF
Rogowski coil – Max current: 500kA
Digital Phosphor Oscilloscope
Digital Measuring Instrument
Operating Terminal

Figure 8.3 shows the complete test set-up. Figures 8.4 and 8.5 show the controlling panel and the Rogowski coil used.
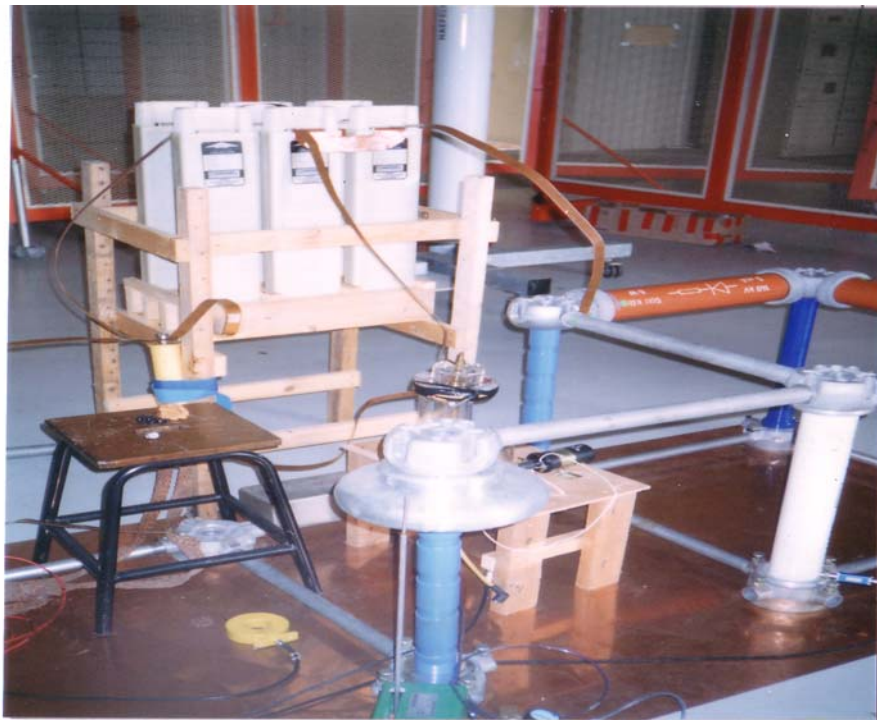
Figure 8.3 (a)

Figure 8.3 (b)

Figure 8.3 (c)

Figure 8.3 (a) to Figure 8.3 (c) : Experimental set-up
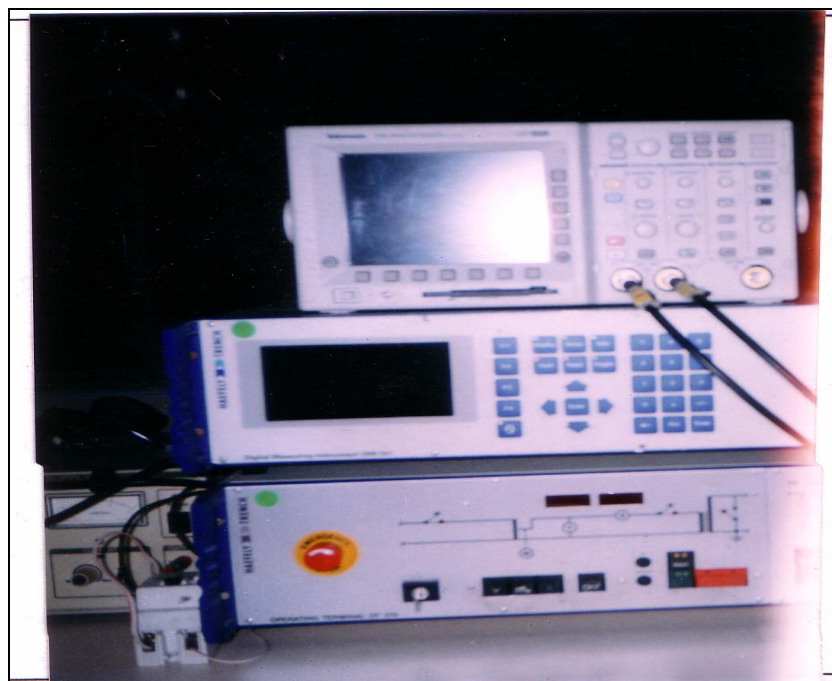
Figure 8.4 : Control Panel
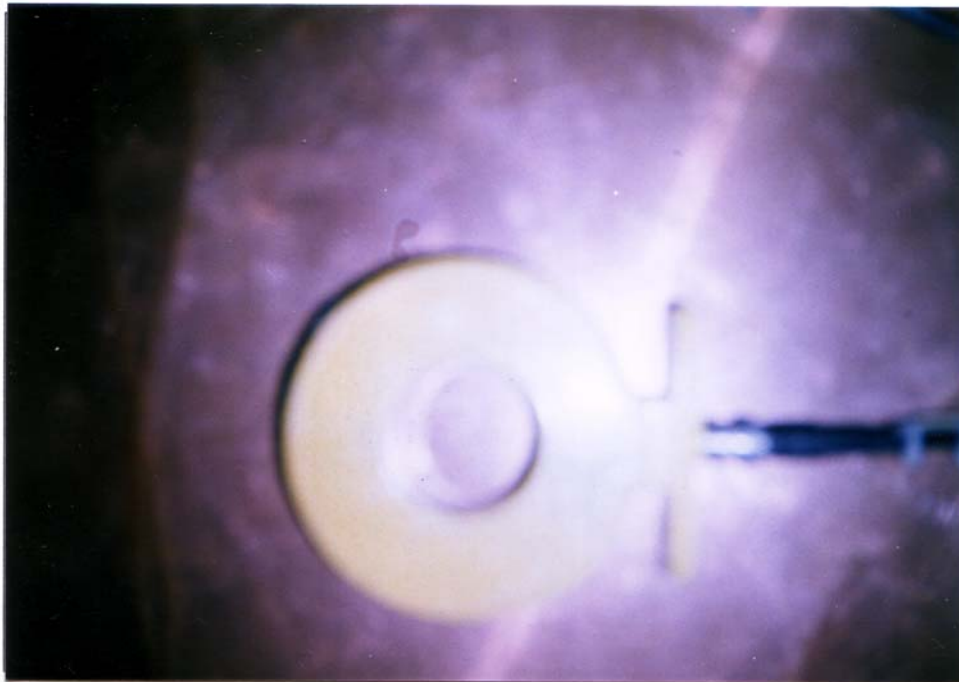
Figure 8.5 : Rogowski Coil

8.3   Methodology

The dc high voltage generation for the charging unit was done using two diodes. A charging resistor was used to limit the current. The wave shaping circuit was made up of the capacitor and R_{tail} as shown in Figure 8.1. The measuring instrument were appropriately installed or situated at their locations.

The surge impedance of the coaxial cable connecting the measuring instruments to the oscilloscope must be chosen correctly to avoid distortion in the waveshape. Correct impedance matching at the termination was ensured for proper signal transmission of the measuring circuit.Usually, a resistor or a series of resistors is used in case of a resistive potential divider, or a single or a number of capacitors in case of a capacitive divider (Naidu, 1995).

The spark gap characteristic used for switching was determined as previously described. The gap length was gradually incremented and the breakdown voltage was

recorded. To raise the breakdown voltage further, the gap was filled with SF_6 gas. The breakdown voltage increases as the pressure of the gas in the gap is increased.

The fast transient impulse was first generated with an open circuit load. There was no load or surge arrester connected. The front and tail times were determined from the oscillograms displayed at the oscilloscope. Adjustments were made if the impulse did not indicate the one needed.

A copper sulphate solution was prepared and used as a liquid resistor. It was used to calibrate the set up and to ensure that the transducers are working properly. Under this linear resistive load, similar voltage and current waveshapes were expected to be produced for if the load was replaced by an arrester.

If the magnitude of the waveshape captured at the oscilloscope was too big and was beyond the oscilloscope range, an attenuator should be used. Invariably, the attenuator is stated in terms of decibel (dB). Therefore, the divider ratio calculation shall include the attenuation applied. In this experiment, 20dB and 10dB attenuators were used when the surge arresters were tested. Attenuator was not needed when the liquid resistor was tested instead.

Voltage and current oscillograms of the liquid resistor were obtained up to the peak current of 5kA, which was the rated current of the surge arrester samples. The values of the current peak and the voltage peak at the instant of current peak were recorded for the increasing breakdown voltages. This step was repeated with each of the surge arrester samples. The residual voltage versus the discharge current was later plotted on a logarithmic graph.

Distortions on the waveform and errors in measurement were observed and these could be caused by:

i) Stray capacitances occurring
   a) between the elements;
   b) from section and terminals of the elements to ground;
   c) from the high voltage lead to the elements or sections.

ii) The impedance errors due to

    a) Connecting leads between the divider and the test objects

    b) Ground return leads and extraneous current in ground leads

iii) Parasitic oscillations due to lead and cable inductances and capacitance of high voltage terminal to ground

As this was a high voltage experiment, it was important to take several precautions. Whenever an accident happens, the emergency push button at the control panel must be pushed. Everytime when adjustments were to be made to the circuit, the earthing switch must close. For added safety precaution, the set up should also be grounded manually with a rod.

The details of the experimental setting are as listed below

Attenuator for voltage signal: 20dB

Attenuator for current signal: 10dB

Spark gap: 1 cm

Current monitor sensitivity: 0.001V/A into 50Ω

Max current: 500kA

DC Voltage Divider setup

    High Voltage/Low voltage Ratio: 18666.6V/V

Impulse setting

    Divider ratio: 375.3V/V

    Polarity: Negative

    Signal Input (DMI Channel): Low 400V

8.4 Surge arrester samples

Throughout the experimental work, there were six samples being tested consisting of one liquid resistor and five surge arresters. Each rated 12kV, 5kA.The surge arrester samples were of different manufacturers, year manufactured and housing.They were all gapless ZnO surge arresters. Thus there were no integrated series or parallel spark gaps. Table 8.2 shows the details of the manufacturers, years manufactured and housing materials. Figure 8.5 shows an example of the Rogowski Coil set up used for current measurement. Figures 8.6 to 8.10 show the arrester samples.

Table 8.2: Manufacturer, year manufactured, housing types and other information for various surge arrester samples

Sample	Manufacturer	Date manufactured	Housing	Rated Voltage	Rated Current	Comment
A	Ohio Brass	2002	EDPM	12kV	5kA	New
B	Oblum	1994	Porcelain	12kV	5kA	Used
C	Oblum	1992	Porcelain	12kV	5kA	Used
D	(Manufactured in Japan)	Unknown	Porcelain	12kV	5kA	New
E	Unknown	Unknown	Porcelain	12kV	5kA	Used
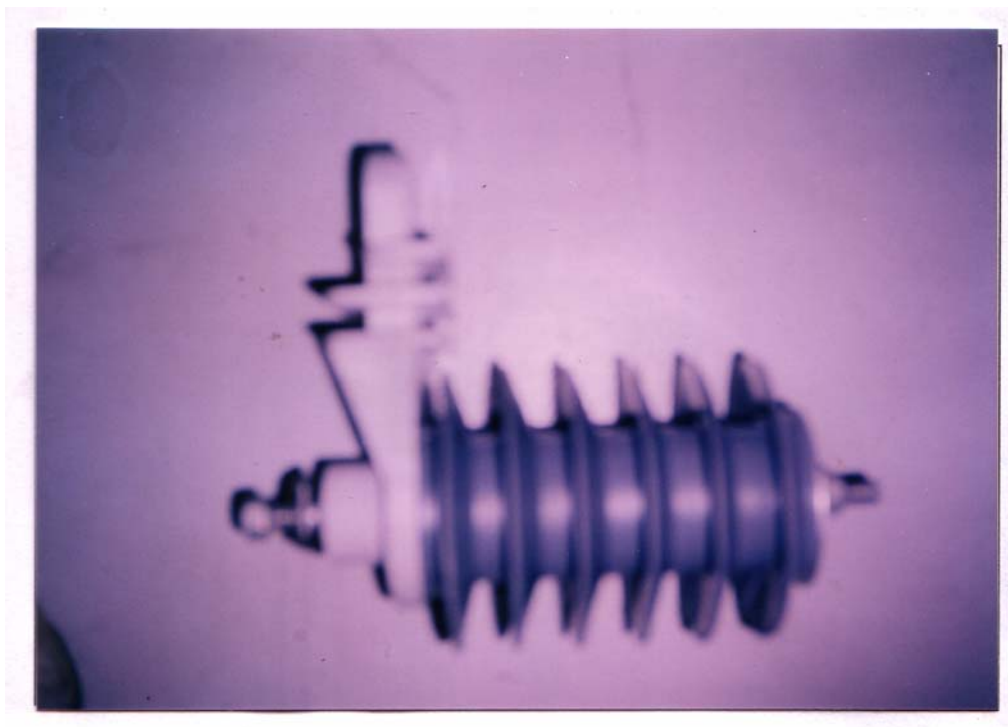
Figure 8.6:   Sample A

Figure 8.7: Sample B

Figure 8.8 : Sample C

Figure 8.9 : Sample D
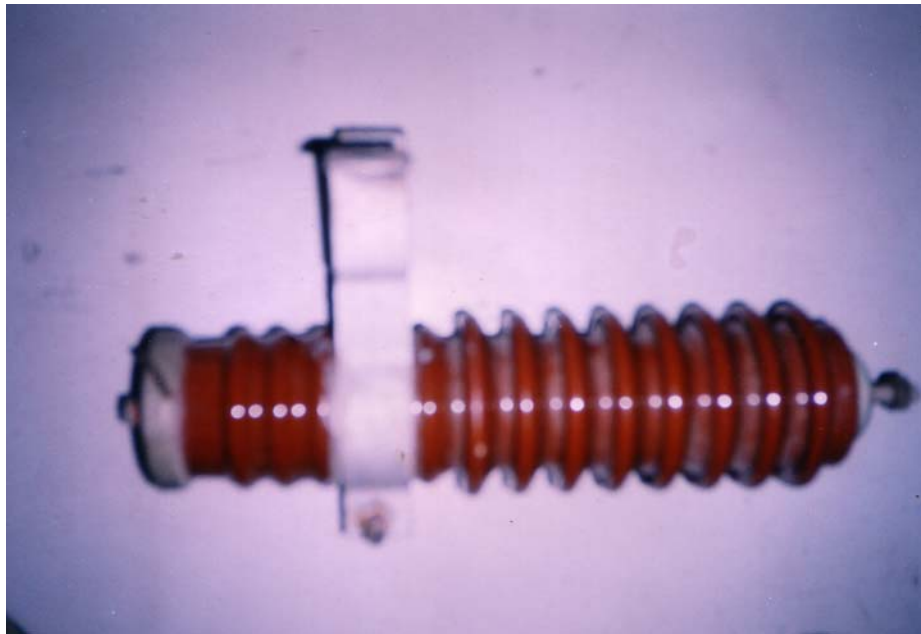
Figure 8.10: Sample E

8.5   Experimental Results

In this section, the results of the tests in the form of voltage-current (V-I) characteristics of the samples will be reported.

The V-I characteristic is dependent upon the type of transients being simulated. The V-I characteristic varies with the waveshape of the arrester current. Current waveshapes with a faster rise time will result in a higher peak voltage. Therefore, theoretically there will be several curves for different impulse current waveforms.
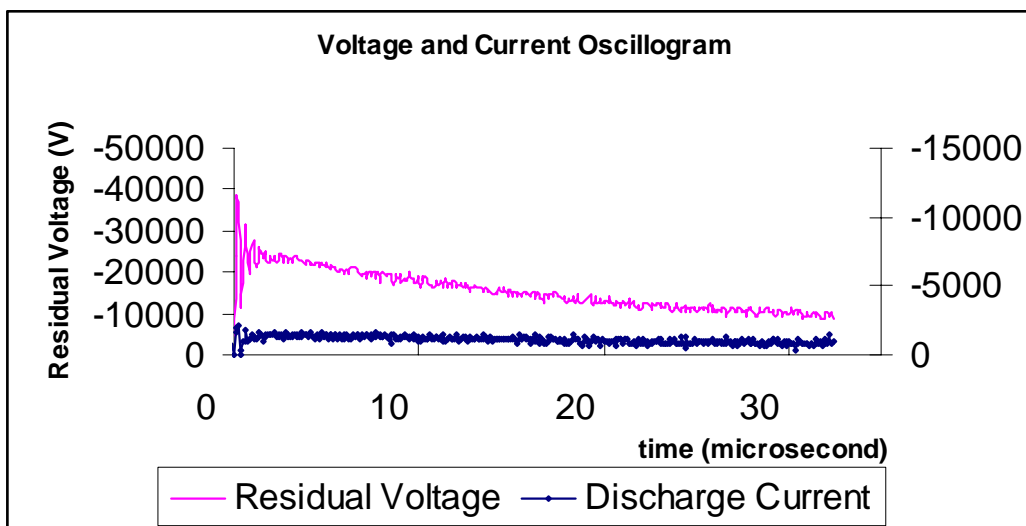
Figure 8.11: Voltage and Current Oscillograms at 1kA
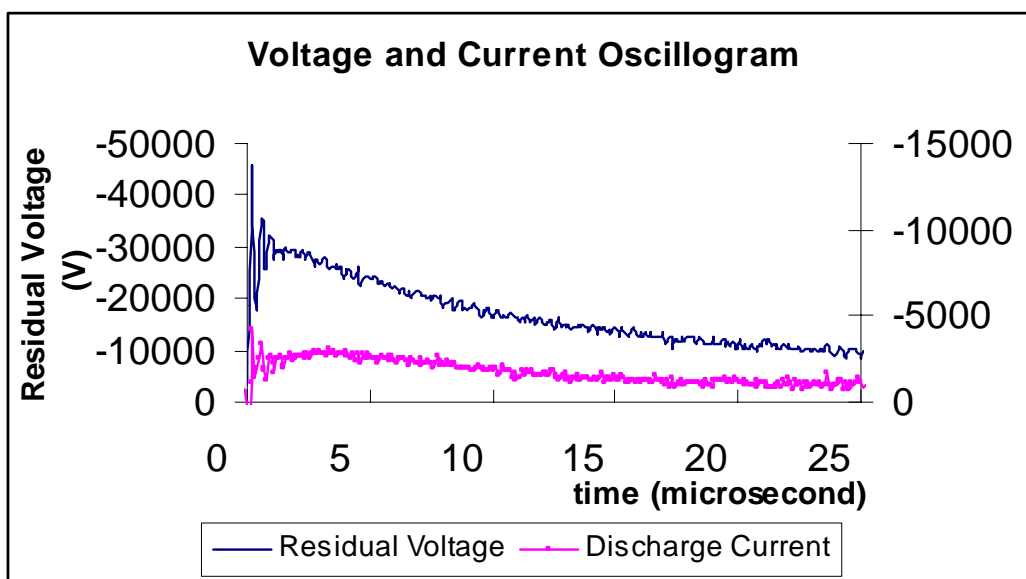
Figure 8.12: Voltage and Current Oscillograms at 3kA
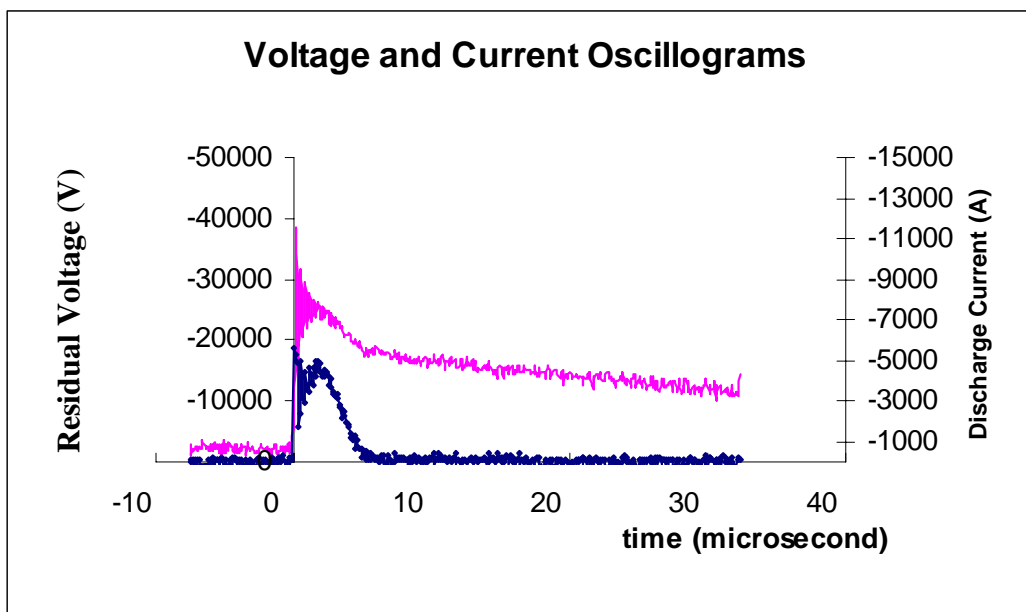
Figure 8.13: Voltage and Current Oscillograms at 5kA

Figures 8.11 to 8.13 show the voltage and current oscillograms for one of the samples. Figure 8.11 shows voltage and current oscillograms at 1kA. Figure 8.12 shows voltage and current oscillograms at 3kA while Figure 8.11 shows voltage and current oscillograms at 5kA. All the other samples also produced similar voltage and current oscillograms. The steep front of current waveshape approaches peak value of 5kA in 1.8μs. The voltage at the same time values at 25.52kV. It is expected when the front time of the current signal goes any faster, the peak voltage at current peak will measure more than 25kV.

For fast front surges such as those with rise time less than 10μs, the peak of the voltage wave occurs before the peak current wave. For typical overvoltage studies where the arrester current exceeds 10 amps, the temperature dependence does not need to be represented in simulations.

Voltage and Current Oscillograms
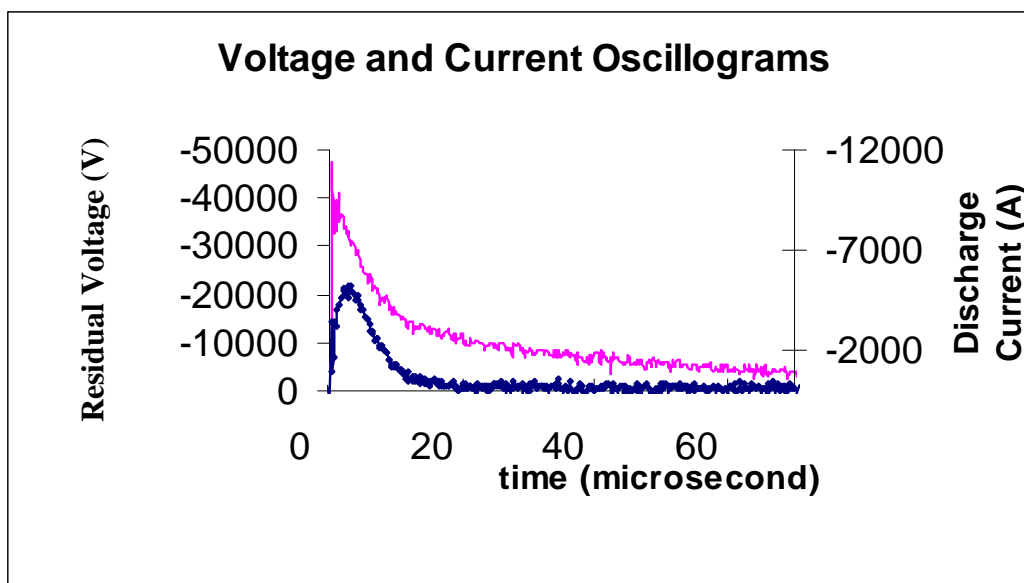
Figure 8.14: Relationship of Peak Voltage and Current Peak for Fast Transient

Figure 8.14 shows the voltage and current oscillograms for one of the samples. It shows the relationship of peak voltage and current peak for fast transient. The current reaches peak value with rise time of 3.2μs (<10μs). However, it only takes approximately 1.4μs to reach voltage peak of 35.6kV. Obviously, the rise time of the current is bigger than that of the voltage.

For current surges with front times faster than about 10μs, the residual voltage across the arrester increases as the time to crest of the arrester discharge current decreases, and the arrester residual voltage reaches a peak before the arrester discharge current reaches its peak. Indeed, the voltage across the arrester is not only a function of the discharge current, but also of the rate of rise. These characteristics are referred as a frequency-dependent behavior.

It also mentioned that for arrester discharge currents with time-to-crest shorter than 4μs, voltage spikes appear on the front of the arrester residual voltage waveform.
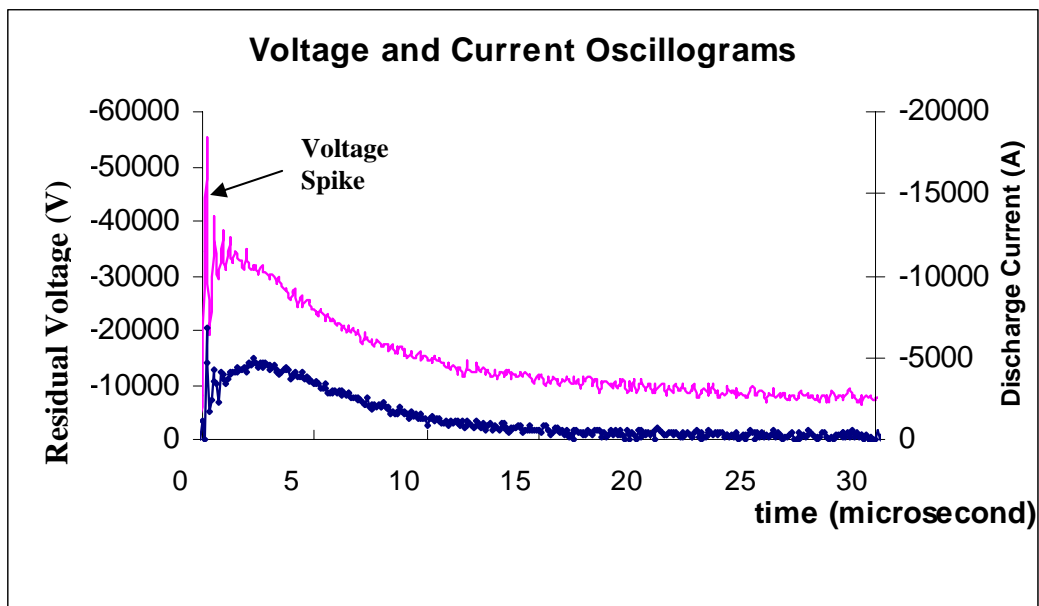
Figure 8.15: Occurrence of Spike in Waveform

Figure 8.15 shows the oscillograms with a smaller time scale. There is an obvious voltage spike at the beginning of the voltage waveform. However, this phenomenon can not be explained theoretically and therefore can be attributed to measurement errors or noise in the voltage transducers.

8.5.1   The V-I characteristic

The V-I characteristic is obtained by plotting the I_{peak} and V (at I_{peak}) with the increasing charging voltage with I values on logarithmic scale. The same is done for each of the samples. The residual voltage is also called the clamping voltage. From Figure 8.16 the V-I graphs plotted, so the appropriate protective level (Figure 8.16) can be determined.
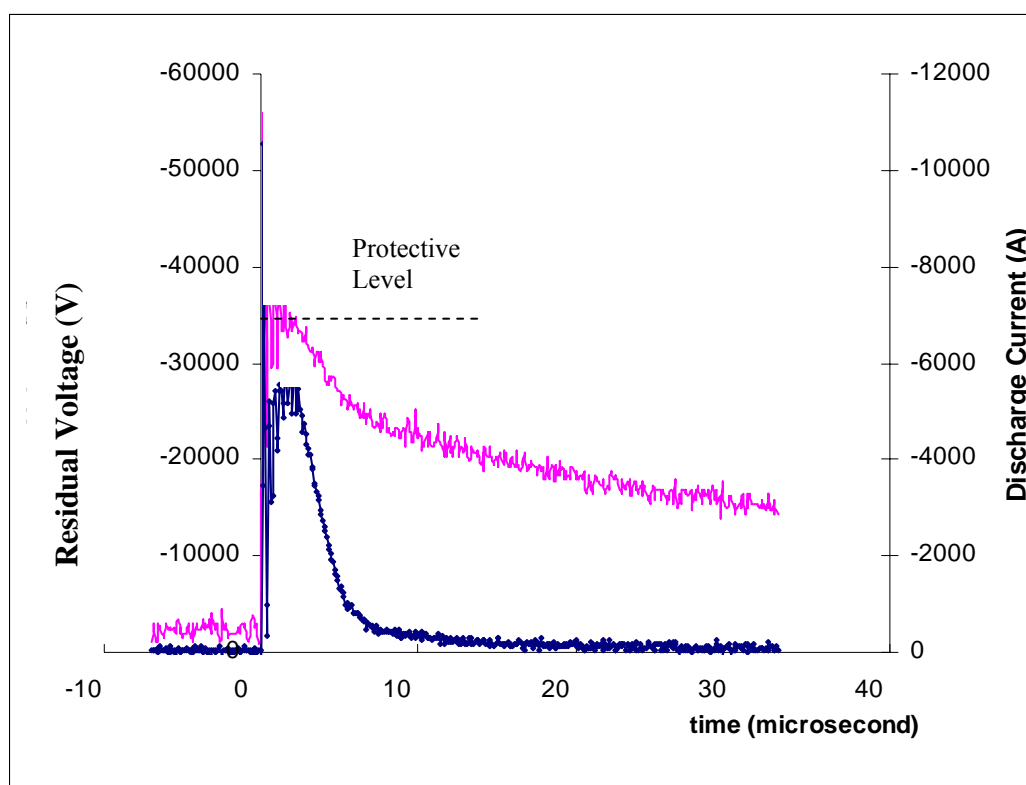
Figure 8.16: The Protective Level Voltage

The V-I characteristic of Sample A are shown in Table 8.3 and Figure 8.17.

Table 8.3: The Protective Level Voltage and Peak Discharge Current of Sample A

Charging Voltage (kV)	Protective Level Voltage (kV)	Peak Discharge Current (kA)
30	22.89	3.16
35	25.14	5.25
40	25.89	7.72
45	30.24	10.12
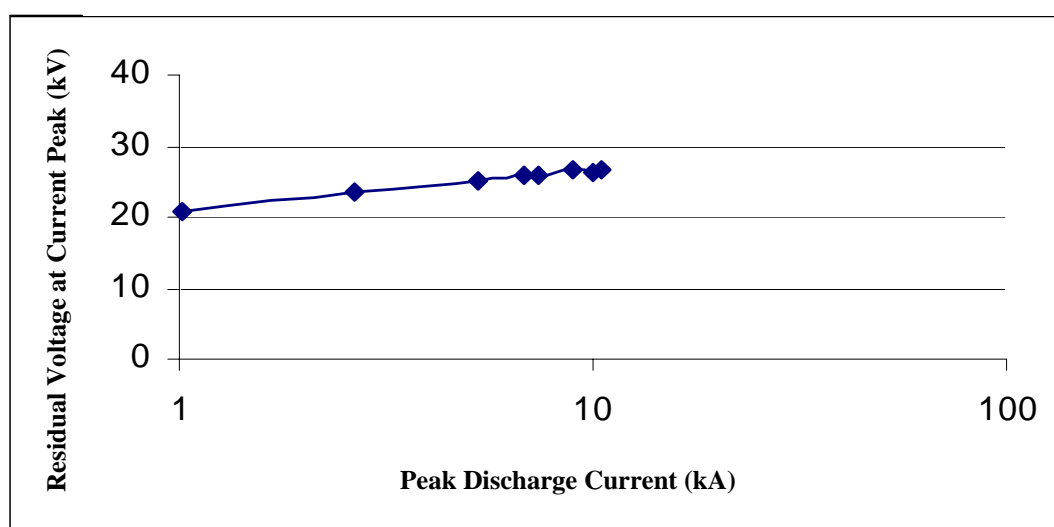
Figure 8.17: The V-I Characteristic of Sample A

As the residual voltage increases, the discharge current also increases. The residual voltage ranges between 20 to 30kV, therefore the protective level should be taken as more than 30kV.

The V-I characteristic of Sample B are shown in Table 8.4 and Figure 8.18.

Table 8.4: The Protective Level Voltage and Peak Discharge Current of Sample B

Charging Voltage (kV)	Protective Level Voltage (kV)	Peak Discharge Current (kA)
40	26.271	2.85
45	29.27	4.68
50	33.40	6.07
55	34.15	6.83
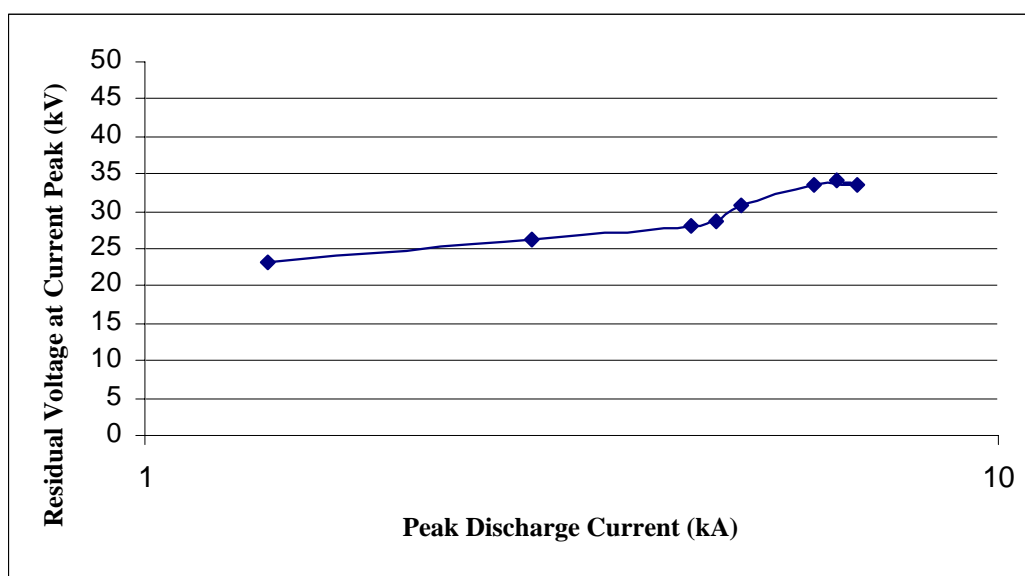
Figure 8.18: The V-I Characteristic of Sample B

From Figure 8.18, it is best to fix sample B onto equipment with protective level of 35kV and above.

The V-I characteristic of Sample C are shown in Table 8.5 and Figure 8.19.

Table 8.5: Protective Level Voltage and Peak Discharge Current of Sample C

Charging Voltage (kV)	Protective Level Voltage (kV)	Peak Discharge Current (kA)
40	27.77	2.40
45	30.02	3.23
50	32.65	5.12
55	33.40	6.32
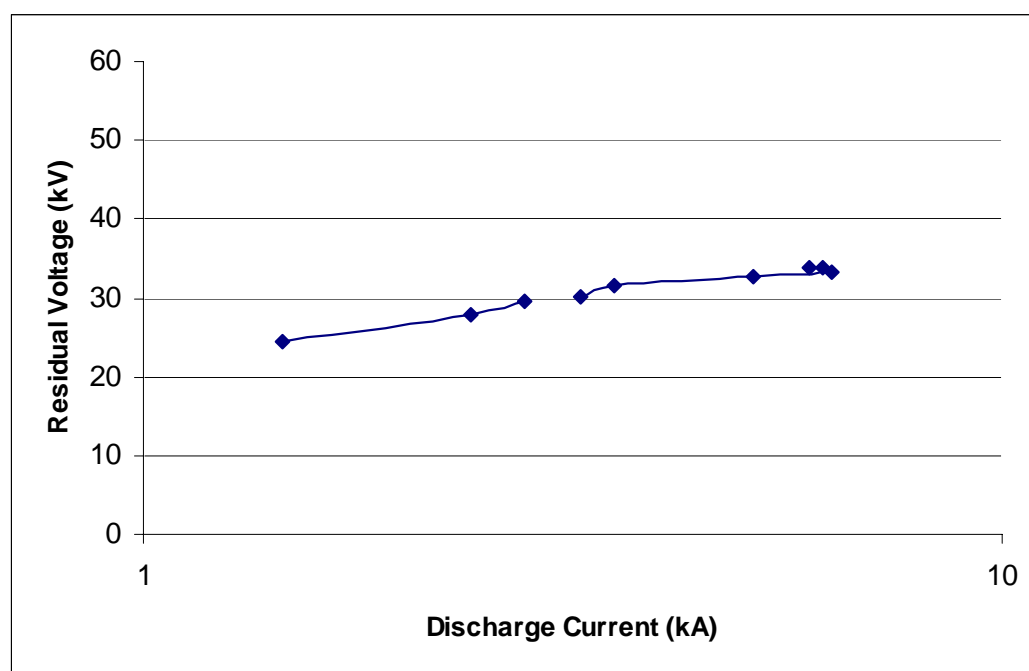
Figure 8.19: The V-I Characteristic of Sample C

From Figure 8.19 the suitable protective level for the use of sample C should be taken as 40kV and above.

The V-I characteristic of Sample D are shown in Table 8.6 and Figure 8.20.

Table 8.6: Protective Level Voltage and Peak Discharge Current of Sample D

Charging Voltage (kV)	Protective Level Voltage (kV)	Peak Discharge Current (kA)
45	33.40	3.38
50	34.53	5.76
55	33.40	5.82
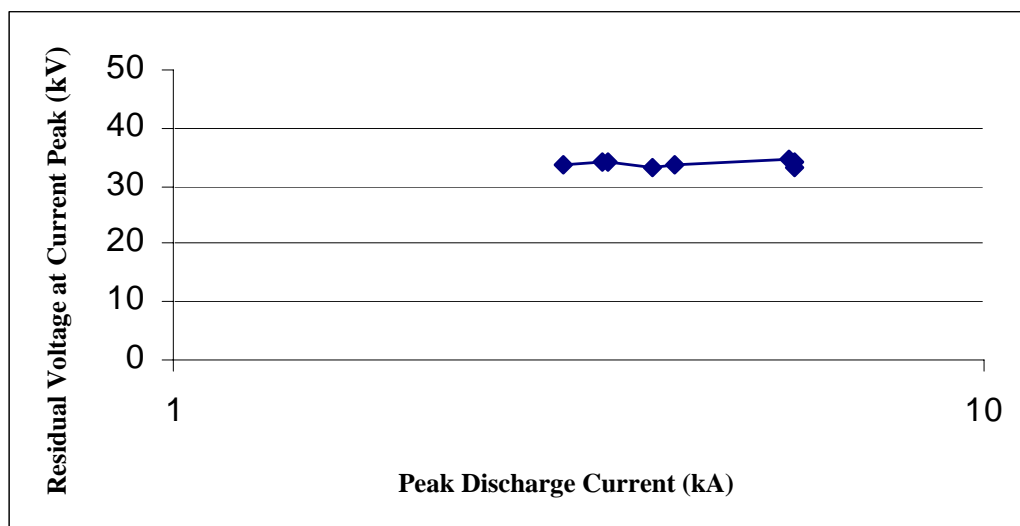
Figure 8.20: The V-I Characteristic of Sample D

From Figure 8.20 the protective level for the use of sample D is taken as 40kV and above.

The V-I characteristic of Sample E are shown in Table 8.7 and Figure 8.21.

Table 8.7: Protective Level Voltage and Peak Discharge Current of Sample E

Breakdown Voltage (kV)	Protective Level Voltage (kV)	Peak Discharge Current (kA)
35	24.39	1.64
40	27.77	2.40
45	29.65	3.48
50	31.15	5.63
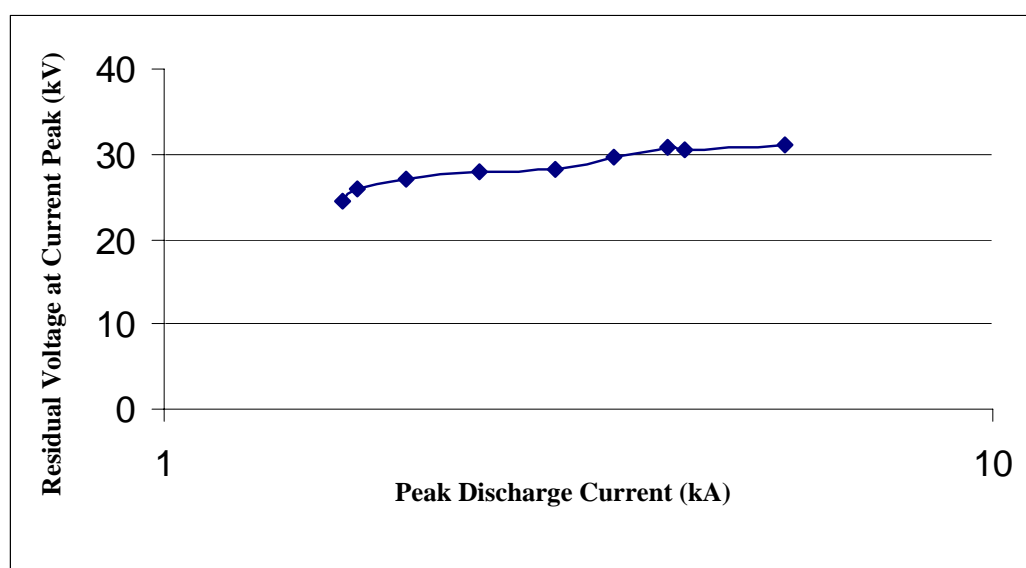
Figure 8.21: The V-I Characteristic of Sample E

From Figure 8.21 the suitable protective level for the use of sample E is 40kV and above.

8.6   Discussions

The residual voltage increases as the charging voltage increases. For each of the surge arrester samples, the charging voltage needed for the residual voltage to reach the rated current 5kA differs. However, the range of the charging voltage is not large, its limits being between 45kV to 50kV.

From Tables 8.3 to 8.7, the charging voltage starts at different values. This is due to the fact that at low charging voltages, the desired waveform was not captured because the surge arrester had not reached its turn-on voltage. From Figures 8.17 to 8.21, the residual voltage ranges from 20kV to 35kV, before it turns to the upturn region.

In implementing the experiment, the major problem was in obtaining the desired impulse. There are many considerations that have to be taken into account. Lacking one could cause the impulse produced not as desired, or worst, the impulse does not appear at all.

The utmost importance is the grounding of the system. As the ground is the common point, it is necessary to make sure a good contact to the ground. Otherwise, there will be lot of noise appearing alongside the impulse. The impedance matching of the terminals is also important. The right coaxial cable should be selected. The setting of the control panel needs to be tuned correctly. Otherwise, the signal could not be captured or captured incomplete.

In high voltage laboratory, the smallest inadequacy could result in a large difference in the data obtained. In the experiment, the gripping of each of the components are loose, especially the connection of the surge arrester. When the gripping loosens, gaps appear in between. It could cause unexpected results, and in this case, the noise. If the gripping is improved, the outcome could be improved.

The result obtained has not considered other factors such as temperature and pressure. It is only tested on a single impulse. Therefore, if the test is performed on several other impulses, the characteristic of the surge arresters can be better determined.

Required fast transient impulse waveform was obtained with unexpected ripple. However, due to the fact that the ripple is within acceptable range and the waveshape is still apparent, analysis was done with the waveform averaged. The calibration test using the liquid resistor has shown that the experimental setup is working properly. Voltage and current oscillograms for various current levels for various surge arresters samples were obtained. Voltage-current curves were then plotted to represent the characteristics of the arresters. Residual voltage was also determined. The constant (k and $\acute{\alpha}$) for each characteristic were then determined. Sample D was found to have the lowest k as well as the highest α value followed by sample A. This shows that sample D diverts the most current with slight change in voltage. On the other hand, the protective level voltage for each of the samples varies in the range of 25kV to 30kV. With the hysteresis curves plotted, self inductances of the surge arrester samples were determined. Generally, the tail inductance (L_t) is larger than the front inductance (L_f). With the analyzed data, the surge arresters were modeled. All in all, every sample is still working properly.

CHAPTER 9

GENERAL DISCUSSIONS AND CONCLUSIONS

Part I

Design of Inclined-Plane Tracking System

A practical on-line monitoring system at a reasonable cost has been designed and evaluated for surface leakage current under Inclined-Plane Test method. The use of such measuring technique permits a better understanding on the performance study of the insulator materials. The higher the total harmonic distortion of the leakage current waveform, the higher the probability of hydrophobic properties lost in the insulating materials. In addition, the characteristics of surface discharge have significantly influenced the on set of material degradation. The results suggest that the combination of leakage current magnitude and waveshapes analysis can provide a reliable indication on the status of insulating materials. The feature of data storage in the designed system could facilitate the researchers to extend the study for further analysis without conducting the test again.

Electrical Tracking Performance of the Newly Formulated LDPE-Natural Rubber (Nr) Blends

Based on the results, the good formulation of LLDPE-NR blends that to be used as a high voltage insulating material can be suggested as follows;

1) For the formulation without ATH loading, the weight of LLDPE component to the weight of natural rubber must be at least of ratio 4:1 (LLDPE:NR)

2) For the compound with a weight ratio of LLDPE to NR contents less than 4:1, an extending filler of alumina trihydrate (ATH) is proposed to be incorporated in the polymer blends. In order to improve the surface tracking and erosion properties, the optimum amount of ATH in the compound is found to be in the range of 50-100 part per hundred of polymer weight.

3) Based on the results of leakage current level as well as the resistance to carbon track development, the weight ratio of LLDPE to NR must be at least of 2:3 (LLDPE:NR). In fact, a higher contents of NR compared to LLDPE in the compound could reduce the mechanical strength properties drastically, and this is not good to be used as an insulating material in high voltage applications. The physical inspection of the compounds with higher contents of NR than LLDPE has proved that a final product of this compound showed bad quality and experienced a difficulty during processing and molding.

Part II
D-dot Probe Based Sensor

A 60kV D-dot probe based impulse voltage divider was successfully designed and constructed. Initial results of the probe's performance are very encouraging. The D-dot probe design can be futher improved for marketing and commercial proposes.

Tubular Current Shunt

This work dealt with theoretical consideration in designing resistive tubular shunt for measurement of current pulse with peak magnitude approximately 10kA and pulse duration approximately 10μs. The design of the 10kA impulse current shunt was successfully carried out including specific identification of materials to be used. The shunt was also successfully constructed. However, the test could not be carried out due to the insufficient resources to complete the last activity in the construction, that is, the soldering of the nickel chromium onto the aluminium.

Design of a triggerable high current switch

The triggerable high current switch has been developed according to the design. With a gap setting that can be changed from minimum to a maximum gap of 33mm, the switch is expected to withstand up to 100 kV stress before being triggered to close. This is done using compressed SF_6 as the breakdown medium. The use of SF_6 would help in increasing the breakdown strength of the gap and also to quench the high current flowing through the gap during the breakdown.

However, the developed switch has not been tested up to a voltage higher than 10 kV in operation (to withstand and be triggered to close) and 33 kV (to withstand only). In both cases, air is used as the breakdown medium. The current flowing through the gap can reach up to 5 kA from the tests done. The risetime of the impulse produced by the impulse current generator used to test the circuit is 1 μs. This is much higher than the objective due to the relatively high inductance of the overall circuit (mainly from the source capacitor and the connecting ground wire).

As a conclusion, the developed switch is a success in terms of its operation, but the capability of the switch needs to be further tested. It needs to be tested with higher voltages (to produce higher currents) and also the use of SF_6 as the breakdown medium need to be observed. Furthermore, the impulse current generator needs to be

improved in reducing its overall inductance. This will be done in the further stages of building the coaxial test module for ZnO surge arresters.

High Current High Voltage Surge Arrester Test Facility

Tests had been carried out using the designed D-dot probe based on high voltage impulse divider on distribution level high voltage surge arresters.The current was measured using a commercial Rogowski coil instead of the supposedly constructed current shunt due to its inavailability at the time of this report.

REFERENCES

ASTM, ASTM D3426-97 (1998). "Standard Test Method for Dielectric Breakdown Voltage and Dielectric Strength of Solid Electrical Insulating Materials Using Impulse Waves"

Barker, P.P., Mancao, R.T., Kvalfine, D.J. and Parrish, D.E. (1993). "Characteristic of Lightning Surges Measured at Metal Oxide Distribution Arresters." IEEE Transactions on Power delivery, Vol.8, No. 1, pp.301-3 10.

Bowider, G.W. (1973). "Measurement in High Voltage Test Circuits" Pergamon Press, Oxford.

Brody & Clause. (1986). −"Material Handbook." 12~h ed. McGrawhill Book Company.

Callister, W.D. (2000). "Materials Science and Engineering – An Introdued. Von Hoffman Press, N.Y.:John Wiley & Sons, Inc. 496-508.

Chang, R.J., *et.al* (1997). "Optimization of Tracking Resistance, Erosion Resistance and Hydrophobicity for Outdoor Insulation Materials." *Int. Conf. On Properties and Applications of Dielectric Materials*. 782-785.

Chang, R.J. and Mazeika, L. (2000). "Analysis of Electrical Activity Associated with Inclined-plane Tracking and Erosion of Insulating Materials." *IEEE Trans. Dielectrics and Electrical Insulation*. **7 No. 3**. 394-400.

Costa, R.A., Hattori, R.S. and Redondo, E.G. (1991). "Optimization of EPDM Compounds for Resistant Insulators to Electrical Tracking." *Proc. 3rd Int. Conf. On Properties and Applications of Dielectric Materials*. 300-304.

Deng, H., Hackam, R. and Cherney, E.A. (1995). "Role of the Size of Particles of Alumina Trihydrate Filler on The Life of RTV Silicone Rubber Coating." *IEEE Trans. Power Delivery*. **10 No. 2**. 1012-1024.

Fernando, M.A.R.M. and Gubanski, S.M. (1999). "Leakage Current Patterns on Contaminated Polymeric Surfaces." *IEEE Trans. Dielectrics and Electrical Insulation*. **6 No. 5**. 688-694.

Feser, K., PtA W., Weyreter, G., Gockenbach, E. (July 1988). "Distortion Free Measurement Of High Impulse Voltages." IEEE Transactions on Power Delivery. **3 No. 3**.

Gallagher, T.J. and Pearmain, A.J. (1983). "High Voltage Measurement, Testing and Design." John Wiley& Sons, Chichester.

Gorur, R.S., *et.al* (1997a). "A Rapid Test Method for Evaluating the Tracking and Erosion Resistance of Polymeric Outdoor Insulating Materials." *IEEE Annual Report-Conf. On Electrical Insulation and Dielectric Phenomena*. 402-405.

Gorur, R.S., *et.al* (1997b). "A Laboratory Test for Tracking and Erosion Resistance of HV Outdoor Insulation." *IEEE Trans. Dielectrics and Electrical Insulation*. **4 No. 6**. 767-774.

Gubanski, S.M. (1999). "Modern outdoor electrical insulation." *IEEE Trans. Dielectrics and Electrical Insulation*. **6 No. 5**. 517.

Hackam, R. (1998). "Outdoor High Voltage Polymeric Insulators." *Proc. Int. Symp on Electrical Insulating Materials*. **IM-1**. 1-15.

Hackam, R. (1999). "Outdoor HV composite polymeric insulators." *IEEE Trans. Dielectrics and Electrical Insulation.* **6. No. 5**. 557-585.

Haddad, A., Naylor, P., German, D.M., Waters, R.T. (1995): "A Low Inductance 60kV Test Module for Distribution Surge Arresters" Ninth International Symposium on High Voltage Engineering, Graz (Austria), **No. 4559.**

Haddad, A., Naylor, P., Metwally, I.A., German, D.M. and Waters, R.T. (1995): "An Improved Non Inductive Impulse Voltage Measurement Technique for ZnO Surge Arresters" IEEE Transactions on Power Delivery, **10 No. 2**. 778-785.

Katada, K. *et.al* (2000). "Corona Discharge Characteristics of Water Droplets on Hydrophobic Polymer Insulator Surface." *Proc. The 6th Int. Conf. On Properties and Applications of Dielectric Materials.* 781-784.

Khalifa, M. (1990): "High Voltage Engineering Theory and Practice" Marcel Dekker Inc, New York.

Kikuchi, et.al (1999). "Survey on the use of non-ceramic composite insulators." *IEEE Trans. Dielectrics and Electrical Insulation.* **6. No. 5**. 548-556.

Kim, S.H. and Hackam, R. (1994). "Temperature distribution in RTV silicone rubber coating following dry band arcing." *Int. Symp. On Electrical Insulation.* 599-602.

Kind, D. (1978): "An Introduction To High-Voltage Experimental Technique" Vieweg & Sohn Verlagsgesellschaft mbH, Braunschweig.

Kuffel, E. and Abdullah, M. (1970): "High Voltage Engineering" Pergamon Press, New York.

Kuffel, E. and Zaengl, W.S. (1984): "High Voltage Engineering Fundamentals" Pergamon Press, New York.

Kumagai, S. and Yoshimura, N. (2001). "Tracking and erosion of HTV silicone rubber and suppression mechanism of ATH." *IEEE Trans. Dielectrics and Electrical Insulation*. **8 No. 2**. 203-211.

Mackevich, J. and Shah, M. (1997a). "Polymer outdoor insulating materials Part I: Comparison of porcelain and polymer electrical insulation." *IEEE Electrical Insulation Magazine*. **13, No.3**. 5-12.

Mackevich, J. and Simmons, S. (1997b). "Polymer Outdoor Insulating Materials Part II-Material Considerations." *IEEE Electrical Insulation Magazine*. **13 No. 4**. 10-16.

Metwally, I.A. (1985): "Coaxial D-Dot Probe: Design and Testing" Electrical Insulation and Dielectric Phenomena, Annual Report, Mansoura University, Egypt, 298-301.

Naidu, M.S. and Kamaraju, V. (1995): "High Voltage Engineering" McGraw-Hill, New York.

Naylor, P. (1995): "The Transient Response of High-Voltage Surge Arresters" PhD Thesis, University of Wales, Cardiff (UK).

Rifijin, L., Caixin, S. and Xiaoguang, Z. (1993). "Development of A Transient Voltage Measuring System." Eight International Symposium on High Voltage Engineering, Yokohama (Japan), **4 No. 54.16**. 141-144.

Risino, A.J., Auckland, D.W. and Varlow, B.R. (1994). "A New Test Method for the Measurement of Surface Tracking Resistance." *IEEE Int. Symposium on Electrical Insulation*. 79-81.

Ryan, H.M. (1994): "High Voltage Engineering and Testing" Peter Peregrinus Ltd, London.

Schwab, A.J. (1972): "High Voltage Measurement Technique" M.I.T. Press, Cambridge, Massachusetts.

Skitek, G.G,, Marshall, S.V. (1990): "Electromagnetic Concepts and Applications" 3rd Edition, Prentice Hall.

Sundhar, S. *et.al* (1992). "Polymer insulating materials and insulators for high voltage outdoor applications." *Int. Symp. On Electrical Insulation*. 222-228.

Ugur, M., Kuntman, A. and Merev, A. (1999a). "Investigation the Effect of Environmental Factors on the Performance of Polymeric Outdoor Insulation." *Conf. On Electrical Insulation and Dielectric Phenomena*. 743-746.

Van Deursen, A.P.J., Gulickx, P.F.M. and Van der Laan, P.C.T. (1993): "A Current and Voltage Sensor Combined in One Unit." Eight International Symposium on High Voltage Engineering, Yokohama (Japan), **2 No. 56.027**. 463-466.

Van Heesch, E.J.M., Van Deursen, A.P.J., Van Houten, M.A., Jacobs, G.A.P., Kersten, W.F.J. and Van Der Laan, P.C.T. (1989): "Field Tests and Response of The D/I H.V. Measuring System." Sixth International Symposium on High Voltage Engineering, New Orleans (USA): **3 No. 42.23**.

Xuguang, L., Yougong, W. and Fuyi, L. (2000). "Study on Improving the Tracking and Erosion Resistance of Silicone Rubber." *Proc. The 6th Int. Conf. On Properties and Applications of Dielectric Materials*. 342-345.

Young, Y.D., *et.al* (1992). "The Effect of Acid Rain on the Tracking Deterioration of Elastomer." *IEEE Int. Symp. On Electrical Insulation*. 258-261.

Z. Abdul-Malek. (1999): "Fast Transient Response of High-Voltage Surge Arresters" PhD Thesis, University of Wales, Cardiff (UK).

Z. Abdul-Malek. (1995): "Lightning Impulse Test on High Voltage Surge Arresters" Master Thesis, University of Wales, Cardiff (UK).